Observations of Jupiter's Decametric Radiation with a Very-Long-Baseline Interferometer

By

MICHEL ALLAN LYNCH

A DISSERTATION PRESENTED TO THE GRADUATE COUNCIL OF
THE UNIVERSITY OF FLORIDA IN PARTIAL
FULFILLMENT OF THE REQUIREMENTS FOR THE DEGREE OF
DOCTOR OF PHILOSOPHY

UNIVERSITY OF FLORIDA
1972

ACKNOWLEDGMENTS

The author wishes to express his appreciation for direction and aid furnished by his research advisor, Dr. Thomas D. Carr. The very-long-baseline interferometer studies have been a continuing interest of Dr. Carr's, and it has been the author's privilege to have served under him in this project. It has been an instructive experience to have studied under Drs. A. G. Smith, K. R. Allen, G. R. Lebo and K-Y. Chen. Each contributed time and thought in the form of consultation, reading of the manuscript of the dissertation and encouragement.

While the author wrote most of the programs used in the research reported in this dissertation, several programmers supplied specific programs to help the project. The work of Mr. Jamie Stone, Jr., in writing the digitization programs, was vital to the data processing and is greatly appreciated. Miss Carol Vilece contributed the early versions of the data handling programs for the IBM 1800 and operated the machine during digitization. The author is in debt to both Mr. Stone and Miss Vilece for expediting his work under the difficult scheduling conditions that obtain on the IBM 1800 at the University of Florida Medical Center. Mrs. Mary Coates Lynch wrote the program to convert the column-binary card code to a useable form for the IBM 360/65 at the University of Florida Computing Center. Both her aid

as a programmer and her encouragement as a wife determined, in no little way, the success of this research.

The author wishes to acknowledge the aid of Mr. W. W. Richardson and Mr. H. W. Schrader in the preparation of the drawings and photographs. He wishes to thank Mrs. Terrie Campbell for her care in typing the original draft of the dissertation.

This investigation was supported in part by the National Science Foundation and the Office of Naval Research.

TABLE OF CONTENTS

LIST OF TABLES

LIST OF FIGURES

LIST OF FIGURES (Continued)

LIST OF FIGURES (Continued)

LIST OF FIGURES (Continued)

Abstract of Dissertation Presented to the Graduate Council of the
University of Florida in Partial Fulfillment of the
Requirements for the Degree of Doctor of Philosophy

OBSERVATIONS OF JUPITER'S DECAMETRIC RADIATION
WITH A VERY-LONG-BASELINE INTERFEROMETER

By

Michel Allan Lynch

June, 1972

Chairman: Dr. Thomas D. Carr
Major Department: Astronomy

This dissertation presents the results of several types of measurements made on the decametric electromagnetic radiation from the planet Jupiter using a very-long-baseline interferometer. Jovian signals were received at stations located at Old Town, Florida, St. Petersburg, Florida, Maipu, Chile, and Bowling Green, Kentucky. The interferometer baselines ranged from 11,150 to 456,000 wavelengths of the 18 MHz receiving frequency. Interference of the signals was accomplished by using the cross correlation function with digitized data in a program for the IBM 360/65 at the University of Florida Computing Center.

By interpreting the amplitude of the cross correlation function as the fringe visibility, an upper limit on the angular size of the source of the radiation was determined to be 0.1 seconds of arc, if it were assumed that the source was incoherent and had a Gaussian brightness distribution. The high correlation of the envelopes of the two L-Bursts studied using the very long baseline (over 7,000 km) indicated that the time dependence of the strength of the burst was probably intrinsic to

the source. The stability of the fringes formed by interference of the L-Burst data indicates that the source did not "jump about" more than 85 km for the 2.2 seconds' duration of the 1971 burst. The "jumping about" motion is superimposed upon a constant drift of the source with respect to the interferometer power pattern. The analysis of a series of S-Bursts received in 1970 indicates that, if the radiation from Jupiter is beamed and the beams rotate with respect to the Earth-Jupiter line, then the minimum sweep rate of the beams must be greater than 10°/second in the north-south direction and greater than 0°.4/second in the east-west direction. The method of sweep-rate measurement involved comparing the time of arrival of an identifiable phase point on the heterodyned Jupiter signal with that of a similarly identifiable amplitude point on the envelope of the detected signal at various pairs of stations.

While the use of the interferometer for the determination of source size is restricted to a source that is an incoherent radiator, the remaining analyses place new limits on any type of source.

CHAPTER I

A GENERAL INTRODUCTION

I-1. Jupiter's Electromagnetic Radiation and the Wavelength Dependence of Its Characteristics

The electromagnetic radiation received from Jupiter is the main key available for man to use in determining the nature of the giant planet. The visible spectrum from the planet is that of sunlight reflected off the tops of clouds. The presence of absorption lines due to gases above the reflecting level serves to modify the solar spectrum. In the infrared a disk temperature of about 130°K was measured by D. H. Menzel and others as early as 1926. This measurement is thought to represent the temperature at the cloud tops, or even somewhat higher, if the radiation is considered to be due to a source obeying the black body radiation laws. It was reported by Mayer, McCullough and Sloanaker (1958) that radiometer measurements at a wavelength of 3 cm gave a disk temperature of about 140°K. The value is in approximate agreement with the infrared value, and it is thought to indicate that the radiation at this wavelength is still thermally generated. A measurement at 10 cm by Sloanaker (1959) was quite different. If the source of the radiation received at this wavelength is considered to be a black body, then its temperature must have been about 600°K.

Succeeding measurements at the longer wavelengths of 21 cm and 31 cm seemed to confirm the trend with disk temperatures of 2000°K and 5000°K, respectively. Radhakrishnan and Roberts (1961) reported that the source region for this wavelength was about three times the diameter of the visible planet in the plane of the equator and that the radiation had a moderate amount of linear polarization. A model of the source of the radiation at this wavelength was proposed. The model accounts for the linear polarization by having relativistic electrons emit synchrotron radiation as they spiral in a magnetic field.

While radiation between the frequencies of 400 MHz and 40 MHz has yet to be detected with certainty, Jupiter is very active in the decameter wavelength region. The decameter region contains frequencies from 40 MHz downward to about 5 MHz where the earth's ionosphere becomes opaque. The flux density reported by Carr, et al. (1964) increases very rapidly with wavelength, seemingly with a spectral index on the order of + 8. Radiation in the decameter region was first reported by Burke and Franklin (1955) and confirmed by Shain, who used old records dating back to 1950. Shain (1955 and 1956) reported that the source of the radiation did not emit isotropically but seemed to radiate into preferred directions in a coordinate system attached to the planet. System II coordinates, with a rotation period of $9^h55^m40^s.6$ (based on the temperate zone visual markings), provided a rotating frame in which the radio sources appeared to be at rest. This later was modified, due to the sources drifting in System II, to a longitude coordinate frame with a rotation period of $9^h55^m29^s.37$ based on the work of Shain (1956), Carr, Smith, Bollhagen, Six and Chatterton (1961) and other groups.

I-2. The Nature of the Decametric Radiation

The most noticeable feature of Jupiter's decametric radiation is its extreme intensity variation with time. Radiation at this wavelength comes in the form of noise storms that last on the order of a few minutes to a few hours. Gallet (1961) further breaks down the noise storms into burst groups (with durations on the order of minutes) and into two types of pulses that make up the burst groups. The L-pulse is characterized by having a length of from 0.1 to 5 seconds while the S-pulse is shorter with a length of from less than 10 to about 100 milliseconds. Flagg and Carr (1967) reported that bursts substantially shorter than this have been detected. Theories for the formation of the two types of pulses are given later in this chapter.

Due to the extreme time variability of the radiation, it is usually more convenient to use the probability of occurrence of an event as the dependent variable. The location of the sources with respect to System III was accomplished by plotting the probability of occurrence of Jupiter radiation versus the central meridian longitude (that longitude in System III that is directly below the earth as viewed from Jupiter). Source A is located at approximately 250°, Source B at about 160° and Source C at about 320° in System III. The source regions are each about 60° wide. Bigg (1964) found a correlation between the superior geocentric longitude of Io, the innermost Galilean satellite, and the probability of occurrence of radiation from the previously described sources. Prediction of Io-Source events can now be made. The events described in this dissertation occurred during Io-B predicted storms. The Io-B storms occur when Io is about 90° from superior geocentric conjunction and Source B is crossing the central meridian.

Jupiter radiation is generally of relatively wide bandwidth. Work by Carr, et al. (1964), Riihimaa (1964) and Dulk (1965) characterizes the bursts as having bandwidths on the order of a MHz with center frequencies that move in time. Some interesting features in the form of modulation lanes visible in the amplitude-frequency domain have been reported by Riihimaa (1970). Since the receivers in the experiments described here have bandwidths on the order of a few kHz, the interaction of a frequency-drifting band of noise with the narrow-band, fixed-frequency receivers must be borne in mind.

Decametric radiation from Jupiter exhibits strong circular polarization. Emission from Source B is almost always polarized in the right hand sense at the commonly studied frequencies in the decametric part of the spectrum.

I-3. A Brief History of Jovian Decametric Measurements Using Long-Baseline-Interferometry.

It was indicated early in the investigation of Jovian radiation that the source was in the vicinity of the planet and was probably rather small. It was therefore necessary to resort to interferometric methods to measure the size of the source. Gardner and Shain (1958) found no burst-for-burst correlation between signals received at the ends of a 20 km baseline. Douglas and Smith (1961) reported a few bursts, especially of the S-type, that were correlated over a baseline of 100 km. Slee and Higgins (1963) used a radio-linked phase sensitive interferometer with a baseline of 32 km and frequency of 19.7 MHz. They found that the fringe visibility was not reduced, hence the source was not resolved, with this baseline.

The University of Florida group used a Brown and Twiss Post-Detection-Correlation Interferometer before 1965 with a baseline of 55 km, as reported by Carr, et al. (1965). May (1965) employed data from this interferometer to determine a maximum source size of 50 seconds of arc. A phase interferometer was also used by this group that employed the cross correlation of the heterodyned radio frequency noise. Brown, et al. (1969) used this system with a baseline of 880 km to reduce the maximum possible source size to less than one second of arc. The phase interferometer of the University of Florida group used tape recorders for the storage of data before cross correlation was done.

Meanwhile Dulk, Rayhrer, and Lawrence (1967) used detected, tape-recorded receiver output to form an interferometer of the Brown and Twiss type with a baseline of 175 km at 34 MHz. They obtained an upper limit of 3 seconds of arc on the size of the sources of both L- and S-bursts. Dulk (1970) and Stannard, et al. (1970) extended the baseline to 487,000 wavelengths at the operating frequency of 34 MHz. By using the instrument in the phase interferometer mode, they were able to explore the phase stability of the source. If the source were assumed to be incoherent, they found that its maximum size was less than 0.1 second of arc.

A preliminary report of part of the work detailed in this dissertation was made by Carr, et al. (1970) in the form of a history of the University of Florida 18 MHz interferometry experiment. At that time a 456,000 wavelength baseline was in use, but only small samples of the data had been hand reduced.

I-4.1. Early Theories Concerning the Production of Jovian Noise Storms

The earliest suggestions as to the origin of the Jovian decametric radiation included Jovian lightning storms and dynamo effects created by slippage of the cloud bands relative to one another. These early proposals ran into energetic problems in accounting for the high intensity of the bursts.

Warwick (1963) proposed Cerenkov radiation of relativistic electrons as a source. This was followed by Zheleznyakov (1965) with a theory involving plasma waves in Jupiter's ionosphere. Ellis (1965) is the first to have published a model that involved cyclotron radiation from electron streams. This model stands as the direct ancestor to most of the seriously considered theories in use today. The discovery of the Io effect by Bigg in 1964 required the inclusion of an interaction mechanism between the satellite and the emitting region. Gledhill (1967) proposed that Io interacted with an implausibly dense plasma discus about the planet by producing waves in it. Piddington and Drake (1968) had Io disturbing the plasma as a result of its having a high degree of conductivity or, alternatively, a permanent magnetic moment. References to these papers are contained in Schatten and Ness (1971).

Goldreich and Lynden-Bell's theory (1969), which is discussed in the next section, requires that Io be about 100 times as conductive as the earth's moon. This problem is alleviated in two more recent theories. One, by Schmahl (1970), treats Io as the source of Alfvenic waves that travel down the magnetic field lines to the ionosphere of the planet. The waves become shockfronts that cause radiation from coherent electron groups. The theory is still not finished in that it does not develop the interaction mechanism between the Alfvenic waves and the electromagnetic waves. Another more recent theory by Schatten and Ness (1971) does

not require the high conductivity for Io that the theory of Goldreich and Lynden-Bell does. They propose that Io is Moon-like and that Jupiter's magnetic field lines slide through Io relatively unaffected. It causes local perturbations in the pitch angle of the electrons spiralling in the field near it, however, thus causing them to emit radiation when they reach the top of the Jovian ionosphere. Schatten and Ness propose that radiation is emitted into a plane perpendicular to the flux line that passes through Io. Their paper presents a computer solution to the geometry problem involving the orientation of the magnetic dipole of Jupiter and the Earth-Jupiter line. The solutions agree with the locations of the three commonly observed sources, and also the rarely seen fourth source. The geometry of the theory shows promise, but, as in Schmahl's theory, the mechanism for the production of radiation is not fully explored.

I-4.2. The Theory of Goldreich and Lynden-Bell

A possible explanation of the effect of Io on the Jovian radiation is given by P. Goldreich and D. Lynden-Bell (1969). They propose that the satellite acts as a unipolar inductor which generates currents along a magnetic flux tube connecting it with Jupiter's ionosphere. The electron currents are thought to undergo cooperation instabilities near the planet, where they radiate by a form of MASER action into preferred directions at frequencies just above the local gyrofrequency.

From the mapping of the source of the decimeter radiation and the investigation of its linearly polarized component, it has been found that a magnetic field having an approximately dipolar geometry can be assigned

to the planet. The N magnetic pole is located in the northern hemisphere and is tilted 10° from the planet's rotation axis toward the System III longitude of 200°. Figure I.1a illustrates the geometrical relations during Io-related storms.

Goldreich and Lynden-Bell, by assuming the conductivity of Io to be about that of silicates, 10^{-5}mho/cm, show that the Jovian magnetic field would diffuse into Io in about one day. The field lines passing through Io would rotate about the planet at Io's orbital speed. If Io has a finite resistance, the flux tube will not be entirely trapped but will slowly drift through it. The slippage time must be long compared with the time for adjustments to be made in the rest of the "circuit." The adjustments are propagated as Alfven waves. Hence, the slippage of a flux line through Io must take longer than the time for an Alfven wave to travel along the flux tube to the planet and return. Since, in Io's reference frame, the parallel component of the electric field must vanish, an electron current flows toward the planet along the outside of the flux tube and returns to Io along the inside (the side nearest Jupiter). In Jupiter's frame, there is an electric field in the ionosphere at the feet of the flux tube which is directed toward the north for the one in the northern hemisphere. The feet of the flux tube slip relative to the rotation of the planet since the tube rotates about Jupiter at Io's orbital rate (1.77 days). In the ionosphere the flux tube has an elliptical cross section. When the ionization of the ionosphere is high the feet of the flux tube will be pulled ahead of the satellite by the rotation of the planet. The authors of the theory calculate that the feet will lead Io by 12° under these conditions. When the ionization is low, e.g.,night time at the foot of the flux tube, there will be no

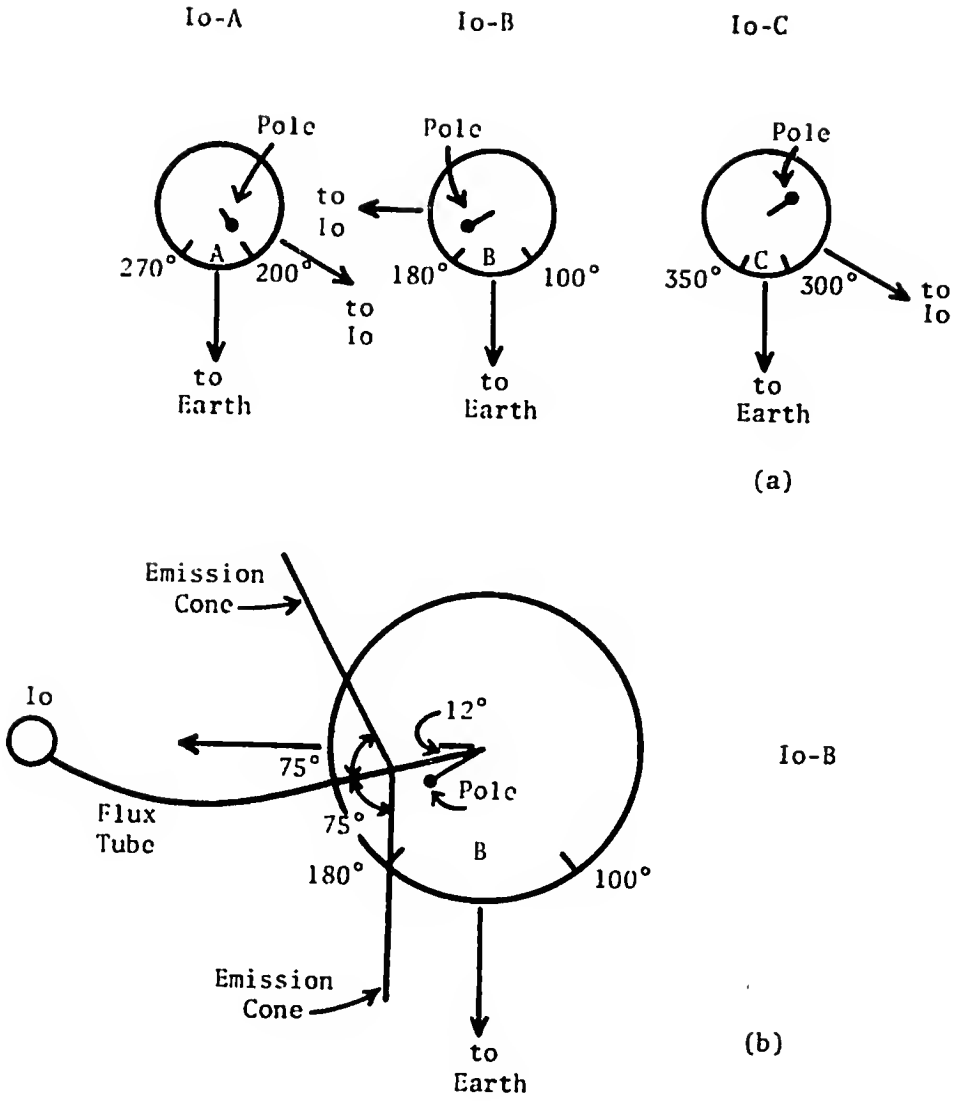

Figure I.1 -- Geometrical Relationship of Jupiter, Io and the Earth for Io-Related Storms.

dragging, and the flux tube will terminate on the same Jovian longitude for which Io is on the Meridian. During the transition from night to day, the foot of the flux tube will be swept from its night position to a point some 12° ahead in about 20 minutes (i.e., at Jupiter's rotation rate of about 36°/hour).

The weakly relativistic electrons spiralling in the flux tube can serve as negative absorbers if their momentum distribution is sufficiently inverted. The greatest amplification occurs in the extraordinary mode for propagation at right angles to the magnetic field as seen in the coordinate system in which the average electron streaming velocity is zero. The linear Doppler effect causes the frequency of the radiation to be raised above the local electron gyrofrequency as seen in the Jovian frame. It also causes the radiation to be directed at large angles with respect to the electron stream velocity.

The radiation from 10 keV electrons spiralling up from the planet along the flux tube will be directed into a conical surface with a half-angle of 79° that opens symmetrically about the flux tube outward from Jupiter. The apex of the cone is located at the foot of the flux tube in Jupiter's ionosphere. Electrons spiralling toward the planet will also emit radiation into a similar cone which, upon reflection of the radiation by the ionosphere, will open outward from the planet. Such a cone will intersect Jupiter's equatorial plane in a pair of diverging lines whose half-angle is between 65° and 75°, depending on the tilt of the magnetic axis with respect to the Jupiter-Io line. The authors of the theory further require that the radiation be beamed only into selected regions of the conical surface. The actual degree of beaming anisotropy cannot be predicted; however, for reasons which seem

plausible, the assumption is made that the preferred beaming angle is at 13° with respect to the east-west direction on Jupiter. The assumed parameters give a model for the Source B emission geometry as shown in Figure I.1b.

Observations show that the sources appear to be narrower at higher monitoring frequencies. In the theory, the local gyrofrequency increases nearer the planet such that the source of the higher frequency radiation must be closer to Jupiter. The axis of the radiation cone is tilted farther from the equatorial plane since the flux tube is more nearly parallel to the magnetic dipole at lower altitudes. The greater the tilt of the cone axis the smaller the angle is between the lines of intersection between the cone and the equatorial plane. This makes the source seem narrower when viewed from Earth since radiation reaching the earth can travel only along the lines of intersection.

The theory gives a model for the formation of the S-Burst. It proposes that a column of electrons spiralling on the surface of the flux tube emits coherently for a period of time. The time duration of the S-Burst is determined by the coherence time of the column of electrons. The bandwidth of the radiation is determined by the altitude range, hence the range of local gyrofrequencies, spanned by the column. S-Bursts may be formed by electrons moving in either direction with respect to the planet during the time for emission of radiation.

The source of the radiation energy is the transverse kinetic energy of the keV electrons spiralling in the magnetic field. The electrons have undergone acceleration from an energy of about 4 eV to the keV region by the electric field generated by Io moving in Jupiter's magnetic field. The ultimate source of energy for the radiation resides in the orbital

energy of Io. Using plausible values for the number density of radiating electrons, etc., the authors show that the doubling of Io's angular momentum is comfortably long compared with the lifetime of the solar system.

A serious weakness in the theory occurs in the assumed value for the conductivity of Io. It was necessary to assume a conductivity of about two orders of magnitude greater than that of the moon, an assumption which may not be realistic.

We wish to consider the theory of Goldreich and Lynden-Bell in this dissertation since it predicts the beaming of the decametric radiation. If the beams sweep across Earth, they should arrive at one station of an interferometer, such as ours, before they arrive at another station. We will report on the measurements of arrival times in a later chapter.

I-4.3. The Theory of Douglas and Smith for the Formation of L-Bursts by the Solar Wind

J. N. Douglas and H. J. Smith (1967) proposed a theory to account for the L-burst structure in the Jovian radiation. Two types of experiments, both involving spaced receivers, led to their conclusion. Gardner and Shain (1958) had found that the burst envelope correlation was often, but not always, poor over baselines of only a few tens of kilometers. Carr, et al. (1964) obtained a similar result over a baseline of 7000 km. The cases of positive correlation indicated that the cause of the amplitude variation in the burst must be more distant than the Earth's ionosphere, since such local variations should not influence the signals at both receivers. Douglas and Smith (1961) started a

continuing program of monitoring Jovian radiation for the purpose of trying to detect differences in arrival times of a given burst at several stations. Results of this work (Douglas and Smith, 1967) indicated that there is a marked dependence of the delay time and the order of arrival at receivers in the east-west orientation on the number of days before (or after) opposition of Jupiter.

In their paper (1967), they argue for a random distribution of phase-changing irregularities in the solar wind located in the space between Jupiter and the earth. They further require that these irregularities be remote from both the earth and Jupiter. The irregularities are stable in structure. Their motion causes an isophotal pattern to drift past the earth-based receivers at a rate of several hundred kilometers per second. Mariner II data concerning the solar wind indicated that the velocity of the wind did not change appreciably with distance from the sun. Douglas and Smith proposed that an inhomogeneity in the solar wind would cause phase changes in the radiation, creating a drifting isophotal pattern as seen at the earth. According to their calculations, using data extrapolated to the region of the Earth-Jupiter line-of-sight, they were able to account for the drift rate of the isophotal pattern. Furthermore, their theory predicted that before Jovian opposition the isophotal pattern should drift eastward, and after opposition the pattern would drift westward. The drift direction is determined by the sense of the solar wind velocity vector projected on a plane perpendicular to the line-of-sight from the earth to Jupiter. It is clear that the vector will switch directions at opposition if the solar wind is assumed to move in a radial direction from the sun. The predicted drift direction was shown to agree with experimental data.

I-5. The Purpose of the Experiments Described in This Dissertation

Theories are the intellectual creations of mankind in the same sense as are the more conventional arts. In the natural sciences, however, man has added the constraint that his theories must represent the way in which a class of natural phenomena may be caused. There is thus the requirement that any prediction concerning a natural phenomenon made by a theory must agree with the measurements made on that natural phenomenon. In case of disagreement, difficulties may lie both in the theory and in the interpretation of the measurements. It is generally not possible to make THE measurement that will unequivocably make the choice between two or more theories obvious.

In astronomy, man is faced with taking data from phenomena that are secondarily related to the information he is seeking. It is therefore necessary to examine not only the performance of the theory in question, but also to be aware of possible failures of theories concerning the way the information is transmitted. A case in point is the determination of the features of Jupiter's magnetic field. The radio astronomer received electromagnetic radiation that, according to Maxwell's equations and the theory of electrical measurements, could be shown to be partially linearly polarized. The synchrotron process had been shown to be a source of linearly polarized radiation having the spectral characteristics observed by the astronomer. Since this demonstration had been made on Earth, one had to make the assumption that such a process could be carried on elsewhere given similar conditions. This assumption is part of a set summarized by Newton in the Principia as a list of Rules of Reasoning. One condition for the occurrence of the

synchrotron process was the presence of a magnetic field. Jupiter, then, must have a magnetic field. Further measurements of the distribution of the source of radiation led to the current understanding of the geometry of the field.

At the same time that an inquiry is being made into the origin of one natural phenomenon, i.e., the radiation from Jupiter in the previous example, many other phenomena are being investigated. There is, for example, exploration of many other features of Jupiter taking place, such as: experimental studies of the atmospheric features of the planet, of the red spot and theoretical studies of the interior of the planet. The aim of man's inquiry seems, in this case, to be that he is hoping to have at some future time a complete picture of Jupiter which can be added to the rest of the pictures he has made of the universe. By that time, if he is successful, he will feel at home in a familiar world, a world of his own intellectual creation.

The experiments in this dissertation are proposed to give man a little more insight into the natural phenomena that he is hoping to understand.

List of Experiments

1. The angular size of the source of Jupiter's decametric radiation will be determined using both a phase and an intensity interferometer.

2. The stability of the position of the source will be examined using the fringe pattern generated by the interferometer.

3. The arrival times of S- and L-Bursts at several stations will be examined to provide experimental information in connection with the theories of Goldreich and Lynden-Bell and of Douglas and Smith. A new method for eliminating the residual timing errors will be used.

CHAPTER II

GENERAL INTERFEROMETER THEORY

The theoretical structure for the understanding of the phase and intensity interferometer is developed in the first two sections of this chapter. Since the interference pattern of the received signals from Jupiter is actually obtained from the computer, the last section of this chapter is devoted to establishing the connection between the classical forms of the interferometer and the experimental technique used here.

II-1. The Phase Interferometer

Classically, the phase interferometer adds the signal voltages from two spaced antennas at some central point. The fluctuation in the combined signal power is dependent on the size and location of the source with respect to the interferometer power pattern. Consider an interferometer formed by placing mixers between each antenna and the signal adding point. A system of this nature allows the signals to be stored on magnetic tape and the interference to be accomplished under more convenient conditions.

Figure II.1a shows a block diagram of the system to be considered. The left half of the system is called receiver one and has an input

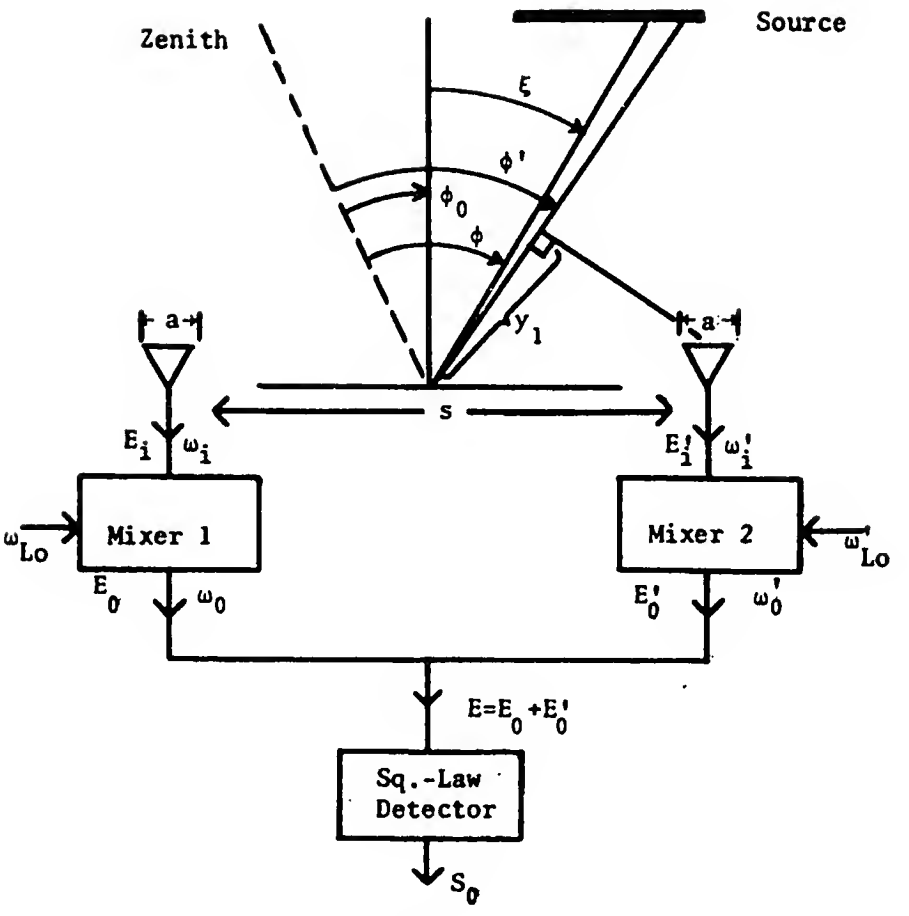

Figure II.1 -- (a) Diagram of the Classical Interferometer,
(b) Graph of the Output S_0 Versus Beam Angle ϕ_0.

frequency ω_i, a local oscillator frequency ω_{Lo}, and a low-passed output frequency ω_o. The right side, receiver two, has similar variables that are given by ω_i', ω_{Lo}', ω_o'. For a single frequency the input voltage to receiver one is $E_i = E_{10}(\xi) \cos(\omega_i t + \Psi)$, where Ψ is the phase lag introduced by the extra path length y_1 with respect to the point halfway between the antennas. Its value is $\Psi = \frac{\pi (s+a) \sin \xi}{\lambda}$. The input voltage to receiver two is $E_i' = E_{10}'(\xi) \cos(\omega_i' t - \Psi)$, where Ψ has the same value. The amplitude factors, E_{10} and E_{10}', are angle dependent since each antenna has a power pattern appropriate to its design. The angle variable, $\xi = \phi_0 - \phi$, denotes a direction in the far field pattern of the interferometer measured from the center of the main lobe. The local oscillator injection voltages take the form: $E_{Lo} = E_{Lo_o} \cos(\omega_{Lo} t)$ and $E_{Lo}' = E_{Lo_o}' \cos(\omega_{Lo}' t + \eta)$, where η is the phase at time = zero. Before low-pass filtering the outputs of the mixers are $E_0 = E_{10}(\xi) \cos(\omega_i t + \Psi) E_{Lo_o} \cos(\omega_{Lo} t)$ and $E_0' = E_{10}'(\xi) \cos(\omega_i' t - \Psi) E_{Lo_o}' \cos(\omega_{Lo}' t + \eta)$. Each of these voltages contains terms that oscillate with frequencies $\omega_i \pm \omega_{Lo}$ and $\omega_i' \pm \omega_{Lo}'$. The summing point will receive only the difference frequencies due to the low-pass filters in each mixer.

Some restrictions are now placed on the variables that are multiplied in the mixers. Let $\omega_i = \omega_i'$. If the source emits over a wide frequency range, these equations apply to each frequency in the bandwidth of the low-pass filters. Specifying $\omega_{Lo}' = \omega_{Lo} + \gamma$ provides a means of distinguishing the fringes from scintillations in the interplanetary medium. It has been shown, Dulk (1970), that these scintillations have

a power spectrum that contains very little power above a frequency of a few Hz. If γ is greater than this amount, then several fringes will pass during one phase fluctuation due to the interplanetary medium. It is convenient to let $E_{Lo_o} = E'_{Lo_o} = E_1$, and, since the individual antennas are steered, $E_{1_0}(0) = E'_{1_0}(0) = 1$.

The voltage at the summing point is given by $E = E_0 + E'_0 =$ $E_1\{\cos(\omega_i t + \Psi)\cos(\omega_{Lo} t) + \cos(\omega_{Lo} t + \gamma t + \eta)\cos(\omega_i t - \Psi)\}$. Upon using a trigonometric identity and the condition that $|\omega_i - \omega_{Lo}| >> \gamma$, the summing point voltage becomes $E = E_1\{\cos[(\omega_i - \omega_{Lo})t - \frac{\eta}{2}]$ $\cos(\Psi + \frac{\gamma t}{2} + \frac{\eta}{2})\}$. The power pattern, after smoothing on a $2\pi/(\omega_i - \omega_{Lo})$ time scale and normalizing, is $P_n(\xi,t,\eta) = \cos^2(\Psi + \frac{\gamma t}{2} + \frac{\eta}{2})$. The power pattern can be written as $P_n(\xi,t) = 1 + \cos(\theta + \gamma t)$, where $\theta = 2\Psi$ is the total phase difference due to path length caused by the separation of the antennas. The γ term gives temporal fringes if θ is held constant. The phase, η, does not depend on the source and can be chosen to be zero for convenience.

The observed flux density from a source is given by $S_0(\phi_0,t) = \int_{\text{source}} B(\phi)\, P_n(\phi_0 - \phi)\, d\phi$, where $B(\phi)$ is the true source brightness distribution, ϕ_0 is the hour angle of the main lobe of the interferometer power pattern, and ϕ is the hour angle of a point in the source. Using the previously calculated normalized power pattern, $P_n(\xi,t)$, the observed flux density becomes $S_0(\phi_0,t) = \int_{-\frac{\alpha}{2}}^{\frac{\alpha}{2}} B(\phi)\, d\phi + \int_{-\frac{\alpha}{2}}^{\frac{\alpha}{2}} B(\phi)\cos(\theta + \gamma t)\, d\phi$ where the angular width of the source is α and $\xi = \phi_0 - \phi$. The integral $S_0 = \int_{-\frac{\alpha}{2}}^{\frac{\alpha}{2}} B(\phi)\, d\phi$ is the total flux density from the source. If α is

small compared with the lobe spacing, the values of ϕ_0 for which the second integral has any appreciable size are limited to the region $|\phi - \phi_0| << \pi$. Under this condition θ becomes $\theta = 2\pi\, s_\lambda\, (\phi_0 - \phi)$.

The second integral takes the form $\int_{-\frac{\alpha}{2}}^{\frac{\alpha}{2}} B(\phi) \cos\, [2\pi\, (s_\lambda\, \phi_0 + \nu t)]$ $\cos\, (2\pi\, s_\lambda\, \phi)\, d\phi + \int_{-\frac{\alpha}{2}}^{\frac{\alpha}{2}} B(\phi) \sin\, [2\pi\, (s_\lambda\, \phi_0 + \nu t)] \sin\, (2\pi\, s_\lambda\, \phi)\, d\phi$, where $\gamma = 2\pi\nu$ and $s_\lambda = \frac{s+a}{\lambda}$. If $S_0\, (\phi_0, s_\lambda, t)$ is written as $S_0\, (\phi_0, s_\lambda, t) = S_0\, [1 + V\, (\phi_0, s_\lambda, t)]$, the visibility function can be identified as

$$V(\phi_0, s_\lambda, t) = \left(\frac{1}{S_0}\right) \{\cos\, [2\pi\, (s_\lambda\, \phi_0 + \nu t)] \int_{-\frac{\alpha}{2}}^{\frac{\alpha}{2}} B(\phi) \cos\, (2\pi\, s_\lambda\, \phi)\, d\phi +$$

$$\sin\, [2\pi\, (s_\lambda\, \phi_0 + \nu t)] \int_{-\frac{\alpha}{2}}^{\frac{\alpha}{2}} B(\phi) \sin\, (2\pi\, s_\lambda\, \phi)\, d\phi\}.$$

Let $V(\phi_0, s_\lambda, t)$ be written as

$$V(\phi_0, s_\lambda, t) = V_0\, (s_\lambda) \cos\, [2\pi\, (s_\lambda\, \phi_0 - s_\lambda\, \Delta\, \phi_0) + \gamma t]. \quad 1)$$

Figure II.1b is a graph of $S\, (\phi_0, s_\lambda, t)$ plotted against ϕ_0 in which the local oscillator offset, γ, is made to be zero.

It will be useful for later derivations to identify the following terms in an expansion of $V\, (\phi_0, s_\lambda, t)$ above (eq. 1):

$$V_0\, (s_\lambda) \cos\, (2\pi\, s_\lambda\, \Delta\, \phi_0) = \frac{1}{S_0} \int_{-\frac{\alpha}{2}}^{\frac{\alpha}{2}} B(\phi) \cos\, (2\pi\, s_\lambda\, \phi)\, d\phi$$

$$\rightarrow \left(\frac{1}{S_0}\right) F_{\cos}\, B(\phi) \qquad 2)$$

and

$$V_0 (s_\lambda) \sin (2\pi s_\lambda \Delta \phi_0) = \left(\frac{1}{S_0}\right) \int_{-\frac{\alpha}{2}}^{\frac{\alpha}{2}} B(\phi) \sin (2\pi s_\lambda \phi)\, d\phi$$

$$\rightarrow \left(\frac{1}{S_0}\right) F_{sin}\, B(\phi)\ , \qquad 3)$$

where F_{cos} and F_{sin} are the Fourier cosine and sine transforms of the brightness distribution $B(\phi)$. In order to make the identification of the transforms it is necessary to require that there are no other sources of appreciable strength in the antenna pattern.

If Equation 3) is multiplied by i and added to Equation 2), and the Fourier transform is taken, the following equation results:

$B(\phi_0) = S_0 \int_{-\infty}^{\infty} V_0 (s_\lambda)\, e^{-i2\pi s_\lambda (\phi_0 - \Delta\phi_0)}\, ds_\lambda$. If the visibility function's amplitude, $V_0 (s_\lambda)$, can be determined for all baseline lengths, the brightness distribution of the source can be reconstructed by an integration over the baseline. In the classical interferometer this quantity is determined by evaluating the equation $V_0 (s_\lambda) = \frac{S_{max} - S_{min}}{S_{max} + S_{min}}$ for many different baselines. A practical limitation on this method's use is that many measurements are required with increasingly longer baselines. In the case of a small source emitting at long wavelengths, as for Jupiter, the earth's diameter may form the limit on the integral. An added requirement was made when the Fourier transform took place. The source was required to be the only one in the antenna pattern. This is reasonably true of Jupiter. Subject to these conditions, the brightness distribution of the source can be determined from a knowledge of the visibility function, $V (\phi_0, s_\lambda, t)$.

It is possible to calculate $V(\phi_0, s_\lambda, t)$ by a method that is more easily realized on a digital computer. The technique uses the cross correlation function which is defined as

$$C(s_\lambda, \xi, t) = \frac{\overline{E_0(t)\, E_0'(t+\tau)}}{[\overline{E_0^2(t)}]^{\frac{1}{2}}\, [\overline{E_0'^2(t+\tau)}]^{\frac{1}{2}}}$$

where $E_0(t)$ is the voltage output, after low-pass filtering, of the first mixer and $E_0'(t+\tau)$ is that of the second mixer at time, τ, later (see Figure II.2a). The voltages are given by

$$E_0(t) = a \int_{-\frac{\alpha}{2}}^{\frac{\alpha}{2}} \sum_r a_r(\phi) \cos\left[\{\omega_r(\phi) - \omega_{Lo}\}\, t + \eta_r(\phi) + \Psi_r(\phi)\right] d\phi \text{ and}$$

$$E_0'(t+\tau) = b \int_{-\frac{\alpha}{2}}^{\frac{\alpha}{2}} \sum_\ell a_\ell(\phi') \cos\left[\{\omega_\ell(\phi') - \omega_{Lo}\}(t+\tau) + \eta_\ell(\phi') - \Psi_\ell(\phi')\right] d\phi',$$

where $a_\ell(\phi')$ and $a_r(\phi)$ are the amplitudes of the frequencies ω_ℓ and ω_r. The same restrictions as for the classical interferometer are added, i.e., $E_{Lo_0} = E'_{Lo_0}$ and $\omega'_{Lo} = \omega_{Lo} + \gamma$. The phases of each component frequency of the source are $\eta_r(\phi)$ and $\eta_\ell(\phi')$, and the initial relative phase of the local oscillators is ignored. It should be noticed that the amplitudes and phases of the ℓ and r components depend on positions in a random way. It is further required that $B(\phi) \alpha \sum_{\ell,r} a_r(\phi)\, a_\ell(\phi)$. The summation on ℓ and r is carried only over the frequencies passed by the low-pass

filters to the multiplier. The filters are assumed to have a flat response inside their passband with no response outside, and the bandwidth of each is much less than the center frequency.

The numerator of $C(s_\lambda, \xi, t)$ becomes $\overline{E_0(t)\, E_0'(t+\tau)} =$

$$\frac{ab}{T} \int_t \int_\phi \sum_r a_r(\phi) \cos[\omega_{ro}(\phi)\, t + \eta_r(\phi) + \Psi_r(\phi)]\, d\phi$$

$$\int_{\phi'} \sum_\ell a_\ell(\phi') \cos[\omega_{\ell 0}(\phi' + \gamma)(t+\tau) + \eta_\ell(\phi') - \Psi_\ell(\phi')]\, d\phi'\, dt$$

where $\omega_{ro}(\phi) = \omega_r(\phi) - \omega_{Lo}(\phi)$ and $\omega_{\ell 0}(\phi') = \omega_\ell(\phi') - \omega_{Lo}(\phi')$. The variable Ψ is defined as before, $\Psi = \pi s_\lambda (\phi_0 - \phi)$, where the small angle approximation has been made. The integration period T is taken as being long with respect to $2\pi/\omega_{ro}$ and short compared to $2\pi/\gamma$ and the fringe rate due to the source moving across the interferometer pattern. A diagram of the interferometer is given in Figure II.2a. Such a system is called a multiplying interferometer and has the varying part of the observed flux density as its output. By rearrangement of the integrations the voltage product becomes $\overline{E_0(t)\, E_0'(t+\tau)} = \int_\phi d\phi \frac{ab}{T} \int_t \int_{\phi'} \sum_{r,\ell} a_r(\phi)$

$\cos[\omega_{ro}(\phi)\, t + \eta_r(\phi) + \Psi_r(\phi)]\, a_\ell(\phi') \cos[(\omega_{\ell 0} + \gamma)(t+\tau) +$

$\eta_\ell(\phi') - \Psi_\ell(\phi')]\, d\phi' dt$. It is necessary to examine the behavior of the amplitudes and phase factors under the integrations over time and ϕ. The amplitudes and phases, $a(\phi)$ and $\eta(\phi)$, of the frequencies are random functions of position. This requires that the integration over ϕ' be zero except where $\phi' = \phi$. Also if the integration over time at any point is

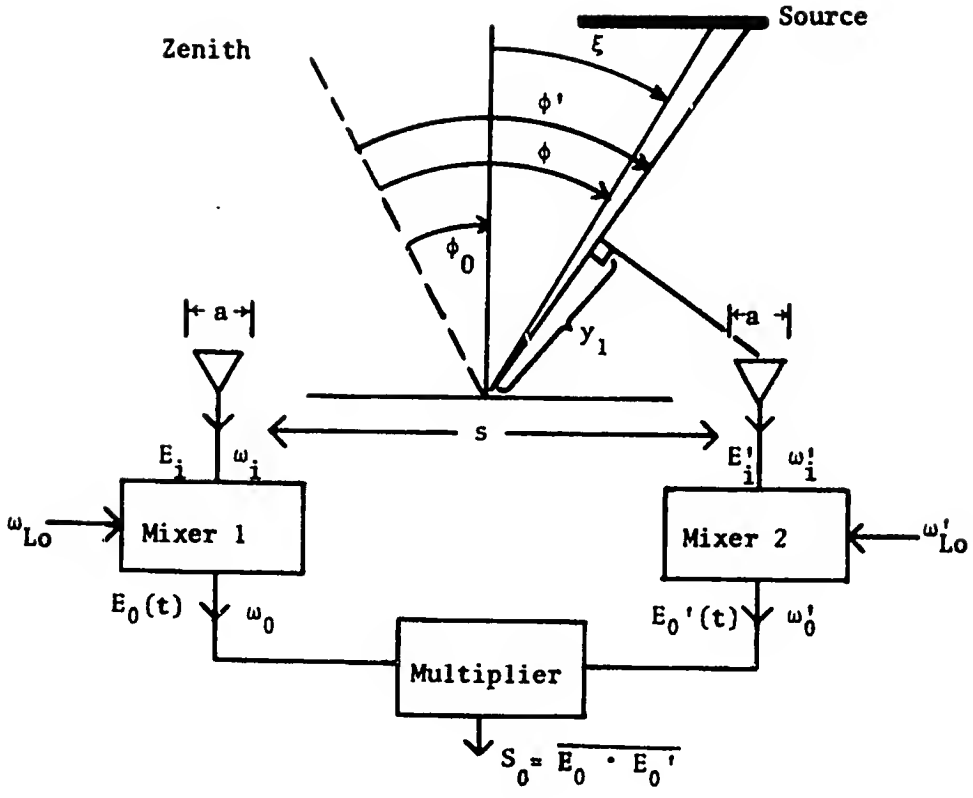

Figure II.2 -- (a) Diagram of the Multiplying Interferometer, (b) Graph of the Output S_0 as It Depends on γ (solid line) and on ϕ_0 (dashed line).

considered, the integral will be zero unless $\omega_{ro} - \omega_{\ell 0} < \frac{2\pi}{T}$. This is caused by the random relation of phases for two different frequencies and the integration time. If this term serves as the integrand for an integral over position, the result will be zero unless $\omega_{ro} = \omega_{\ell 0}$, which is again due to the random nature of the phases and amplitudes of different frequencies with position.

We are left with the product term having the form $\overline{E_0(t)\, E_0'(t+\tau)} = \frac{ab}{2} \int \sum_{r=\ell} a_r(\phi)\, a_\ell(\phi) \cos[\xi t + 2\Psi(\phi)]\, d\phi$, where the integration time is short compared to $2\pi/\gamma$ and to the time for the source to pass through one fringe. This is the same form as the varying component of the observed flux density as derived for the voltage adding interferometer.

The denominator of $C(s_\lambda, \xi, t)$ can be written as $[\overline{E_0^2(t)}]^{\frac{1}{2}} = \{\frac{a^2}{T} \int [\int\int \sum_{r,s} a_r(\phi)\, a_s(\phi') \cos[\omega_{ro} t + \eta_r(\phi) + \Psi_r] \cos [\omega_{so} t + \eta_s(\phi') + \Psi_s(\phi')]\, d\phi'\, d\phi]\, dt\}^{\frac{1}{2}}$, where the product of the spatial integrals has been replaced by the double integral over the position variables. By the arguments used in the previous part, $\phi' = \phi$ and $\omega_{ro} = \omega_{\ell 0}$ or the integral will be zero. Then $[\overline{E_0^2(t)}]^{\frac{1}{2}} = \{\int d\phi\, \frac{a^2}{T} \int \sum_{r=s} a_r(\phi)\, a_s(\phi) \cos^2[\omega_{ro} t + \eta_r(\phi) + \Psi_r(\phi)]\, dt\}^{\frac{1}{2}}$. After the time integration this becomes $[\overline{E_0^2(t)}]^{\frac{1}{2}} = \{\frac{a^2}{2} \int \sum_{r=s} a_r(\phi)\, a_s(\phi)\, d\phi\}^{\frac{1}{2}}$, where, upon substituting $B(\phi)$ for the sum on frequency, we recognize $[\overline{E_0^2(t)}]^{\frac{1}{2}} = \{\frac{a^2}{2} \int B(\phi)\, d\phi\}^{\frac{1}{2}}$ to be a $S_0^{\frac{1}{2}}/\sqrt{2}$. A similar term for the rms value of the second receiver's voltage is also demonstrable.

The cross correlation function can then be written as

$$C(s_\lambda,\xi,t) = \frac{\overline{E_0\ (t)\ E_0'\ (t+\tau)}}{[\overline{E_0^2\ (t)}]^{\frac{1}{2}}\ [\overline{E_0'^2\ (t+\tau)}]^{\frac{1}{2}}} = \frac{\frac{ab}{2}\ V(s_\lambda,\phi_0,t)S_0}{\frac{a}{\sqrt{2}}\ S_0^{\frac{1}{2}}\ \frac{b}{\sqrt{2}}\ S_0^{\frac{1}{2}}} =$$

$$\frac{S_0\ V_0\ (s_\lambda)\ \cos\ [\gamma t + 2\pi\ s_\lambda\ (\phi_0 - \Delta\phi_0)]}{S_0}\ .$$

It is then seen that the cross correlation function is just the fringe visibility. The amplitude of the fringes generated by plotting the cross correlation function against time is just $V_0\ (s_\lambda)$. The cross correlation function lends itself to being calculated with digitized data in the computer. Figure II.2b is a graph of the output of this form of interferometer plotted against time. The envelope represents fringes due to the motion of the source with respect to the interferometer fringes and the solid curve is the cross correlation function. The amplitude variations are due to the relative local oscillator offset and source motion.

II-2. The Intensity Interferometer

A new form of interferometer was proposed by R. Hanbury Brown and R. Q. Twiss (1954) that had the advantages of being operable over a very long baseline and of being relatively insensitive to phase distortions caused by electron density variations in the ionosphere. A diagram of the system is given in Figure II.3a. The Michelson (phase) interferometer is sensitive to phase shifts that occur to the signals before they

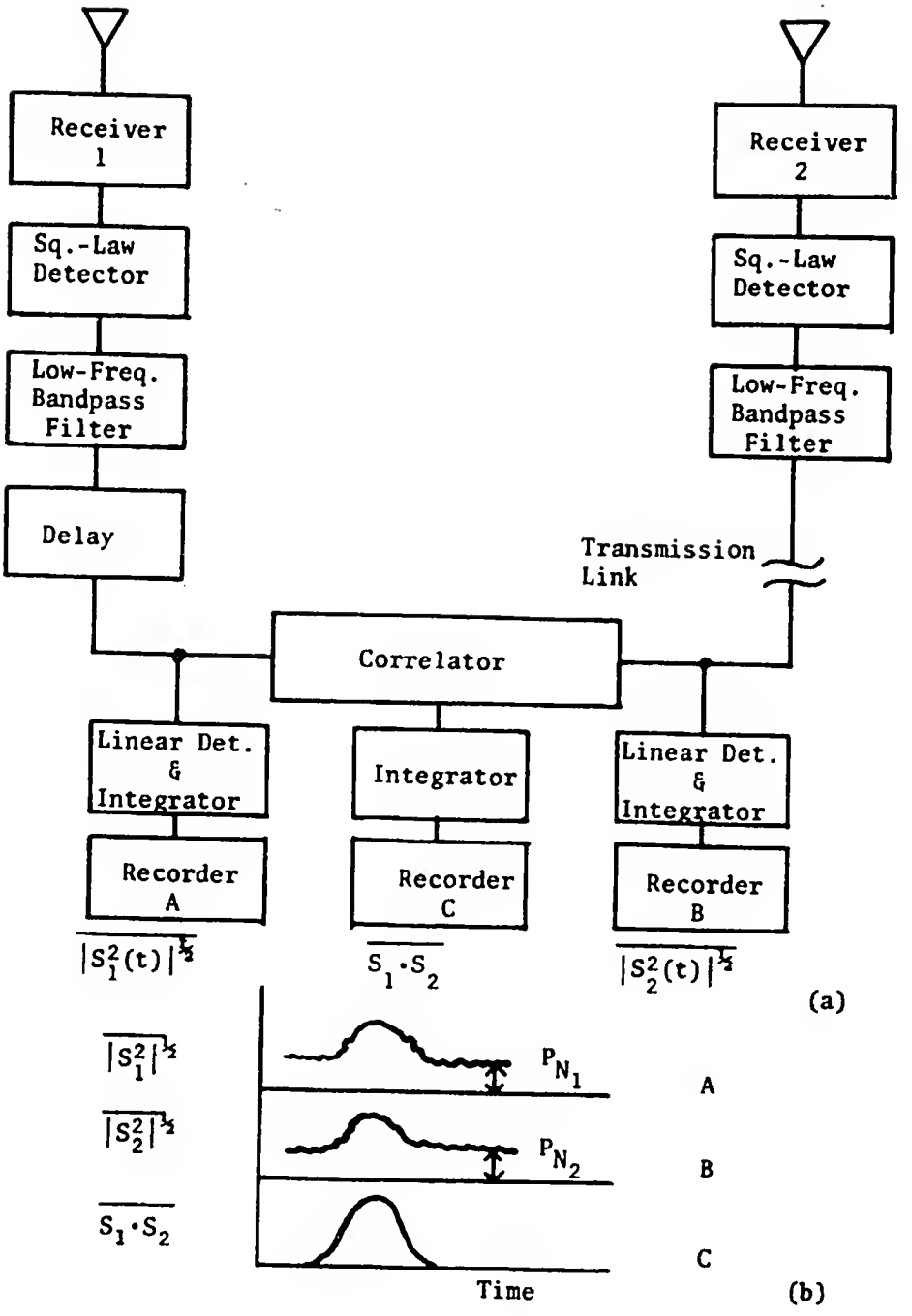

Figure II.3 -- (a) Diagram of the Brown and Twiss Post-Detection-Correlation Interferometer, (b) a Sample Record.

reach the summing point. The system described here is not as sensitive to this problem since the data sent from the remote station is square-law detected and filtered. This data undergoes two types of treatment at the time that interference is applied. Each signal is linearly detected, filtered and plotted on a chart recorder. A third channel is formed by multiplying the original signals, filtering and then plotting the product. A delay network is incorporated into one leg to compensate for the time delay, τ, caused by the data transmission link. The normalized correlator output c (ℓ,t) is given by the equation,

$$c\ (\ell,t) = \frac{\overline{S_1\ (t) \cdot S_2\ (t - \tau_0)}}{\{[\overline{S_1^{\,2}\ (t)}]^{\frac{1}{2}} - P_{N1}\}\{[\overline{S_2^{\,2}\ (t - \tau_0)}]^{\frac{1}{2}} - P_{N2}\}}$$, where the

numerator is the filtered multiplier output signal at a given time, t, and $[S_1{}^2]^{\frac{1}{2}}$ and $[S_2{}^2]^{\frac{1}{2}}$ are the values of the individual, linearly detected channels at the same time. P_{N1} and P_{N2} are the average values of the low-frequency filtered outputs observed when the source is outside the antenna beam. C (ℓ) is formed by averaging c (ℓ,t) over a number of passes of the source through the beam. The variable ℓ is the separation of the two antennas.

Brown and Twiss show, in the first part of their paper, that a term they call the correlation coefficient, $\rho\ (\ell)$, is given by

$$\rho\ (\ell) = \frac{[F_{cos}{}^2\ (s_\lambda) + F_{sin}{}^2\ (s_\lambda)]^{\frac{1}{2}}}{F_{cos}\ (0)}$$ for the Michelson interferometer.

It is seen that the numerator can be formed by referring to the square root of the sum of the squares of Equations 2) and 3) in the previous section. The denominator is just Equation 2) evaluated for a baseline

length of zero; in other words, the antennas are adjacent. This shows that the correlation coefficient of Brown and Twiss is just the amplitude of the fringe visibility function derived in the first section of this chapter. It was also shown at that time that the amplitude of the fringes generated by the cross correlation function was equal to the fringe amplitude of the visibility function.

They continue in their paper to show that c (ℓ,t) is given by

$$c\ (\ell,t) = \frac{F_{cos}^{\ 2}\ (s_\lambda) + F_{sin}^{\ 2}\ (s_\lambda)}{F_{cos}^{\ 2}\ (0)}$$, which is just the square of $\rho\ (\ell)$.

We will use such a method in the computer to determine the best time shift of the envelopes of bursts received at two different stations in order to determine relative arrival times. The integration period used in the averages of the functions is long compared with any time variation in the arguments of the voltages sent to the square-law detectors. Figure II.3b is a sample record of data taken as a source crosses the antenna pattern of the individual antennas.

II-3. The Formation of an Interferometer Using the Cross Correlation Function

A phase interferometer can be formed using data that is tape recorded at the antenna locations. The receivers must heterodyne the signal from the observing frequency, in this case 18 MHz, to a frequency compatible with the tape recorder. The data must be digitized and is then used in the equation for the cross correlation function

$$C(s_\lambda,\xi,t) = \frac{\overline{E_0(t)\,E_0'(t+\tau)}}{[\overline{E_0^2(t)}]^{\frac{1}{2}}\,[\overline{E_0^2(t+\tau)}]^{\frac{1}{2}}}$$. The form actually employed must, of course, perform the integrations discretely. The cross correlation function takes the form

$$C(s_\lambda,\xi,t) = \frac{\sum_{j=1}^{N} E_{0j}(t)\,E'_{0j}(t+\tau)}{\left[\sum_{j=1}^{N}(E_{0j}^2)\sum_{j=1}^{N}(E'^2_{0j})\right]^{\frac{1}{2}}}$$. The variable τ, is a time correction factor to account for any relative timing errors generated by such things as transmission time for timing signals, timing resolution, etc. The method involves the calculation of $C(s_\lambda,\xi,t)$ for many different values of τ, and the selection of the value of τ that maximizes the amplitude of $C(s_\lambda,\xi,t)$. Further description of the procedure follows in the next chapter.

A post-detection-correlation interferometer as introduced by Brown and Twiss is formed by first square-law detecting the heterodyned data on the magnetic tape. After smoothing, the envelopes are cross correlated. A value for the best relative shift of the envelopes is determined by finding that value of τ that maximizes the cross correlation function for a given region of integration. A comparison of the best shifts found for the two methods gives a means to detect the presence of a sweeping beam of Jupiter decametric radiation.

Occasionally a combination of circumstances can occur in which a segment of data that has been interfered is so short in time that the fringe does not reach maximum value. This makes the determination of the fringe amplitude difficult if not impossible. If the local oscillator

initial phase term had not been ignored in the development of the cross correlation function, $C(s_\lambda,\xi,t)$, a function of the form $C(s_\lambda,\xi,\eta,t) = V(s_\lambda,\xi,\eta,t)$, where η is the initial phase, would have resulted. Equation 1) in section II-1 would have the form $V(s_\lambda,\xi,\eta,t) = V_0(s_\lambda) \cos[2\pi s_\lambda(\phi_0 - \Delta\phi_0) + \eta + \gamma t]$. If the receiver at one station were arranged such that two equal local oscillator frequencies with phases shifted 90° were injected into two mixers, the signals from another station cross correlated with the first station would exhibit fringes with a 90° phase shift. The fringe amplitude $V_0(s_\lambda)$ could be obtained by taking the square root of the sum of the squares of the cross correlation function for each pair of signals. The derivation is given below:

$$V_{\text{1st pair}} = V_0(s_\lambda) \cos[2\pi s_\lambda(\phi_0 - \Delta\phi_0) + \eta_0 + \gamma t]$$

$$V_{\text{2nd pair}} = V_0(s_\lambda) \cos[2\pi s_\lambda(\phi_0 - \Delta\phi_0) + \eta_0 + 90° + \gamma t] =$$

$$V_0(s_\lambda) \sin[2\pi s_\lambda(\phi_0 - \Delta\phi_0) + \eta_0 + \gamma t]$$

$$[V^2_{\text{1st pair}} + V^2_{\text{2nd pair}}]^{\frac{1}{2}} = V_0(s_\lambda)[\cos^2\{2\pi s_\lambda(\phi_0 - \Delta\phi_0) + \eta_0 + \gamma t\} + \sin^2\{2\pi s_\lambda(\phi_0 - \Delta\phi_0) + \eta_0 + \gamma t\}]^{\frac{1}{2}}$$

therefore

$$V_0(s_\lambda) = [V^2_{\text{1st pair}}(\eta_0) + V^2_{\text{2nd pair}}(\eta_0 + 90°)]^{\frac{1}{2}} .$$

For a strip source with a Gaussian spatial distribution of radiators, Equation 2) can be used to calculate a set of values for the amplitude of the visibility function, $V_0(s_\lambda)$, if the source is symmetrical.

Since it has been shown that the cross correlation function and the fringe visibility function are equal, the experimental values of the amplitude of $C(s_\lambda,\xi,\eta,t)$ should lie on the curve representing the source. Figure II.4 is a graph of $V_0(s_\lambda)$ plotted versus baseline length for sources with angular widths of 0".1, 0".25, and 0".5 of arc. Values for the amplitude of the cross correlation function determined in later chapters will be compared with this graph to determine the size of the source. This graph is adapted from Dulk (1970).

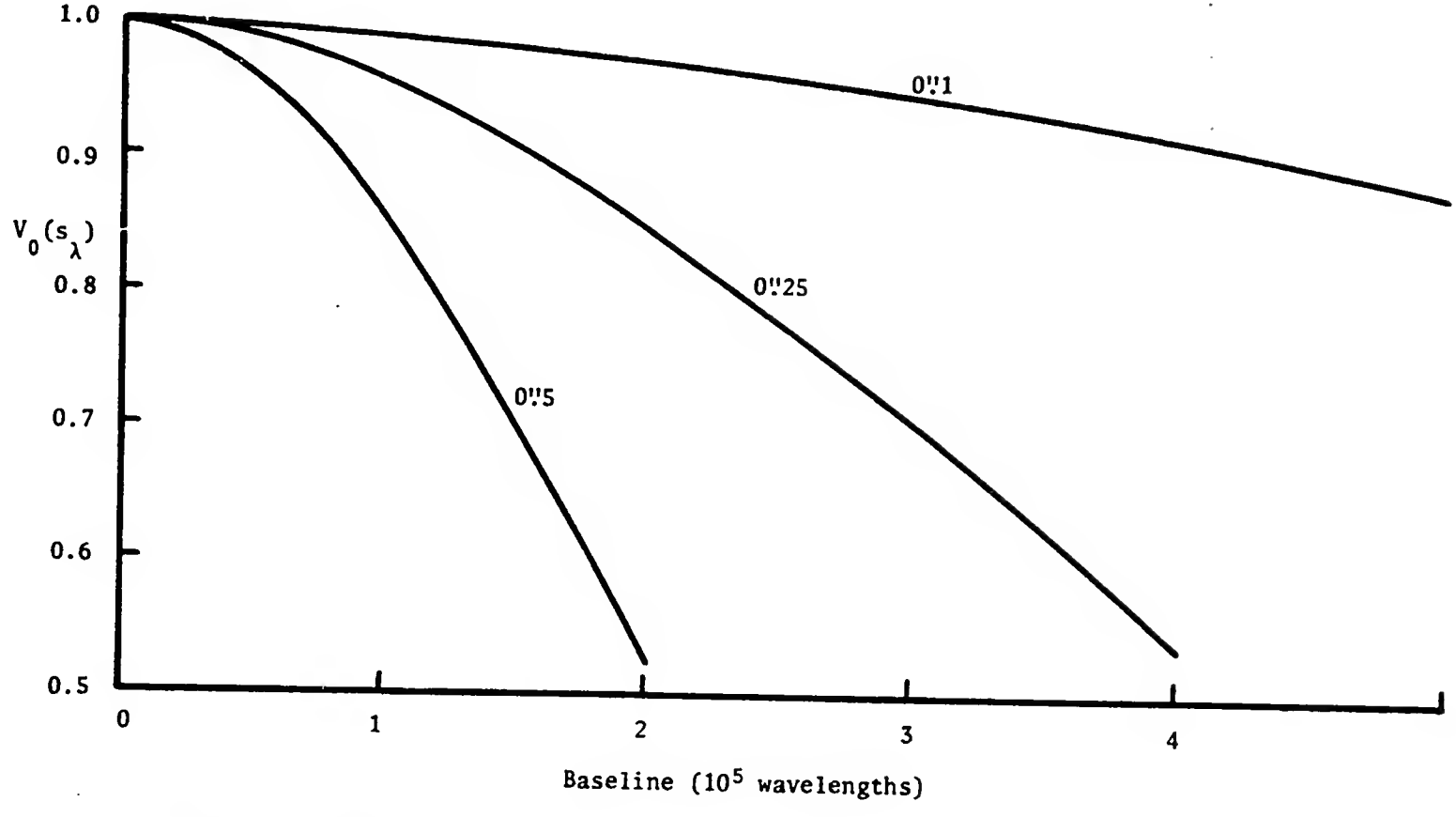

Figure II.4 -- Graph of $V_0(s_\lambda)$ Versus Baseline Length for a Gaussian Source of Various Angular Widths.

CHAPTER III

THE TAPE RECORDING INTERFEROMETER

III-1. The Signal Receiving Systems

In 1969 receiving systems as diagrammed in Figure III.1 were located at Western Kentucky University, University of Florida Radio Observatory, Florida Presbyterian College, and the Observatorio Radioastronomico de Maipu in Chile. At each station a steerable, linearly polarized Yagi antenna provided the Jupiter signal to a Collins 75S-1 communications receiver. The receiver used crystal-controlled local oscillators throughout and employed a mechanical filter to establish the overall bandpass of the receiver. The mechanical filter had a 455 kHz center frequency and a 2.1 kHz bandwidth. A 50-ohm resistor serving as a dummy load could be switched to the receiver input in place of the antenna. A WWV time standard receiver was operated concurrently with the system to provide real time synchronization of the composite time channel. A data channel multiplexer received the audio signals from the Collins and WWV receivers and placed them on one channel of a Magnecord stereo tape recorder. The multiplexer placed the Jupiter signal on the tape most of the time. WWV was keyed in for two seconds every minute for the double tick and for 20 seconds every five minutes for the voice announcement.

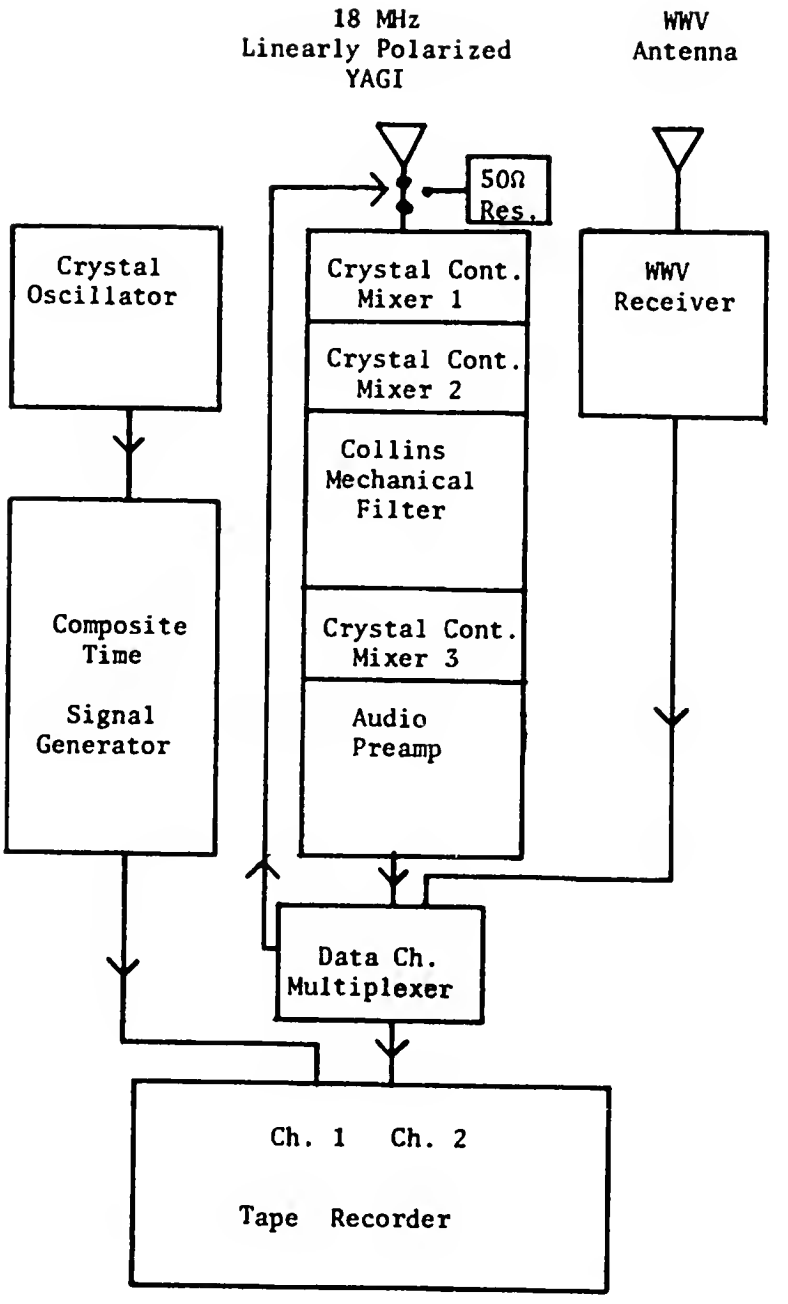

Figure III.1 -- Diagram of 1969 Receiving System.

Before the voice announcement the dummy load was keyed into the receiver input in place of the antenna for a few seconds at 5-minute intervals to serve as a system check. A crystal oscillator was used as the source of a stable frequency to drive a divider chain to provide the composite time signal. All stations had the one pulse-per-second and 60 pulses-per-second outputs. All but Western Kentucky University used the 960 pulses-per-second output. A 600 pulses-per-second output was used by WKU. The composite timing signal was formed by pulse-height coding the tick. The one-second pulse was tallest, followed by the 1/60th-second pulse with the 1/960th-second (or 1/600th) pulse the shortest. The pulses could be identified on a chart recording or oscilloscope by this means. The composite time signal was recorded on the other channel of the Magnecord tape recorder. Real time synchronization of the composite time signal was accomplished by comparing the time marks in one channel with the onset of the WWV tone or double ticks that were keyed into the other channel.

The processing of data from this system revealed two shortcomings. The local oscillators, although they were crystal controlled, were not stable enough. One could not predict the fringe rate generated by the local oscillator offset, γ, since this offset was, in itself, not predictable. The other shortcoming occurred when two stations were interfered at a time when their fringe was passing through zero, or was a value other than a maximum. If the fringe could not be reconstructed for a long enough time to show the peak, then the amplitude of the fringe could not be determined. The data processed for this dissertation from 1969 fortunately had a duration longer than one fringe cycle.

A receiving system was designed for the 1970 Jupiter season to overcome these shortcomings. Figure III.2 is a block diagram of the system operated at the University of Florida Radio Observatory. A very stable crystal in a double oven was used as the source of all frequencies employed in the system. The composite time signal was produced as in the 1969 system, except the frequencies were changed to 1 pulse per second, 50 pulses per second and 1000 pulses per second. The time signal was recorded continuously on one channel of a four-channel Viking tape recorder. The 1.8 MHz crystal standard also drove a frequency synthesizer that provided the local oscillator injections to the receiver. The first and second local oscillator frequencies were produced by a combination of multiplying and dividing. The second local oscillator frequency was switch selectable between 3.15 MHz and 4.05 MHz to provide a means of tuning the receiver off of an interfering station. The product detector local oscillator input was produced by dividing and phase shifting. Two product detectors were sent the signal from the receiver I.F. stage. Their local oscillator inputs were the same frequency, 450 kHz, but one was phase shifted 90° with respect to the other. The interference of both of the product detector outputs with another station allows the reconstruction of the fringe amplitude without having either combination actually reach a fringe peak. The receiver was designed around a Collins mechanical filter of the type used in the earlier system. Two different bandwidths were used, 2.1 kHz and 6 kHz, at the center frequency of 455 kHz. The R.F. preamp and mixers were made using dual-gate, metal-oxide-silicon-field-effect transistors (MOSFET). They provide a much wider dynamic range and superior resistance to cross modulation due to adjacent channel interference. A frequency conversion scheme for two different I.F.

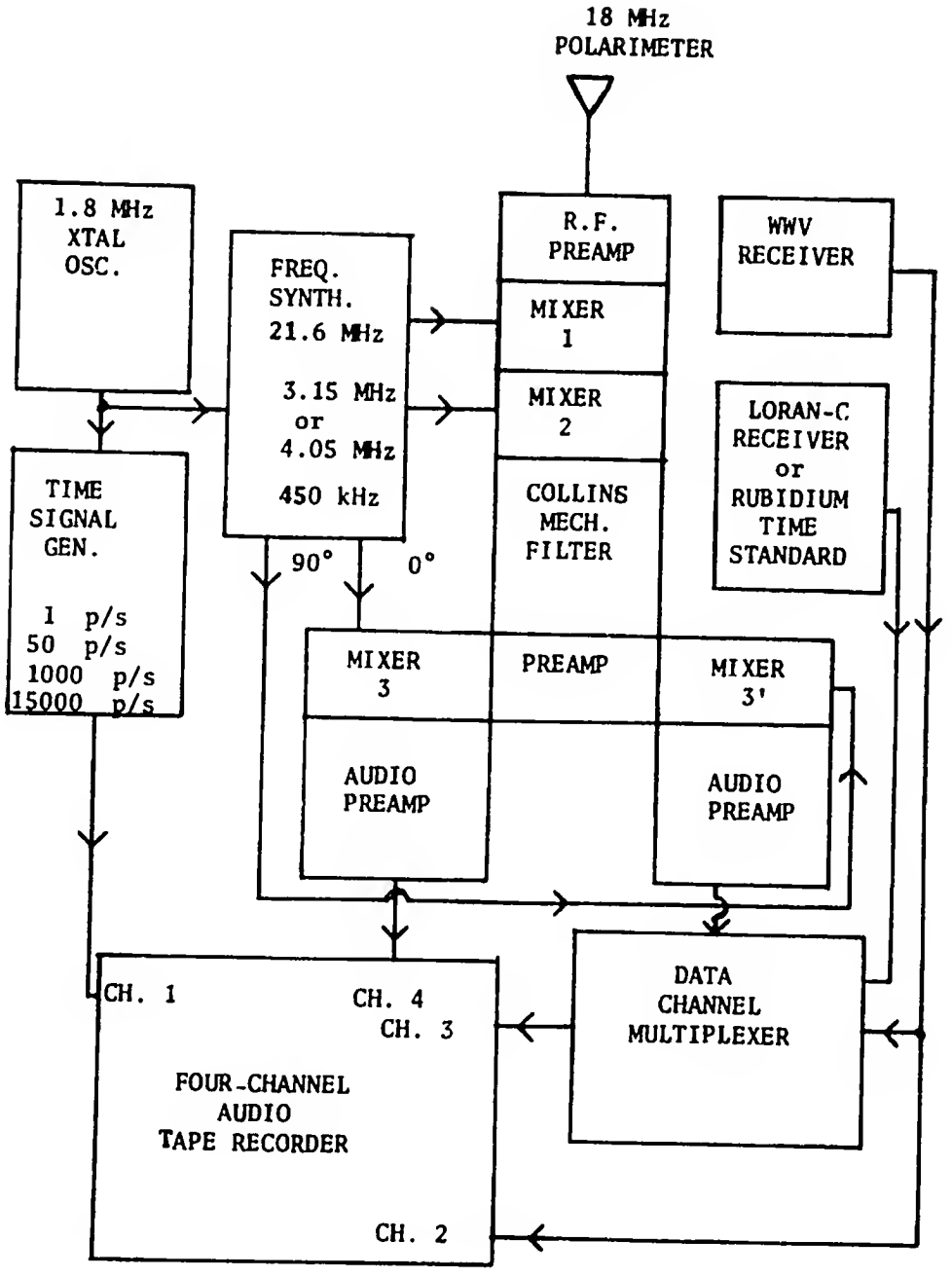

Figure III.2 -- Diagram of 1970 Receiving System.

bandwidths is shown in Figure III.3. A detailed block diagram of the system is shown in Figure III.4. The receiver located at the other station in the network (Maipu, Chile) had a single product detector; otherwise the system was identical.

The real time synchronization for stations in the United States used signals from WWV and LORAN-C. The data multiplexer keyed WWV into the data channel every minute for the double tick and every five minutes for the voice announcement. This was followed by LORAN-C for two seconds to provide as accurate timing as possible. The VLF transmission time from the station is very stable and predictable for ground wave. Information concerning the transmission time delay for WWV time signals came from Application Note 52 by the Hewlett-Packard Company (1965). Information pertaining to the VLF network of LORAN-C came from papers by L. D. Shapiro (1968a and 1968b). The inputs to the four-channel Viking tape recorder consist of: channel 1 - composite time signal; channel 2 - continuous WWV; channel 3 - multiplexed data and time signals; channel 4 - data.

Since it is difficult to receive any of the LORAN-C networks in Chile, they were provided with a rubidium frequency standard on loan from NRAO. The 1 MHz output was divided down to 1 pulse per second and compared with NBS time at the NASA satellite tracking station near Santiago, Chile. The atomic standard was carried while still running to the Jupiter observatory at Maipu, Chile, to calibrate the local standard and to be keyed into the data channel every minute instead of the WWV double tick. The WWV voice announcement was keyed in every five minutes as at the University of Florida station.

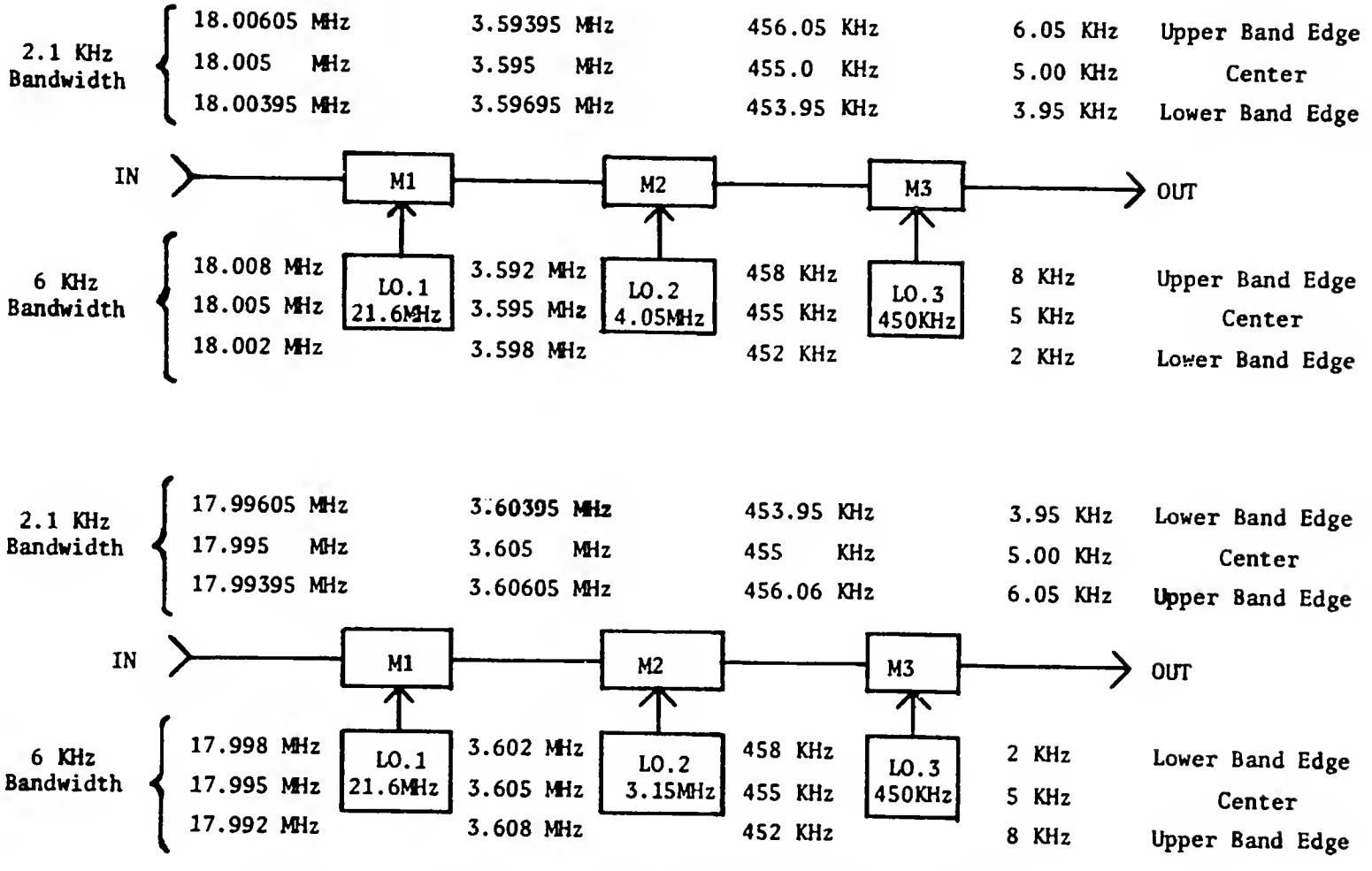

Figure III.3 -- Diagram Showing Frequency Conversion Scheme Used in 1970 Receiving System.

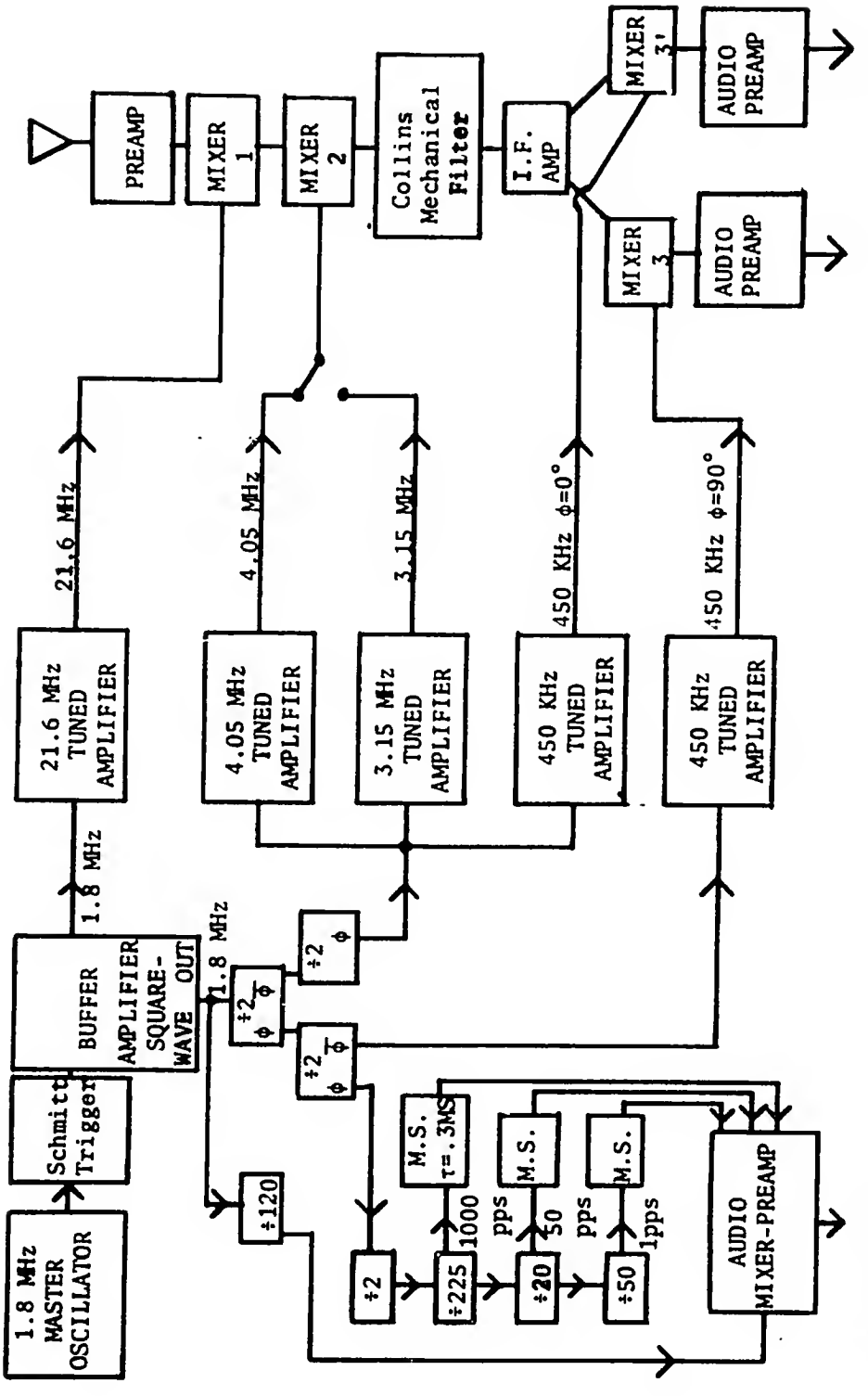

Figure III.4 -- Diagram of Details of 1970 Receiving System.

The antenna system at Chile consisted of a polarimeter that was used near the meridian and a steerable Yagi for sources away from the meridian. The 1970 data processed here uses the linearly polarized Yagi. The Florida antenna was a manually steerable polarimeter or, on the night when the data was recorded, a linearly polarized Yagi.

The network has since been enlarged to include stations at Western Kentucky University (a single product detector model) and San Antonio, Texas. All recording in the network in 1971 was done using right hand circular polarization except at WKU (linear).

III-2. The Treatment of the Data on the Computer

Interference fringes are formed for various pairs of stations by calculating the cross correlation function for a given integration period as a function of time. In order to use the computer to aid in the calculations, it was necessary to present the data to it in a digital form.

The data tapes were digitized using an analog-to-digital converter as a data source for an IBM 1800 computer. Two forms of the digitization program were used. The 1969 data was digitized by passing a burst, that had been located earlier, to the digitizer using the original magnetic tape. The operator, listening with ear phones to the time channel, counted from a known starting time (usually the WWV minute mark) to the second tick before the second tick that preceded the part to be digitized. He pushed the START button on the computer, which searched for the next second mark. Upon finding this mark, it waited for a length of time given to it on a data card. After the wait, the computer

began digitizing until it filled a data array which was allotted 3520 words. The time channel was digitized by alternate samples with the data channel and stored in a similar array. Both arrays were transferred to a disk and plotted on an incremental plotter. Figure III.5 shows a composite plot of the digitized data and time channels and an expanded plot of the data channel for Chile. The time channel is digitized to allow the exact time interval of digitization to be determined. By careful comparison with the chart recordings of the raw data the exact starting and ending times of the digitization period can be determined.

The data from 1970 was handled a bit differently. The Computer Sciences Division of the University of Florida Medical Center, where the previous work had been done, had produced a general purpose digitization program that would digitize up to 509,440 words of data at speeds in excess of 7 000 data points per second per channel. After the data was discovered, from the search of chart records, it was slowed down by a factor of eight-to-one and presented to the machine. Approximately six seconds of data were digitized, with points being taken alternately from the data channel and time channel. The tape had been started by the operator and digitization begun immediately. A program called LOOK was provided that searched the data for the addresses of the bursts and the second ticks. The interesting bursts, which were previously seen on chart records, were then located and transferred with a program called TRNFR to another disk for storage and plotting on the incremental plotter. The method used was theoretically easier than that used the previous year, but tape recorder instabilities complicated the efforts.

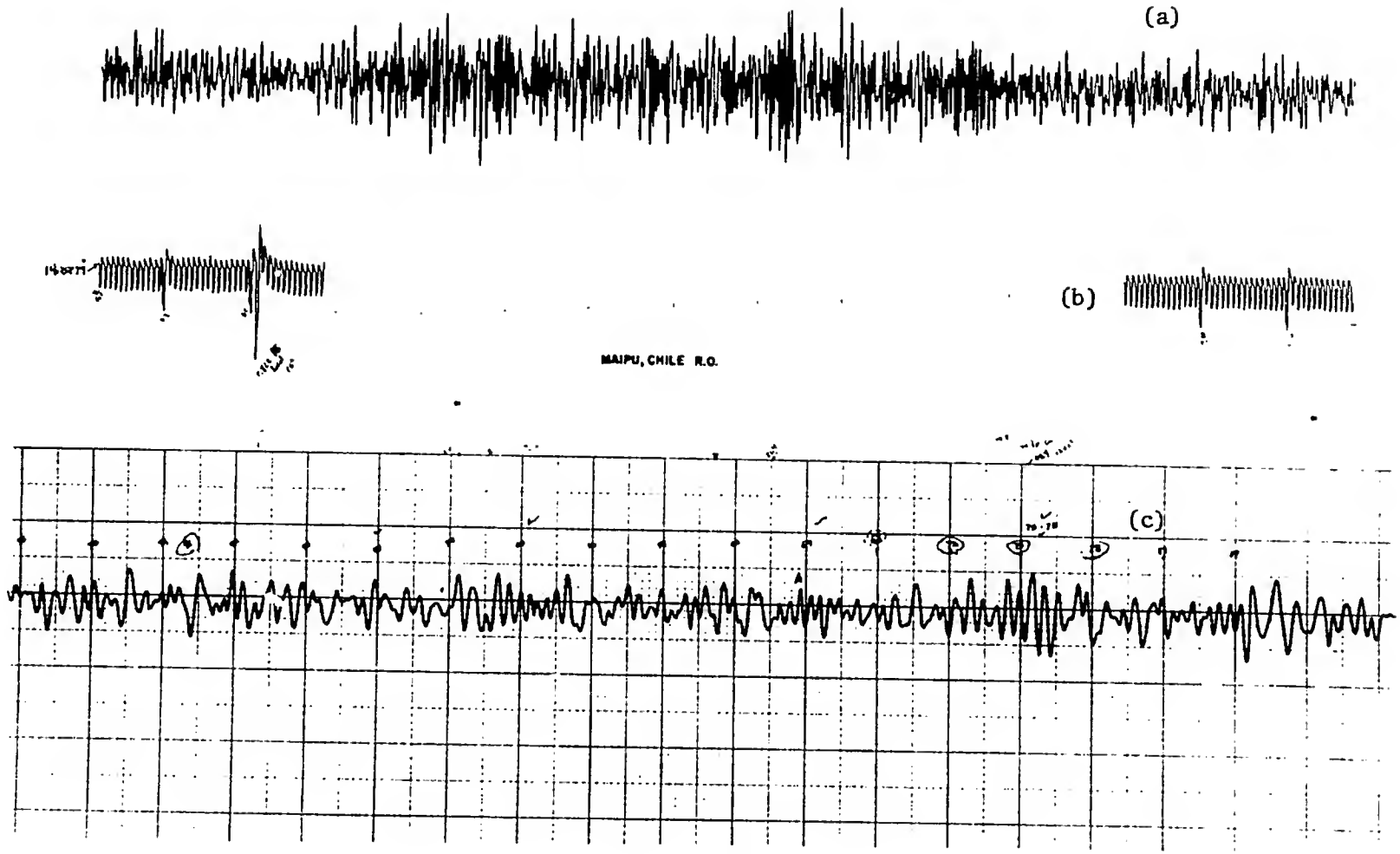

Figure III.5 -- (a) Computer Plotted Data of Entire Burst as Received at MAIPU.
(b) Portion of Time Channel Digitized Simultaneously with Data in (a).
(c) Computer Plotted Expanded Portion of the Center of the Burst in (a).

Data was transferred from the IBM 1800 on cards. The remainder of the data processing was done on an IBM 360/65. The 1970 data was transferred in a column binary format in order to require the punching of fewer cards by the IBM 1800. An Assembler program was written to convert the column binary information on the cards to files on a tape that could be read by a FORTRAN program such as CROCO, which is described later.

In order for interference to be achieved properly, the two tapes from a pair of stations must present data to the multiplier at the same rate in real time. Tape stretch and other inconsistencies made some correction in the digitized data necessary. A program called BADE was written by the author to adjust the number of data points in a table to represent the same real time period and to move the zero value of the data to the average value for the table. The program also adjusted each data table to begin at the same point in real time by correcting for time signal transmission time and errors in the starting time of digitization. In 1969 a data table of 2240 data points was prepared by BADE such that the first point in each table occurred at the same time. This left an error due to the geometrical path length differences for the Jupiter signal and some residual timing errors, since WWV was the prime source of real time that year.

Two programs were written by the author to prepare data for the intensity interferometer mode and the envelope correlation experiment. The program, BASQ, square-law detected the data in each of the data tables prepared by BADE and integrated it over 20 data points. The integration period was sufficient to remove the audio and leave the slowly

time-varying envelope. A post-detection-correlation interferometer of the Brown and Twiss type was formed with this data. The other program, BABS, took the absolute value of the BADE data, integrated over 20 data points, and adjusted the baseline of the data to the average. It played the part of a full-wave, linear detector with integrator, followed by a coupling capacitor. BABS provided the data to examine the relative arrival times of the fine structure in an L-Burst.

The program, called CROCO, was the main analysis tool used on the data. Its purpose was to calculate the cross correlation function, $C(s_\lambda,\xi,\eta,t)$. It was written by the author to be very flexible in its choice of integration times, number of values of C calculated for a data table, and where (in a data table) it started and ended calculations of C. CROCO performs the calculation of the cross correlation function,

$$C_{ITAU}(s_\lambda,\xi,\eta,t) = \frac{\sum_{j=1}^{N} E_{0\,j}\, E'_{0\,j+ITAU}}{\left[\sum_{j=1}^{N} E_{0\,j}^{2} \sum_{j=1}^{N} E'^{2}_{0\,j+ITAU}\right]^{1/2}}, \qquad 4)$$

in two parts. The numerator is formed by summing the product $E_{0\,j}$ $E'_{0\,j+ITAU}$ over N values of j, where N is the selected integration time and ITAU is the initial shift of the two data tables with respect to each other. The denominator is formed by computing the sum of the square of $E_{0\,j}$ and the sum of the square of $E'_{0\,j+ITAU}$. The two sums are multiplied together and the square root is taken. The cross

correlation function is formed and given the name PXC(J), an element of an array. The denominator is saved and stored as PNM. The program steps LDELT data points further into the data tables and calculates another value for C and the denominator. After calculating three values of C, a line of print is generated. The line of print consists of the denominator (PNM), three values of C (XCOR1, XCOR2, XCOR3) and the line number. In addition, the program assigns an asterisk to one of the 100 remaining spaces in the line at a position that is proportional to the value of the first C calculated. Since C ranges from -1 to +1, each space represents a change in C of .02. The process is repeated until the index for the selection of the data points to be multiplied reaches NDPS, which is the number of data points in each table. The program increments the relative shift variable K by KDELT and repeats the calculation. When K has the value JTAU, the program will repeat the cycle once more and stop.

Some essential quantities which must be provided by the user are the following:

1. IDATE(1), IDATE(2), AND IDATE(3) are the numbers of the month, day and year, respectively, e.g., 1, 2, 69, on which the burst occurred.

2. IFIL1 and IFIL2 are used to denote the portion of an input array in which data from each station has been placed. The initial array usually must be changed for different batches of data.

3. JHOUR and XSEC are the hour and second at which the burst of interest occurred.

4. ITAU and JTAU are the beginning and ending relative shifts. They are calculated by the formulas ITAU = (initial time shift) x (digitization rate) and JTAU = (final time shift) x (digitization rate).

If the two shifts are on the same side of zero-relative-shift, ITAU is given a negative sign.

5. N is the integration time in data points. N = (integration time) x (digitization rate).

6. KDELT is the increment of shifting in data points.

7. LDELT is the increment of stepping through the data tables.

8. DPS is the digitization rate in data points per second.

9. NDPS is the number of data points in each data table. All tables are assumed to contain the same number of data points.

The program is run on data from a pair of stations for a given range of relative shifts. The best shift is selected by noting the shift that makes the fringes have the greatest amplitude and have the smoothest curve.

A modification of CROCO was made that incorporated statements to control an incremental plotter. CROCOCAL produced the graphs of the fringes shown in a number of the figures. It was hoped that it would be inexpensive enough to use as an analytic tool in place of CROCO, since the smoothness of the curves is much easier to see. Unfortunately, it turned out to be anything but inexpensive. A listing of a combination version of BADE and BASQ is included in the Appendix, followed by a listing of CROCO.

A refinement in the method of setting the digitization rate was added during the processing of the 1970 data. An integrated circuit phase-lock detector made by Signetics (NE 565) was used to lock an oscillator to the 15 KHz tone that had been placed on the time channel. Since the tone had been derived from the crystal-frequency standard, it remained in phase with the timing marks on this channel. The analog-to-digital converter in the IBM 1800 Data Acquisition System was driven

from the synchronized oscillator. The synchronization of the converter eliminates any change in the effective digitization rate due to changes in tape speed (caused either by differences in tape recorder speeds or wow and flutter in a given tape recorder). The time channel of the digitized data was printed by the IBM 1800 in such a form as to make detection of any loss of coherence between the timing channel and the phase-locked oscillator obvious. For further checking the data channel was plotted on the incremental plotter. The data was punched on cards in a column binary format for transportation to the IBM 360 for use in CROCO.

CHAPTER IV

AN ANALYSIS OF THE DATA RECEIVED IN 1969

IV-1. Spatial Orientation of the Receiving System

The Jovian decametric burst that is analyzed in this chapter was received on the morning of 2 January 1969 at $08^h22^m14^s$ UT by the four stations that were members of the interferometer network that year. The stations were located at Bowling Green, Kentucky (lat. 36°57' N, long. 86°25' W), Old Town, Florida (lat. 29°31'50" N, long, 82°1' 55" W), St. Petersburg, Florida (lat. 27°45'45" N, long. 82°38' W), and Maipu, Chile (lat. 33°23'50" S, long. 60°42'12" W). The primary timing source was the National Bureau of Standards radio station WWV, located in Boulder, Colorado (lat. 40°40'48" N, long. 105°2'25" W), as shown in Figure IV.1. The local one-second ticks were delayed by approximately one second from the one-second tick transmitted by WWV due to the transmission time delay and the manual method used for aligning the local tick with that from WWV. The total delays for the stations were 1.0016 seconds for Bowling Green, 0.4202 seconds for Old Town, 0.8917 seconds for St. Petersburg, and 0.2555 seconds for Maipu. The actual transmission delay from WWV ranged from 6.1 milliseconds for Bowling Green to about 33 milliseconds for Maipu. The latter

Figure IV.1 -- Western Hemisphere Map Showing the Locations of the Receiving Stations and WWV. MAIPU Is near Santiago, Chile.

time is uncertain by at least 2 milliseconds since it is not known, a priori, how many hops were required for transmitting the timing signal that was received at Maipu.

Figure IV.2a shows the arrangement of the earth, Jupiter, and the sun on 2 January 1969 as seen from the North Pole of the ecliptic. The right ascension of Jupiter was $12^h22^m19^s.2$ and its declination was -0°59'28". The right ascension of the sun on that date was approximately 18^h41^m or 280° east of the Vernal Equinox. The North Pole of the earth is pointing to the right as the observer looks along the line-of-sight from the earth to Jupiter, since this is the northern hemisphere winter.

The receiving stations will be referred to by the initials of the university radio observatory that operated them. They were Western Kentucky University (WKU) at Bowling Green, University of Florida Radio Observatory (UFRO) at Old Town, Florida Presbyterian College (FPC) at St. Petersburg, and Observatorio Radioastronomico de Maipu of the Universidad de Chile (MAIPU) at Maipu, Chile. Table IV.1 gives the baseline lengths of pairs of these stations for the baselines projected

Table IV.1

Station Pair	D_{EW} (km)	D_{NS} (km)	D (km)
UFRO - FPC	83.1	166	185.8
WKU - UFRO	44.7	697	698
WKU - FPC	89.6	896	905
FPC - MAIPU	2000	6520	6820
UFRO - MAIPU	1913	6690	6980
WKU - MAIPU	1875	7380	7620

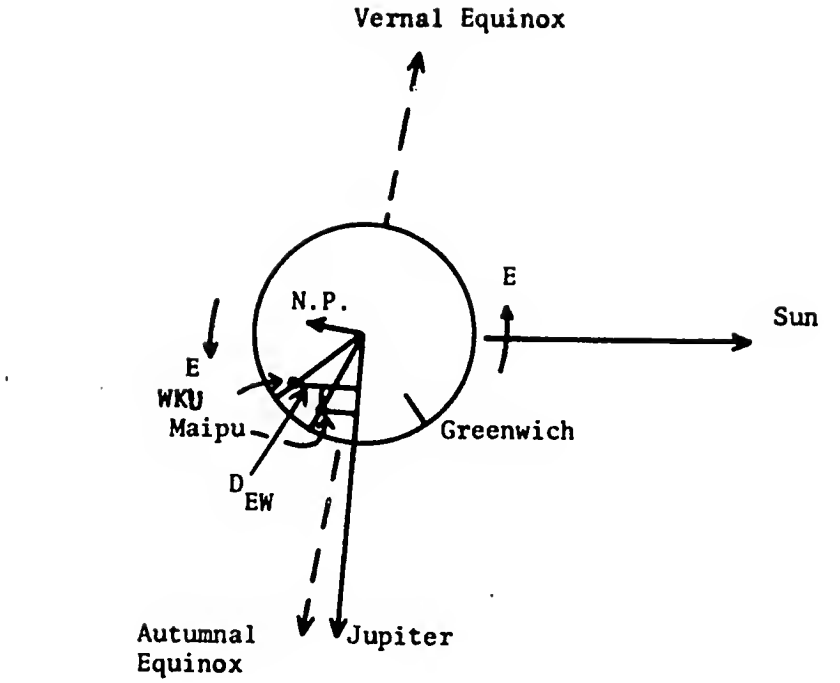

(a)

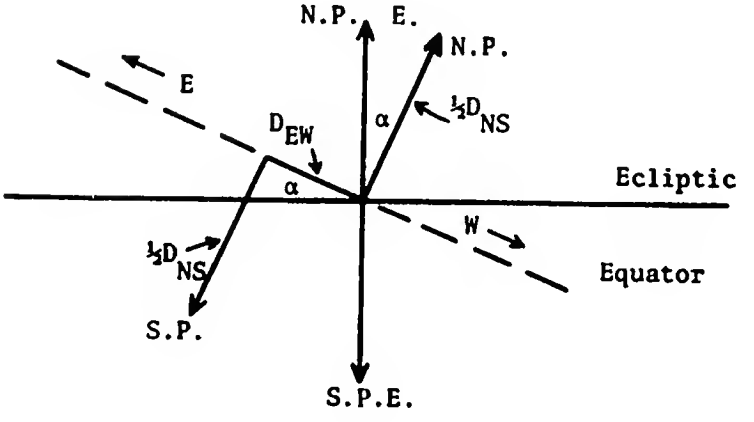

(b)

Figure IV.2 -- (a) View of Earth, Jupiter and the Sun from Above the North Pole on 2 January 1969, (b) D_{NS} and D_{EW} Projected on the Plane Perpendicular to the Line-of-Sight to Jupiter.

on a plane perpendicular to the line-of-sight to Jupiter from the earth. The variable D_{EW} is the length of the baseline projected on a line that is parallel to the equatorial plane and is perpendicular to the line-of-sight. The variable D_{NS} is the length of the baseline projected on a line parallel to the north-south axis of the earth and perpendicular to the line-of-sight to Jupiter. The variable D is the total baseline projected on a plane perpendicular to the line-of-sight to Jupiter. The effective baseline lengths, measured in wavelengths of the 18 MHz received signal of the various interferometers formed by all pairs of stations, range from 11,150 to 456,000.

For the experiment involving the effect of the solar wind on the envelope of the L-Burst (as proposed by Douglas and Smith), it is necessary to know the effective length of the baseline as projected on the plane of the ecliptic. It is the interaction of the solar wind with the radiation travelling from Jupiter along the line-of-sight, which lies in the ecliptic plane, that is proposed to be the cause of the shape of the L-Burst envelope. Figure IV.2b shows the appearance of the WKU - MAIPU baseline components D_{NS} and D_{EW} as seen by an observer at the center of the earth looking toward Jupiter. The direction sense for east and west is that used by an observer at the location of the stations, i.e., on the side of the earth toward Jupiter in Figure IV.2a. The angle, α, is the projection of the polar angle of the earth ($23\frac{1}{2}^\circ$) on the plane perpendicular to the line-of-sight to Jupiter. Its value is given by $\tan \alpha = \tan 23\frac{1}{2}^\circ \cos (RA_J - 180^\circ)$, where RA_J is the right ascension of Jupiter in degrees. On 2 January 1969 the right ascension of Jupiter was $185^\circ.5$. The value of α was then $23^\circ.4$. The east-west baseline, B_{EW}, as projected on the plane of the ecliptic,

is given by $B_{EW} = D_{NS} \sin \alpha + D_{EW} \cos \alpha$ for the orientation shown in Figure IV.2b.

IV-2. The Nature of the Received Signal

According to a classification of Jovian noise storm activity given by Douglas and Smith (1967) and attributed to Gallet, a burst with a duration of from 0.1 second to 5 seconds is an L-Burst. Inspection of Figures IV.3 and IV.11 will reveal that the burst under study here is about 0.130 seconds long; hence, by strict application of the classification scheme, it is technically an L-Burst. Recall that the largest time marks that are visible in the figures occur at 1/60th second intervals. This burst will henceforth be referred to as an L-Burst, even though an added requirement for a burst to be so classified will be shown as a result of the analysis in this chapter.

As can be seen in Figure IV.3, the signals, as received at the several stations, were not all of the same strength. An important requirement for the use of the signals in the interferometer is their signal-to-noise ratio. This number is gotten by comparing the voltage ratio of the peaks of the burst with the peaks of the noise outside of the burst. Expressed in decibels, the (S+N)/N ratios are the following: WKU - 14 db, FPC - 9.5 db, MAIPU - 9 db, and UFRO - 6 db. The signal-to-noise ratio for UFRO is too low to make the fringes detectable. Another factor in the form of the relative frequency effect of the local oscillator at UFRO made the fringes almost indistinguishable from other noise effects. This required the exclusion of the UFRO data from the calculations of the cross correlation function.

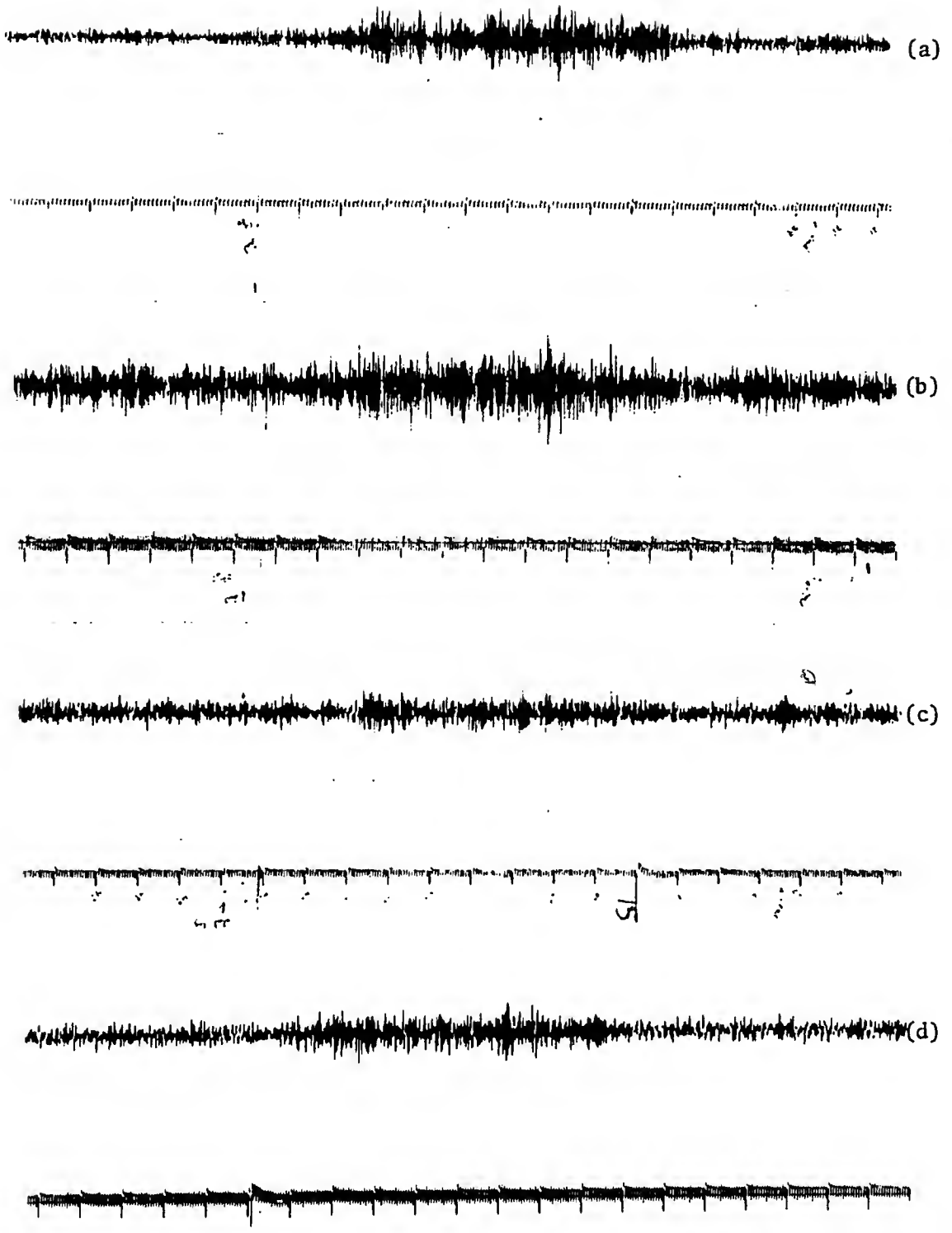

Figure IV.3 -- Actual Chart Records of the Heterodyned Data from WKU (a), FPC (b), UFRO (c) and MAIPU (d) for the L-Burst of 2 January 1969. Alternate Lines Are the Timing Channels for the Corresponding Stations.

IV-3. Measurement of the Size of the Source of Jovian Decametric Radiation

It was shown in Chapter II that the brightness distribution of a source could be calculated from the fringe visibility function $V_0(s_\lambda)$ by the following equation: $B(\phi_0) = S_0 \int_{-\infty}^{\infty} V_0(s_\lambda) e^{-i2\pi s_\lambda(\phi_0 - \Delta\phi_0)} ds_\lambda$. In that chapter it was also shown that the visibility function was equal to the amplitude of the cross correlation function, $C(s_\lambda, \xi, t)$. Therefore, in order to find the angular width (i.e., twice the value of ϕ_0 for which $B(\phi_0)$ is just zero) of the source, one must calculate the cross correlation function for the best relative shift of the data from all pairs of stations. The best relative shift is determined by the relative shift, τ, in Equation 4) in Chapter III that maximizes the amplitude of the curve of the cross correlation function plotted against time. The reason τ was introduced was to make allowance for the relative inaccuracy of the knowledge of real time at each of the stations (due to real time being received from WWV) and for the difference in path length that the signal from Jupiter had to travel to the various stations.

The program CROCO was used on the heterodyned data, which had previously been adjusted in time and length by the program BADE, to calculate and make a plot of the cross correlation function as a function of time. The plot was in the form of a series of asterisks on the computer printout, as is described in Chapter III. After the best shift was discovered, the program CROCOCAL plotted the curves that are shown in Figures IV.4, IV.5, and IV.6. The individual figures are composites of three pages of plotting of the output of CROCOCAL done on a

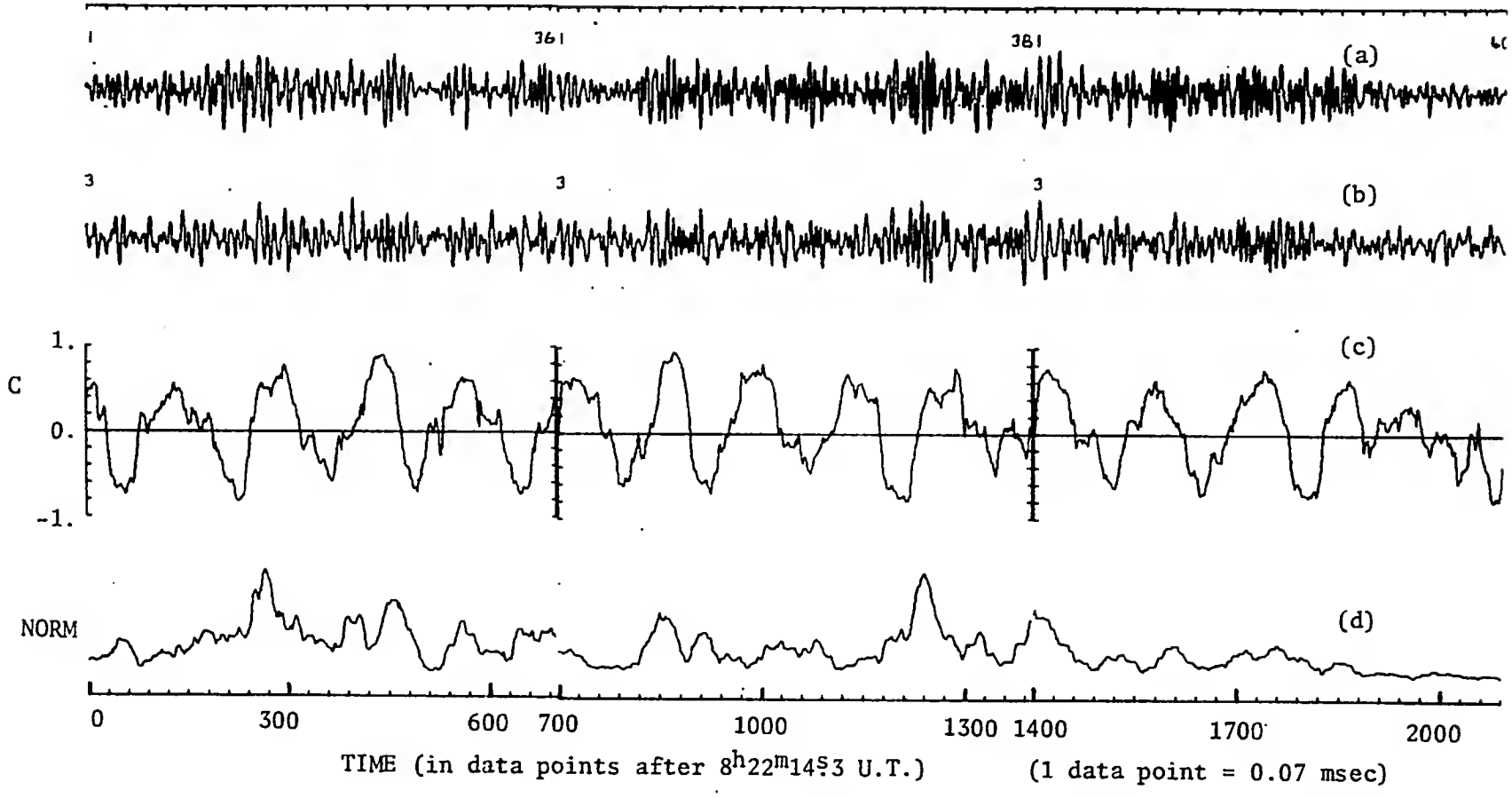

Figure IV.4 -- Plot of Heterodyned Data from WKU (a) and MAIPU (b). Plot of Cross Correlation Function (c) and Normalization (d) Versus Time for L-Burst of 2 January 1969.

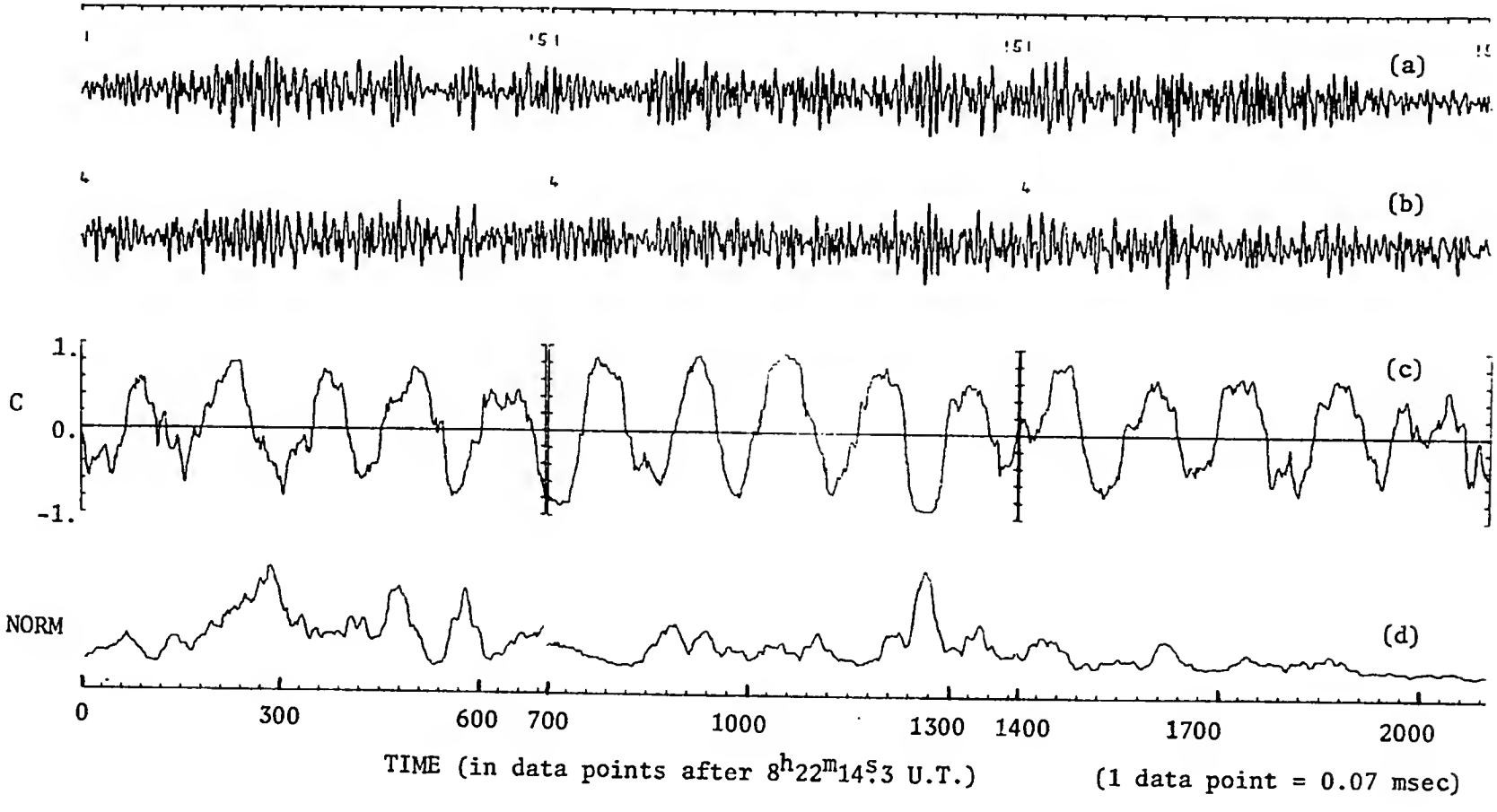

Figure IV.5 -- Plot of Heterodyned Data from WKU (a) and FPC (b). Plot of Cross Correlation Function(c) and Normalization (d) Versus Time for L-Burst of 2 January 1969.

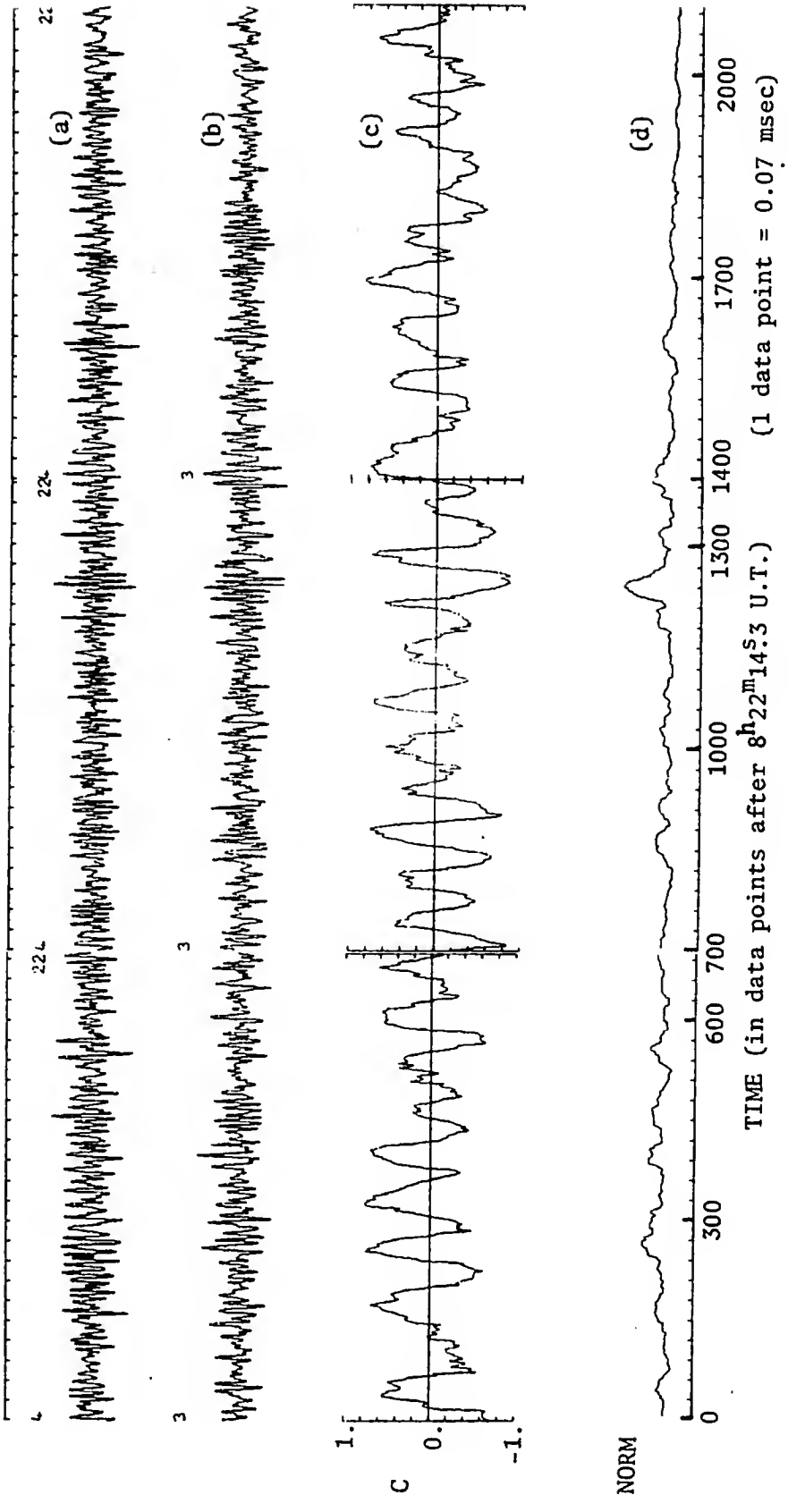

Figure IV.6 -- Plot of Heterodyned Data from FPC (a) and MAIPU (b). Plot of Cross Correlation Function (c) and Normalization (d) Versus Time for L-Burst of 2 January 1969.

Calcomp plotter. The first two lines are a plot of the data as received by the stations (the heterodyned signal), hence can be compared directly with Figure IV.3. The third line in each figure is the cross correlation function plotted against time, and the fourth line is the denominator of $C(s_\lambda,\xi,t)$ which serves as a normalizing factor. The integration time, N, is 2.1 milliseconds. The peaks in the normalization curve indicate where especially strong regions of the burst are located. The time axis is calibrated in data points, such that one data point is 0.07 milliseconds. Time is counted from the beginning of the burst, or $08^h22^m14\overset{s}{.}3$ UT.

Figure IV.4 shows the data from WKU compared with that from MAIPU. Figure IV.5 compares data from WKU and FPC, while Figure IV.6 compares data from FPC and MAIPU. Table IV.2 gives the amplitude of the cross correlation function near the two selected regions of high signal level and shows the fringe rate in this vicinity. As was shown in Chapter II, the fringe rate is due to the relative motion of the source with respect to the far field pattern of the interferometer, together with the relative local oscillator offset frequency. The fringe rate due to the motion of the source through the interferometer pattern for the longest east-west baseline is on the order of 0.1 fringe/second. Most of the fringe rate in Table IV.2 can be attributed

Table IV.2

Stations	$\|C\|$ near D.P. 880	$\|C\|$ near D.P. 1240	F.R.
WKU - FPC	0.90 ± 14%	0.92 ± 14%	107 Hz
FPC - MAIPU	0.80 ± 20%	0.87 ± 20%	216 Hz
WKU - MAIPU	0.95 ± 16%	0.80 ± 16%	103 Hz

to the local oscillator offsets. It is encouraging to note that the sum of two of the fringe rates (the first and the third) is very nearly equal to the fringe rate of the other pair of stations (the second) as is predicted by the theory of operation of the superheterodyne receivers used in this experiment.

It is clear from Table IV.2 that the amplitude of the cross correlation function does not decrease with baseline length. The variation in $|C|$ is closely related to the signal-to-noise ratio of the signals used to calculate it. This effect is also noticed in the relative "fuzziness" of the curve for $C(s_\lambda,\xi,t)$ in regions where the signal is not strong, as is reflected by the normalization curve. The immediate conclusion from this data is that the longest interferometer baseline did not resolve the source of this burst. There is another interpretation of this result, however. If the source is coherent, the assumptions made concerning the random nature of the signal as a function of both time and position on the source are invalid. The result is that the fringe visibility function, V_0 cannot be used to reconstitute the brightness distribution. This consequence will be considered in the concluding portion of the dissertation. At this point, it can be concluded that the angular width of the source is less than the width of one beam lobe, if the source is incoherent. This angle, for the longest baseline, is given by $\theta = \frac{\lambda}{D}$ radians. For the WKU - MAIPU baseline, D is 7620 km, making θ have a value on the order of ½ second of arc. The corresponding linear distance on Jupiter is 1880 km.

A smaller upper limit on the size of the source can be found by using the family of curves for the amplitude of the fringe visibility

function, $V_0(s_\lambda)$, that is given in Figure II.4. Using the interpretation that low values of $|C|$ are due to uncorrelated noise contamination when the signal strength is weaker, it is seen that the data points form a curve that lies above the curve for a 0".1 of arc Gaussian strip source. This implies that, if the source is incoherent, its size is less than 0".1 of arc or a linear distance of 490 km on Jupiter.

An experiment was conducted using a one-bit correlation scheme to compare the method with that already given. Weinreb (1963) and Cooper (1970) have demonstrated the utility of various one- and two-bit correlation techniques in the field of radio astronomy. The sensitivity of the one-bit technique is 64% that of the continuous multiplying correlator used above. The various two-bit correlation methods have a sensitivity on the order of 85% compared with the continuous multiplying correlator. It was felt that by converting the data to the form in which plus one represents excursions of the data voltage above the zero axis and minus one those below the axis, any contribution of the envelope to the cross correlation function would be eliminated. It should be recalled that there are many physical modifications that can occur to the envelope of the Jovian burst, e.g., solar wind interaction, interaction of a Faraday rotated plane-polarized wave and an antenna polarized in another sense, etc. Any frequency effect, having been introduced at the source, is useful for the purpose of giving information about the source itself. Figure IV.7 is a composite of the fringes generated by interfering signals that have been treated in the one-bit method from the stations WKU and MAIPU. The one-bit representations of the signals from WKU and

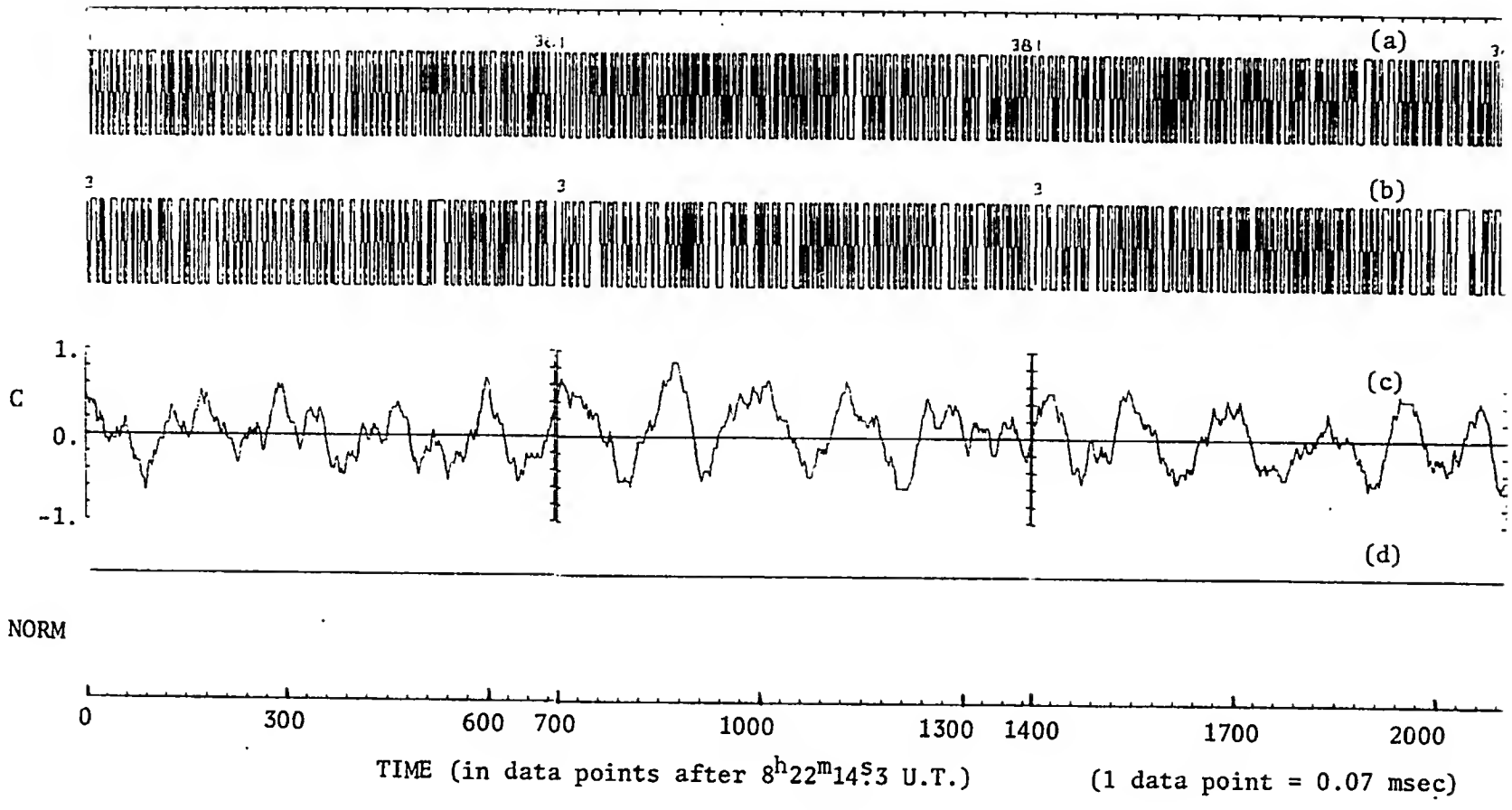

Figure IV.7 -- Plot of Data After Receiving the One-Bit Treatment from WKU (a) and MAIPU (b). Plot of Cross Correlation Function (c) and Normalization (d) for This Data.

MAIPU are shown on lines one and two, respectively. The third line is the cross correlation function plotted against time, with N = 2.1 milliseconds, and the fourth line is the normalization. The normalization has a constant value since the amplitude information in the original signals has been removed. This is one of the attractive features of the method from an instrumentation point of view. The hardware for the correlator is relatively easy to implement with digital logic integrated circuits. The time delay, τ, can be handled by shift registers, for example. The cross correlation function plotted in Figure IV.7 shows the fringes that were seen in Figure IV.4, which is a plot of the same data without the one-bit representation. Some regions, corresponding to highly intense radiation in Figure IV.4, show a fringe amplitude on the order of 0.9. It should be noticed in Figure IV.7 that the fringe amplitude decreases away from the center of the burst. This artifact is caused by the time scaling having some residual error which causes the data at the beginning and end of the burst not to have exactly the same best shift. This is removed in Figure IV.4 by plotting the first and last thirds of the data at the proper best shift for that section of the data. The one-bit correlator is seen to depend very sensitively on relative shift of the data. This feature will be used in the section of Chapter IV dealing with the beam-sweep experiment. The principal shortcoming of the one-bit correlator is that it must integrate over a longer period of time to overcome the loss of information due to the one-bit representation. In normal radio astronomical applications there is no difficulty encountered with this shortcoming since the sources that are studied do not change in intensity over times

that are long with respect to a typical integration period. The Jovian burst envelope, however, changes with time and its shape is not preserved from one burst to another. The S-burst, especially, requires the use of the continuous multiplying correlator.

In Chapter II, it was shown that the Brown and Twiss post-detector-correlation interferometer could be formed using the same form of the cross correlation function as was used for the phase interferometer. The data from the four stations was full-wave detected in the computer by the program BABS. CROCO was run using this data in the same manner as before. The best shift for each pair of stations was found, and the cross correlation function was plotted by CROCOCAL. Figures IV.8, IV.9, and IV.10 show the results of these calculations for the three pairs of stations used in the phase interferometer. In each figure, lines one and two are the detected data from the stations. The full-wave detected data was filtered for an integration time of 1.4 milliseconds. The integration time, N, in the cross correlation function calculation was 70 milliseconds, which is approximately the length of the detail structure in the data. The third line is the cross correlation function, which no longer exhibits fringes. The fourth line is the normalization. Table IV.3 summarizes some values of the cross correlation function near

Table IV.3

Stations	C^2 near D.P. 880	C^2 near D.P. 1240
WKU - FPC	0.84	0.97
FPC - MAIPU	0.64	0.95
WKU - MAIPU	0.90	0.97

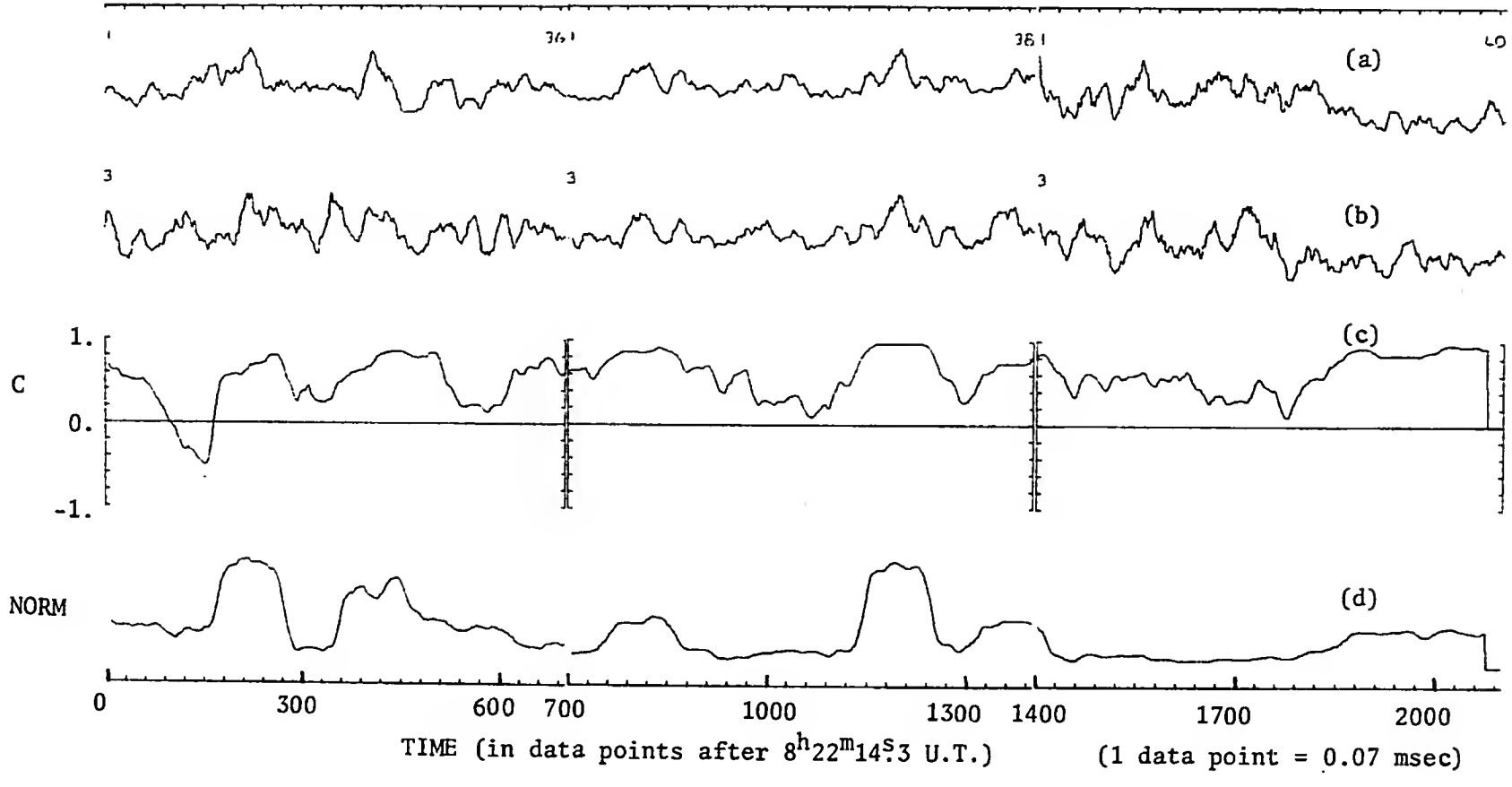

Figure IV.8 -- Plot of Detected Data from WKU (a) and MAIPU (b). Plot of Cross Correlation Function (c) and Normalization (d) Versus Time for L-Burst of 2 January 1969.

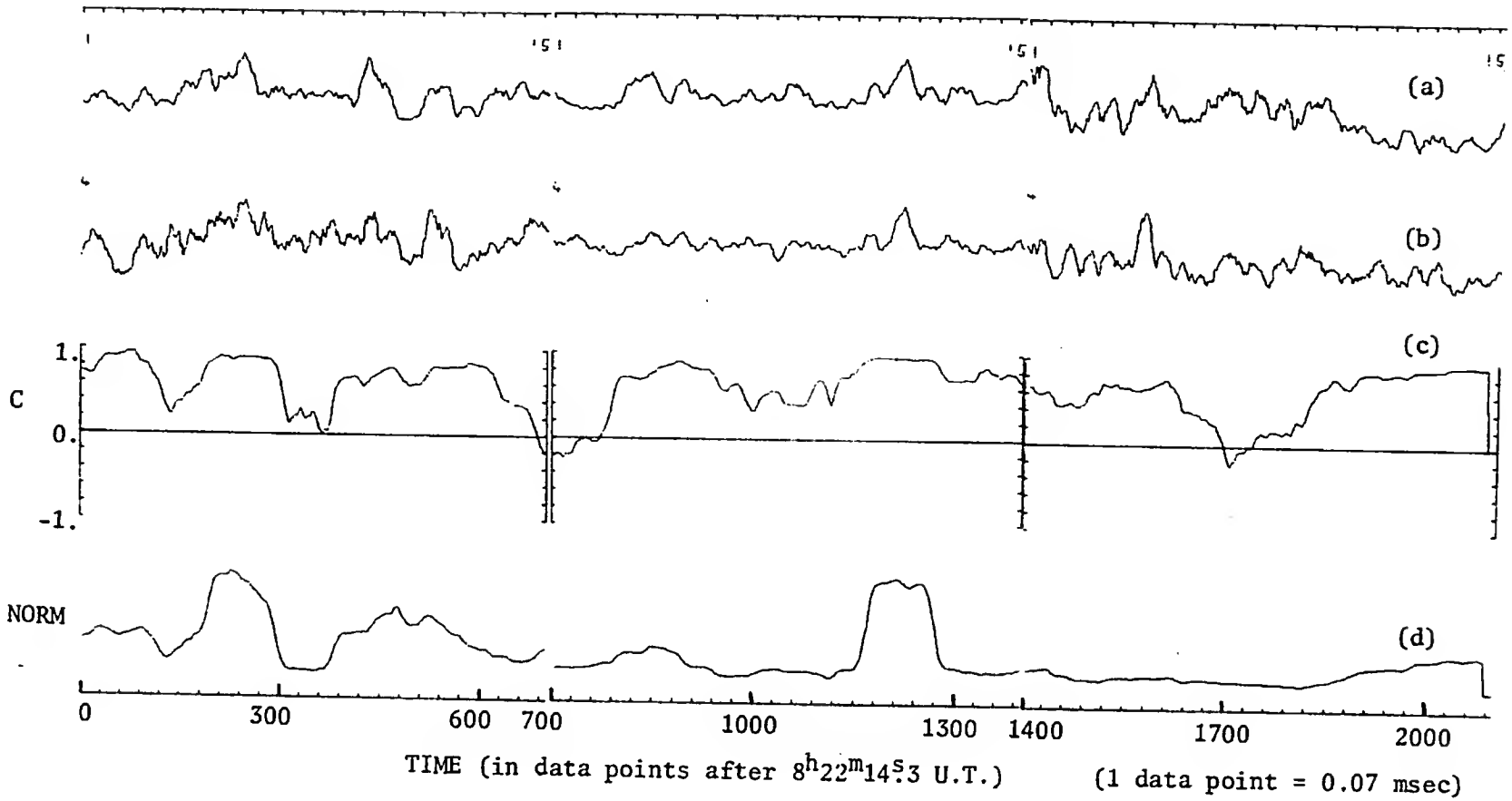

Figure IV.9 -- Plot of Detected Data from WKU (a) and FPC (b). Plot of Cross Correlation Function (c) and Normalization (d) Versus Time for L-Burst of 2 January 1969.

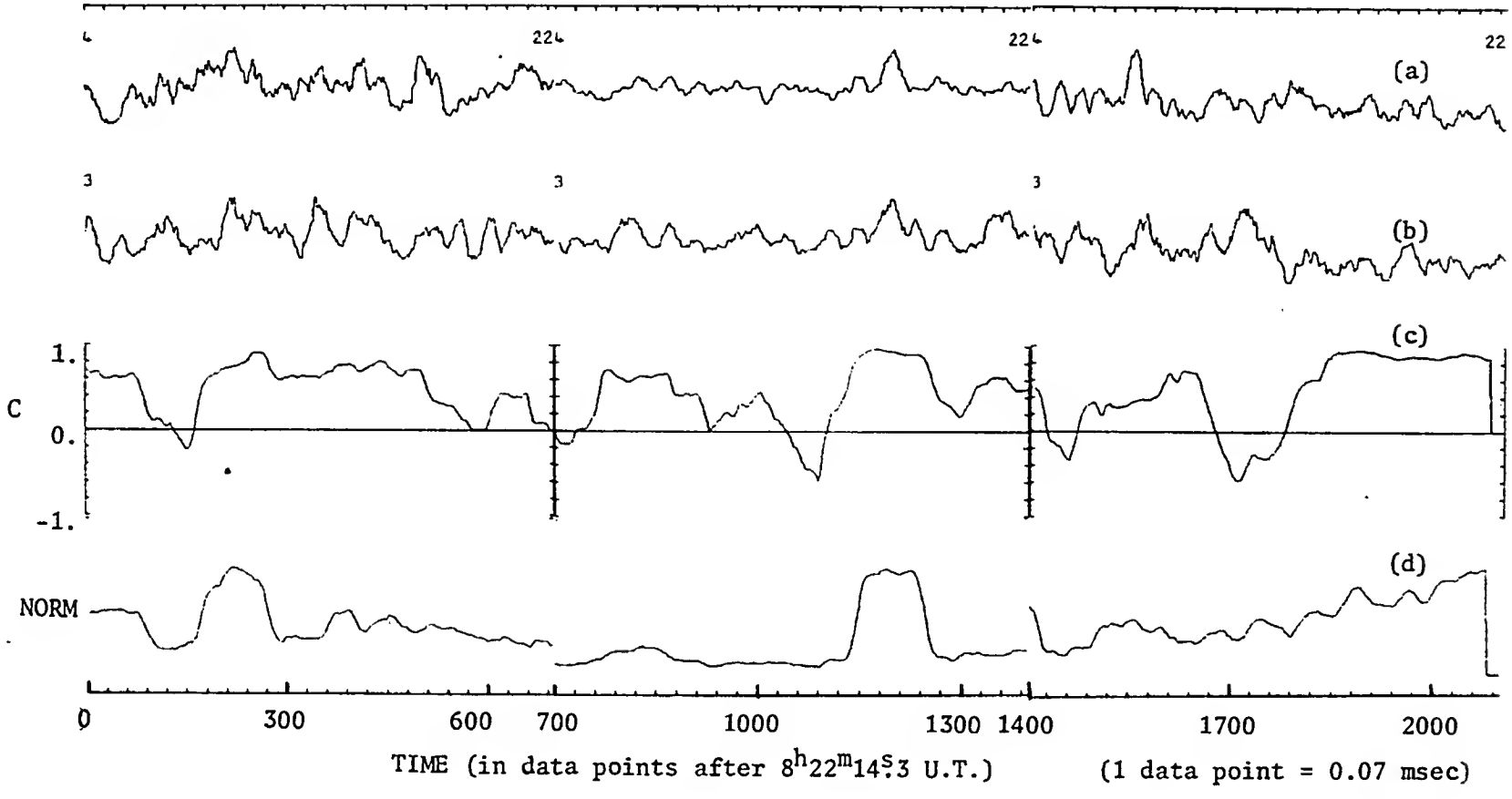

Figure IV.10 -- Plot of Detected Data from FPC (a) and MAIPU (b). Plot of Cross Correlation Function (c) and Normalization (d) Versus Time for L-Burst of 2 January 1969.

regions of especially strong signal (the same regions as were shown in Table IV.2). The symbol C^2 means that this cross correlation function is to be interpreted as the square of the C found using the phase interferometer. It is seen that the values obtained by the two methods are essentially the same. Since the cross correlation function, C^2, also does not decrease with increasing baseline length it can be concluded that, if the source is incoherent, it is not resolved. The beam lobe angle is the same as for the phase interferometer. If the source of this burst was incoherent, it must have been less than 0".1 of arc in angular width.

IV-4. Burst Arrival Time Experiment

Figure IV.11 is a composite of three chart records depicting the envelope of the burst as it was received at WKU, FPC and MAIPU. The envelopes have been aligned in real time, i.e., local tick misadjustment and WWV time delay have been removed. It is clear that this burst arrived at all of the stations at essentially the same time.

A much more accurate technique can be used than that given above. The normal method to measure the burst arrival time consists of providing stable local time marks on the data tape that have been accurately calibrated in real time. The calibration procedure is very difficult and has only recently become practicable for widely separated stations. The method usually involves flying an atomic oscillator by plane to the various stations or comparison with a continuously calibrated time standard in an earth satellite. In the novel technique for measuring burst arrival time given here, Jupiter's signals themselves are used to calibrate the local clocks.

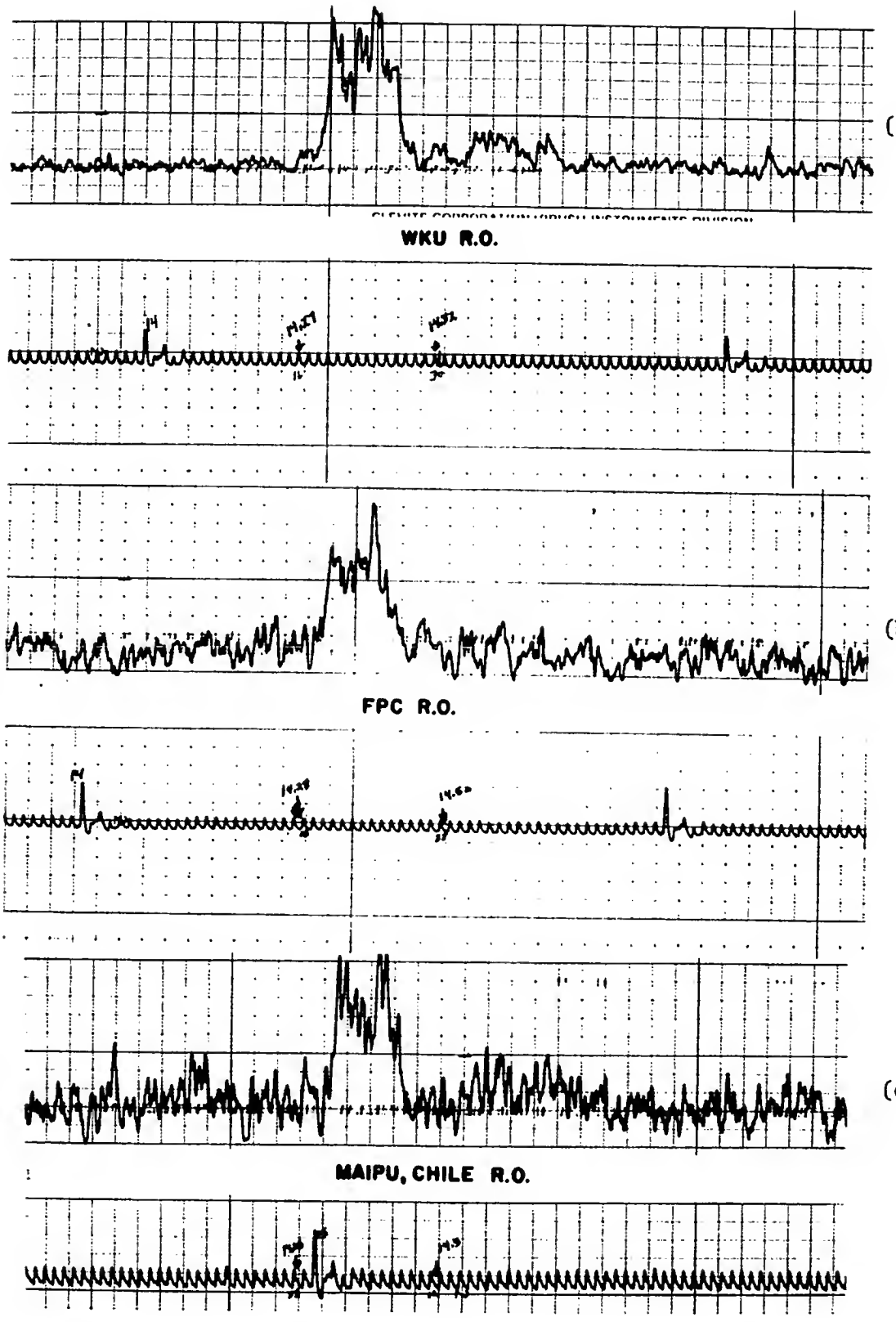

Figure IV.11 -- Actual Chart Records of the Detected Data from WKU (a), FPC (b) and MAIPU (c) for the L-Burst of 2 January 1969. Records Are Laterally Adjusted Such as to Be Aligned in Real Time.

The property of the Jovian signals that is used can be demonstrated by considering a model consisting of a frequency modulated transmitter driving a directive antenna that is located in the vicinity of Jupiter (it is only necessary that the station be a long distance away and in the line-of-sight). If two receiving stations are located such that the beam of the antenna can sweep across them, the output of the receivers will be as shown in Figure IV.12. It is assumed that the station that is not in the center of the beam can still receive some signal. The receivers are superheterodynes and have product detectors, as do those in our interferometer. Figure IV.12 has been drawn in such a way that the phase changes in the frequency modulation are aligned in each of the signals, e.g., the feature at time "7". The frequency modulation features are produced at the transmitter and, except for random Doppler shifting, cannot be altered during transmission after the signal leaves the transmitter. The envelopes, on the other hand, are determined by the location of the receiver with respect to the antenna beam of the transmitter. If the beam sweeps from one station to the other, there will be a noticeable difference in the time relationship of the frequency modulated "carrier" and the envelope when the signals received at each station are compared. The frequency modulation feature at time "7" has a high amplitude at station two, while it is weaker at station one. If the signal underneath the envelope from one station is cross correlated with that from the other, the relative shift for the greatest amplitude of the cross correlation function will be zero for this example. If the envelopes are cross correlated, it is clear from Figure IV.12 that the envelope of station two would have to be shifted

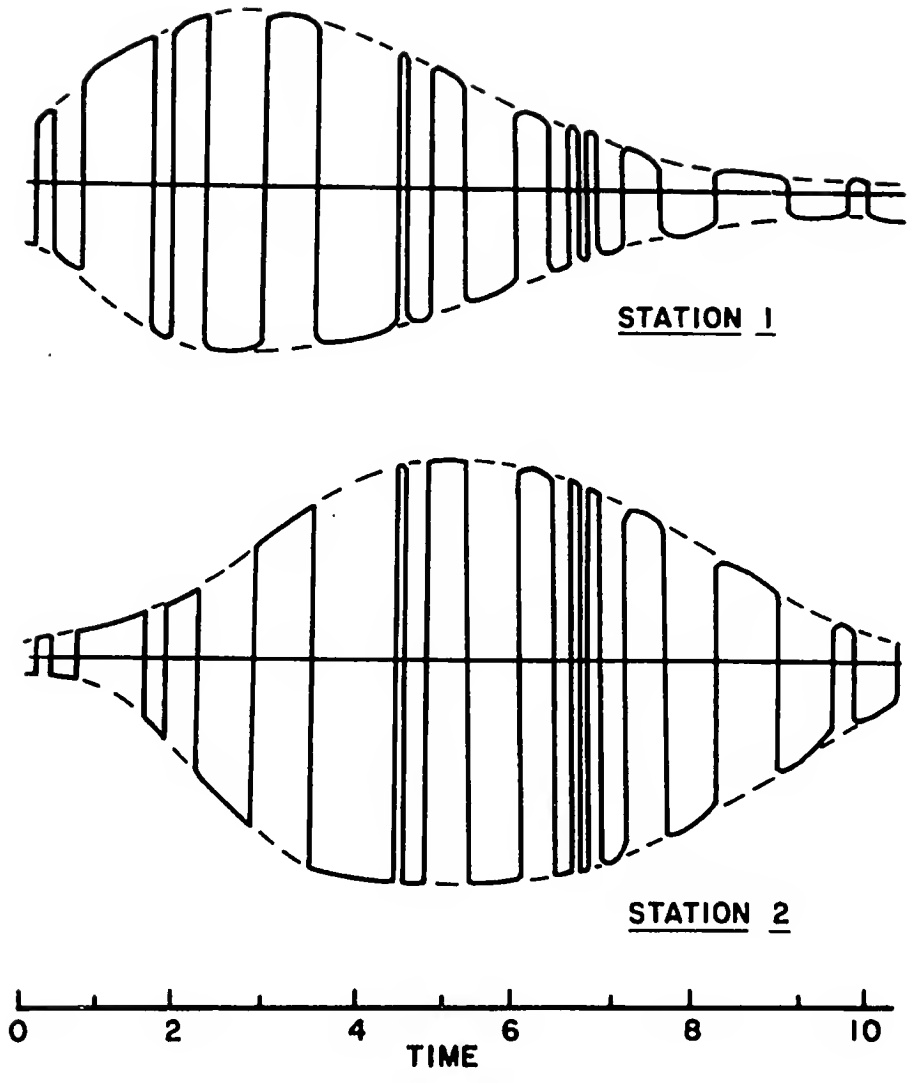

Figure IV.12 -- Plot of the Amplitude of a Constant Intensity Signal as Received at Two Stations as the Beam of Radiation Sweeps from Station 1 to Station 2. Frequency Modulation Features Are Visible Under the Envelopes.

forward by approximately 3 time units to obtain the maximum cross correlation function.

It is proposed by a number of investigators, including Goldreich and Lynden-Bell (1969), that the decametric radiation from Jupiter is highly beamed. A burst envelope received on earth, then, may be shaped by the way that the beam sweeps across the receiving station, if it sweeps rapidly enough. The frequency modulation of the Jovian signal is due to the source being a producer of random noise of moderate bandwidth. It is the interaction of this noise spectrum with the I.F. filter in the receiver that produces the wave forms shown in Figure IV.3. The filters in all of the receivers in the interferometer are identical, hence their effect on the same noise spectrum is the same. There is only one best shift for the heterodyned data due to the random nature of the noise spectrum produced by the Jovian decametric source. The local clocks can be calibrated with each other by using the correction produced by finding the best shift for each pair of stations. The envelopes of the signals can be cross correlated to find the best shift for them. The best shifts for the heterodyned data and the envelopes from a given pair of stations can be compared to determine the rate and direction of motion of a sweeping beam.

Figure IV.13 is a plot of a portion of the burst as received at WKU and MAIPU. The signal is especially strong in this part of the burst. Figure IV.13a shows the heterodyned signal from WKU and MAIPU on lines one and two, respectively. Line three is the cross correlation function plotted versus time for a shift of 38 data points, and line four is the normalization. Figure IV.13b shows the cross

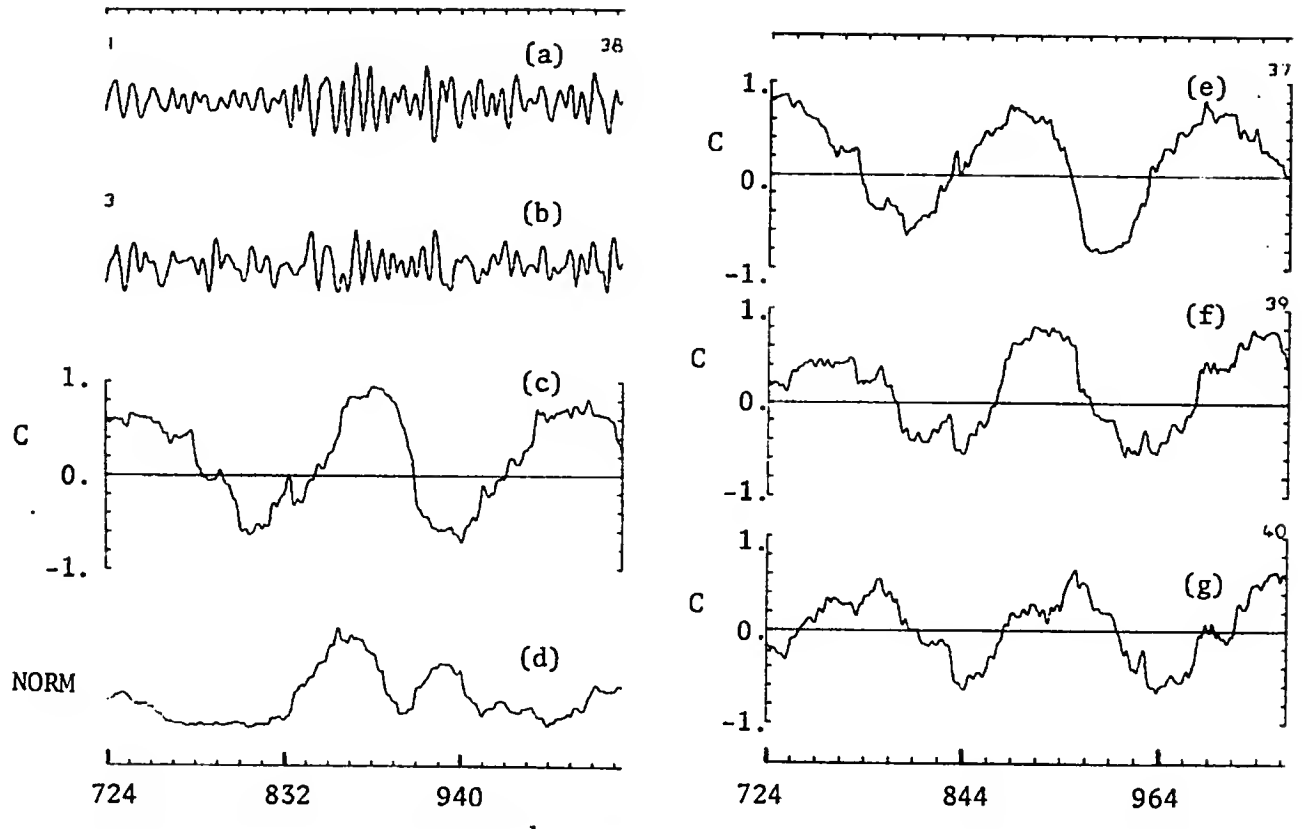

Figure IV.13 -- Plot of Heterodyned Data near Data Point 840 for WKU (a) and MAIPU (b). Plot of Cross Correlation Function (c) and Normalization (d) for Relative Shift = 38 Data Points. Plot of Cross Correlation Function for Relative Shift = 37 (e), 39 (f) and 40 (g) Data Points.

correlation function plotted versus time for other shifts. The shift is 37, 39, and 40 data points in lines one, two and three, respectively. The integration time for calculating C was 2.1 milliseconds. It should be obvious from the two parts of Figure IV.13 that the cross correlation function is very sensitive to relative shift. The value of best shift of 38 data points indicates that the clock at MAIPU must be advanced by 2.65 milliseconds from the time that was indicated by the corrections given to BADE. Figure IV.14 is an illustration of the full-wave detected data from WKU and MAIPU arranged in the same way as for Figure IV.13. Figure IV.14b shows the dependence of the cross correlation function on relative shift. The deviation from the value for the best shift is not as rapid as for the heterodyned data and is the chief error introduced in the technique. Table IV.4 is a summary of the best relative shifts for the data from the three pairs of stations.

Table IV.4

Stations	Best Shift		Data Pt.
	Heterodyned Data	Detected Data	
WKU - FPC	1.05 msec	1.05 msec	1200
FPC - MAIPU	1.54 msec	1.68 msec	1200
WKU - MAIPU	2.66 msec	2.66 msec	840

Figure IV.15a is a graph of the dependence of the cross correlation function on the relative shift for the entire burst as received at WKU and MAIPU. The integration time for calculating C^2 was 112 milliseconds, which covers the entire burst in one summation. While the

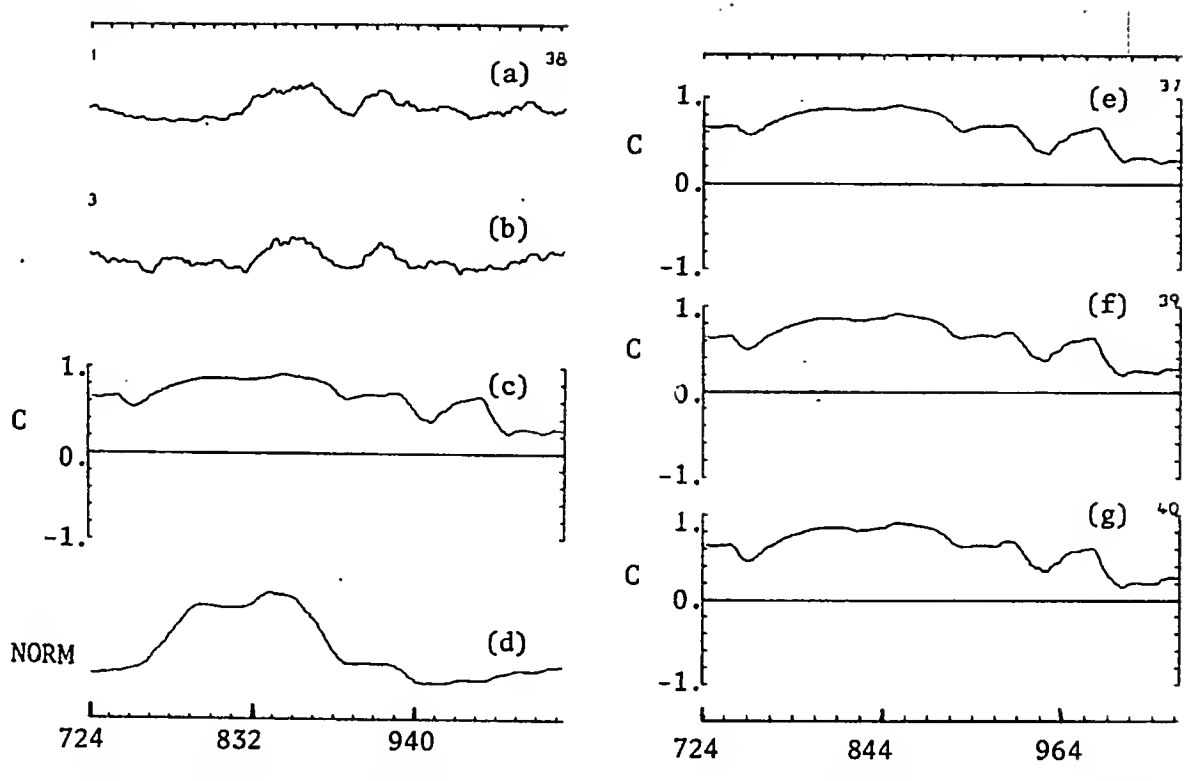

Figure IV.14 -- Plot of Detected Data near Data Point 840 for WKU (a) and MAIPU (b). Plot of Cross Correlation Function (c) and Normalization (d) for Relative Shift = 38 Data Points. Plot of Cross Correlation Function for Relative Shift = 37 (e), 39 (f) and 40 (g) Data Points.

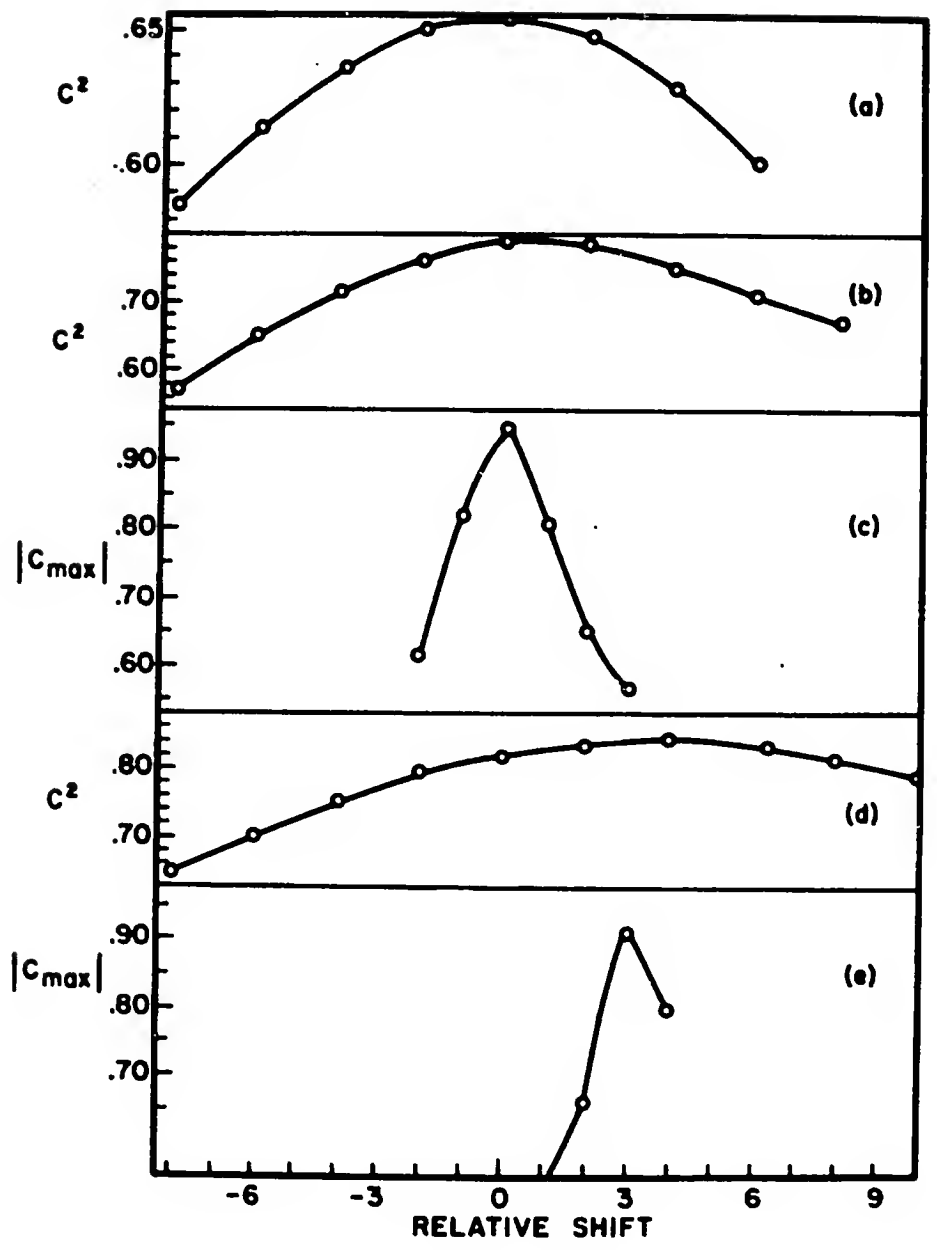

Figure IV.15 -- Cross Correlation Measures Plotted as Function of Relative Shift for the WKU-MAIPU Baseline. (a) C^2 for Detected Data with N=112 Milliseconds. (b) and (d) C^2 for Detected Data in the Vicinity of Data Points 840 and 1240, Respectively, with N=15 Milliseconds. (c) and (e) Amplitude of the Cross Correlation Function Near the Same Two Locations with N=2.1 Milliseconds.

curve is not sharply peaked, it is obvious that the best shift for the entire burst is within 400 microseconds of the best shift for the separate sections of the burst. Figures IV.15b and c are graphs of C^2 and $|C|$ for the detected and heterodyned data, respectively, near the data point 850. Parts d and e are for C^2 and $|C|$ near the data point 1240 in the bursts received at WKU and MAIPU. The time axis is calibrated in multiples of data points (1 dp is 0.07 milliseconds) relative to the best shift for the heterodyned data (2.66 milliseconds). All curves show a peak in the vicinity of a relative best shift of zero. Since there is no consistent deviation between the best shift for the heterodyned data and that for the detected data, it is concluded that there is no measurable beam sweeping effect, and that the observed slight deviation is experimental scatter due to contamination of the Jupiter signal by uncorrelated galactic noise. The uncertainty in timing is on the order of 400 microseconds. If a beam had swept past the two stations at a rate slower than this, its presence would have been detected.

On 2 January 1969 the distance from the earth to Jupiter was 7.81×10^8 km. The north-south baseline in equatorial coordinates for WKU - MAIPU was 1.9 seconds of arc as seen from Jupiter. The east-west baseline in the same coordinate system was 0.50 seconds of arc. The maximum detectable beam sweep rate in the north-south direction was 2°/second and was $0^\circ.5$/second in the east-west direction. For a beam sweeping parallel to the baseline, the maximum detectable sweep rate was on the order of $2^\circ.1$/second.

The theory of Goldreich and Lynden-Bell contains four possible mechanisms that might cause a beam of radiation to be swept across

the earth. Jupiter's ionosphere, where the lower terminus of a flux tube is located, rotates with the planet. If the source, moving with the ionosphere, swept the beam of radiation with it, the beam would rotate with an angular velocity of 0°.01 per second. The flux tube passes through Io and, in this theory, moves with the satellite. The orbital angular velocity of Io is 0°.0023 per second, which would be the sweep rate of a beam influenced by this satellite. The theory proposes that as ionization conditions in the ionosphere change from those at night to the daytime state, that the foot of the flux tube advances from a position below Io to one approximately 15° ahead. If the beam is swept by this mechanism, its angular velocity would be on the order of 0°.004 per second. The advance is assumed to occur in about 20 minutes. It is obvious that any of these beam sweep rates would be easily detectable by the method proposed above. A group of electrons spirals along a field line that lies between Io and the ionosphere of Jupiter. If it is assumed that the radius of curvature of the field line in this region is on the order of 5 times the radius of the planet and that the electrons are moving with a velocity of 0.1 times the speed of light, a beam of radiation generated by them would sweep at a rate on the order of 4°.8 per second. This sweep rate is just beyond the range of measurement by the data that has been analyzed in this chapter. The three sweep mechanisms mentioned earlier are definitely ruled out, however.

Douglas and Smith (1967) proposed a theory that accounts for the structure of the L-Burst. They attribute the L-Burst to an isophotal pattern, caused by inhomogeneities in the solar wind, drifting across the receiving stations. They support their theory with convincing

evidence based upon the time of arrival of a given L-Burst at several receiving stations. Their model predicts that the easternmost station on a baseline parallel to the ecliptic will receive the burst before any stations to the west if Jupiter is before opposition. The westernmost station will receive the burst earliest if Jupiter is after opposition. The L-Burst analyzed in this chapter was received when Jupiter was 82 days before opposition. Their data shows that for a baseline length of about 100 km that the signal will arrive at the station to the east about 0.1 second before it arrives at the western station for this time (82 days before opposition). The WKU - MAIPU baseline, when projected on the ecliptic, B_{EW}, has a length of 4580 km on a plane perpendicular to the line-of-sight from the earth to Jupiter. By scaling the time delay in a linear fashion proportional to the relative baseline lengths, it is seen that the expected delay time should be on the order of 4.5 seconds. No such effect was observed in this case. It is therefore concluded that the source itself may exhibit intensity variations that are at least as long as the burst that has been analyzed here. Although most L-Burst envelopes are probably shaped by the solar wind, some must be intrinsic to the source itself.

IV-5. The Stability of the Position of the Source

While the phase interferometer can give no information about the size of the source that radiates coherently, the fringes are a good source of information about the relative motion of the source during the time of emission. Examination of Figure IV.4 will reveal no

consistent departure of the fringe rate or rapid changes of phase from that shown at the beginning of the burst. There are numerous apparent losses of coherence, but these can be correlated with intervals of low signal level. The effect of these low levels is to allow the uncorrelated noise of the galactic background to cause temporary loss of coherence. When the signal increases again, the fringe regains its coherence, with no shift in phase. The interpretation of this effect is that the source remained in essentially the same position in the interferometer antenna pattern during the emission of the radiation. The spatial resolution is on the order of 0.1 part of a fringe or about 0.05 seconds of arc. This corresponds to the source remaining within 245 km of its original position during the burst.

CHAPTER V

ANALYSIS OF DATA RECEIVED IN 1970

V-1. Instrumentation, Timing and Baseline Orientation

In 1970 the receivers that are diagrammed in Figures III.2, III.3, and III.4 were put on the air at the University of Florida Radio Observatory, Old Town, Florida, and at the Observatorio Radioastronomico de Maipu of the Universidad de Chile near Maipu, Chile. The geographical coordinates of these stations were given in Chapter IV. The great circle distance between UFRO and MAIPU is 7384 km and the chordal distance, D, is 6980 km (419,000 λ); the angle between first nulls for the interferometer is 0.49 seconds of arc. Figure V.1a shows a view of the earth as seen from the North Pole of the ecliptic on 30 April 1970 at the time the bursts that are analyzed in this chapter were received. The celestial coordinates of Jupiter on that date were as follows: right ascension = $13^h53^m54^s$ and declination = -10°5'41". The right ascension of the sun was $2^h27^m22^s$.

The various baseline projections that will be used in the interpretation of the data are shown in Figure V.1b. The projections are drawn in a plane that is perpendicular to the line-of-sight from the stations to Jupiter. D_{NS} is the component of D parallel to the polar axis of the earth projected on the plane perpendicular to the line-of-sight

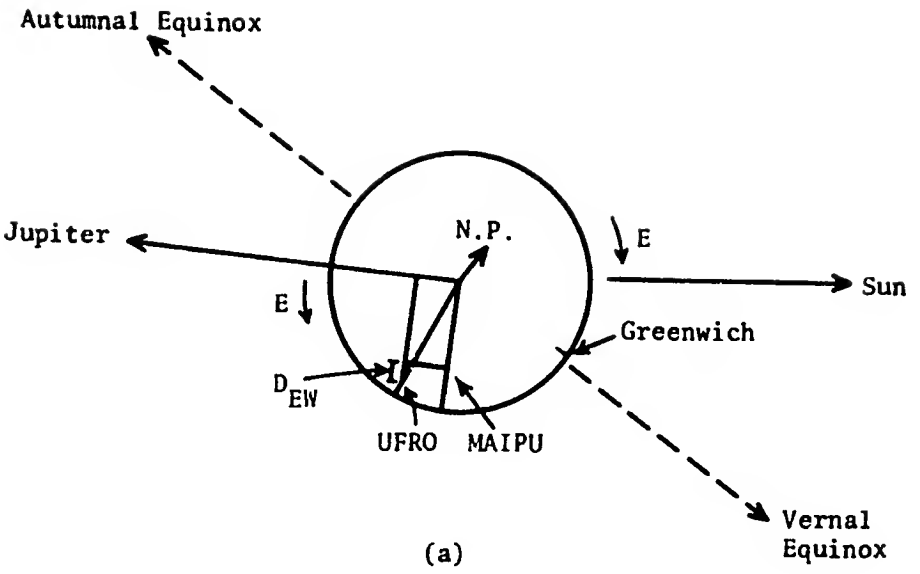

(a)

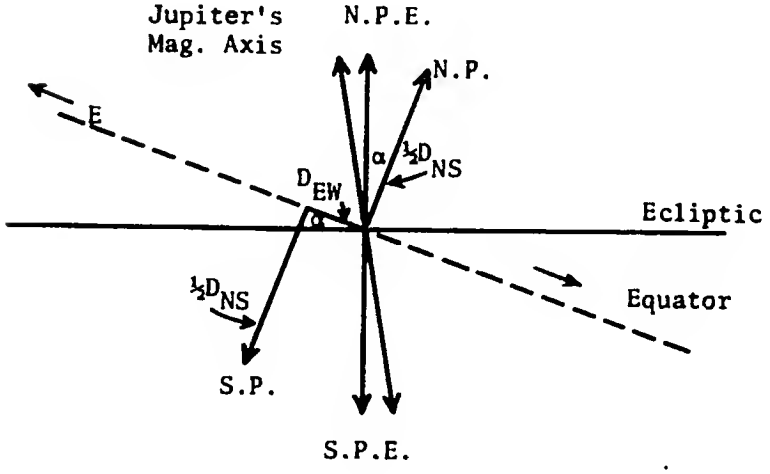

(b)

Figure V.1 -- (a) View of Earth, Jupiter and the Sun from Above the North Pole on 30 April 1970, (b) D_{NS} and D_{EW} Projected on the Plane Perpendicular to the Line-of-Sight to Jupiter.

to Jupiter. D_{EW} is the component of D parallel to the earth's equatorial plane projected on the same plane. Angle α lies between D_{NS} and the North Pole of the ecliptic in the same plane and had a value of 20°.5 when the data was received. The various baseline components had the following lengths: D_{NS} = 6560 km and D_{EW} = 205 km, with MAIPU east of UFRO using the directions for the side of the earth toward Jupiter.

To insure the accurate calibration of the locally generated time signal at MAIPU with respect to real time, a rubidium vapor clock was provided on loan from the National Radio Astronomy Observatory. Without interrupting its operation, the clock could be transported to the NASA satellite tracking station near Santiago for calibration. This procedure was performed at biweekly intervals during the observing season. The data channel was multiplexed in such a way that the WWV voice announcement was recorded for 20 seconds at 5-minute intervals and the rubidium vapor clock signal was recorded for three seconds every minute on the minute.

While it was hoped to use signals transmitted by the East Coast LORAN-C chain to provide very accurate timing at UFRO, the audio preamplifier in the LORAN-C receiver was found to be saturating, and the station identifiers could not be decoded on chart recordings made from slowed-down magnetic tapes. Local timing was determined as accurately as possible by correcting the WWV time marks for transmission time from Boulder, Colorado, which amounted to 8.3 milliseconds (Hewlett-Packard Company, 1965).

The data format, as recorded on magnetic tape at UFRO and MAIPU, was given in Chapter III. Just prior to the installation of the receivers at both stations, a fourth timing signal was added to the

local time channel for the purpose of synchronizing an analog-to-digital converter. The sync pulse had a frequency of 15 kHz and was derived by a separate divide chain from the 1.8 MHz crystal at each station. Synchronization of the A-to-D converter to this signal caused the resulting digitization rate to be constant with respect to the local time standard (hence constant in real time). Since this effectively eliminated the variation in digitization rate caused by tape stretch and speed instabilities in the magnetic tape drives, the most complex part of the program, BADE, could be eliminated.

V-2. The Nature of the Received Data

Figures V.2 and V.3 reproduce chart recordings of the envelope detected data as received at UFRO (both channels) and MAIPU beginning at $9^h35^m51\overset{s}{.}5$ U.T. on 30 April 1970. The time covered by the chart records is about 4.5 seconds. The taller marks in the time channels, which are shown on alternate lines just below the corresponding data channels, occur at one-second intervals, and the shorter marks occur at 20-millisecond intervals. The one-millisecond marks and the 15 kHz sync tone are not distinguishable.

There were approximately 68 S-Bursts in the time period beginning at $9^h35^m51\overset{s}{.}6$ U.T. and ending six seconds later. Of these 68 bursts, only 7% were present at one station and missing at the other. This analysis will be restricted to the eleven bursts that are indicated in Figures V.2 and V.3. Table V.1 gives the beginning times of the intervals that were digitized in terms of the locally generated times at each station and in terms of U.T. The indicated times are in

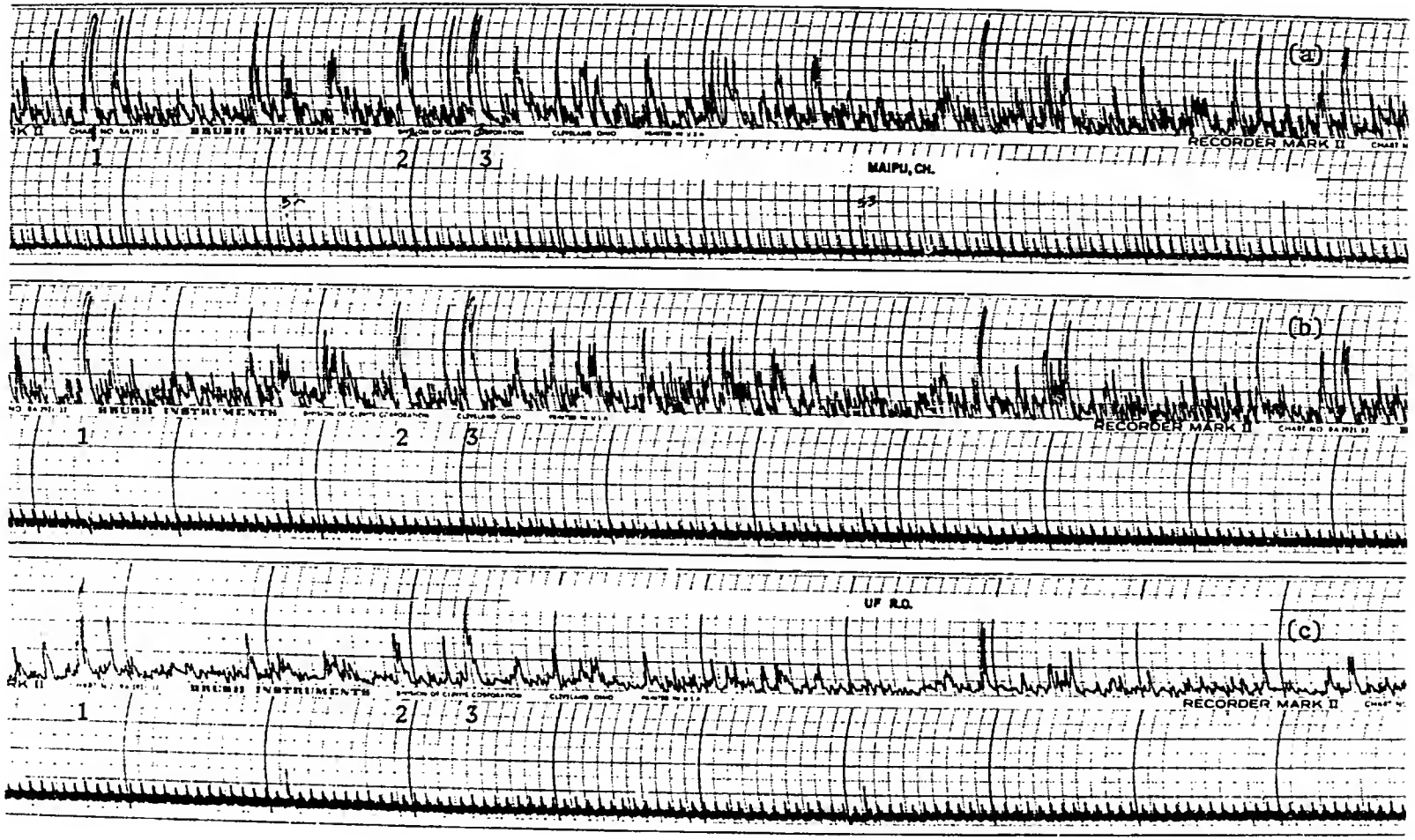

Figure V.2 -- Chart Records Showing Detected Data from MAIPU (a), UFRO Channel A (b) and UFRO Channel B (c) Beginning at $9^h35^m51\overset{s}{.}5$ U.T. on 30 April 1970. Bursts 1, 2 and 3 Are Labelled. The Tallest Marks Visible in the Time Channels Are Second Ticks.

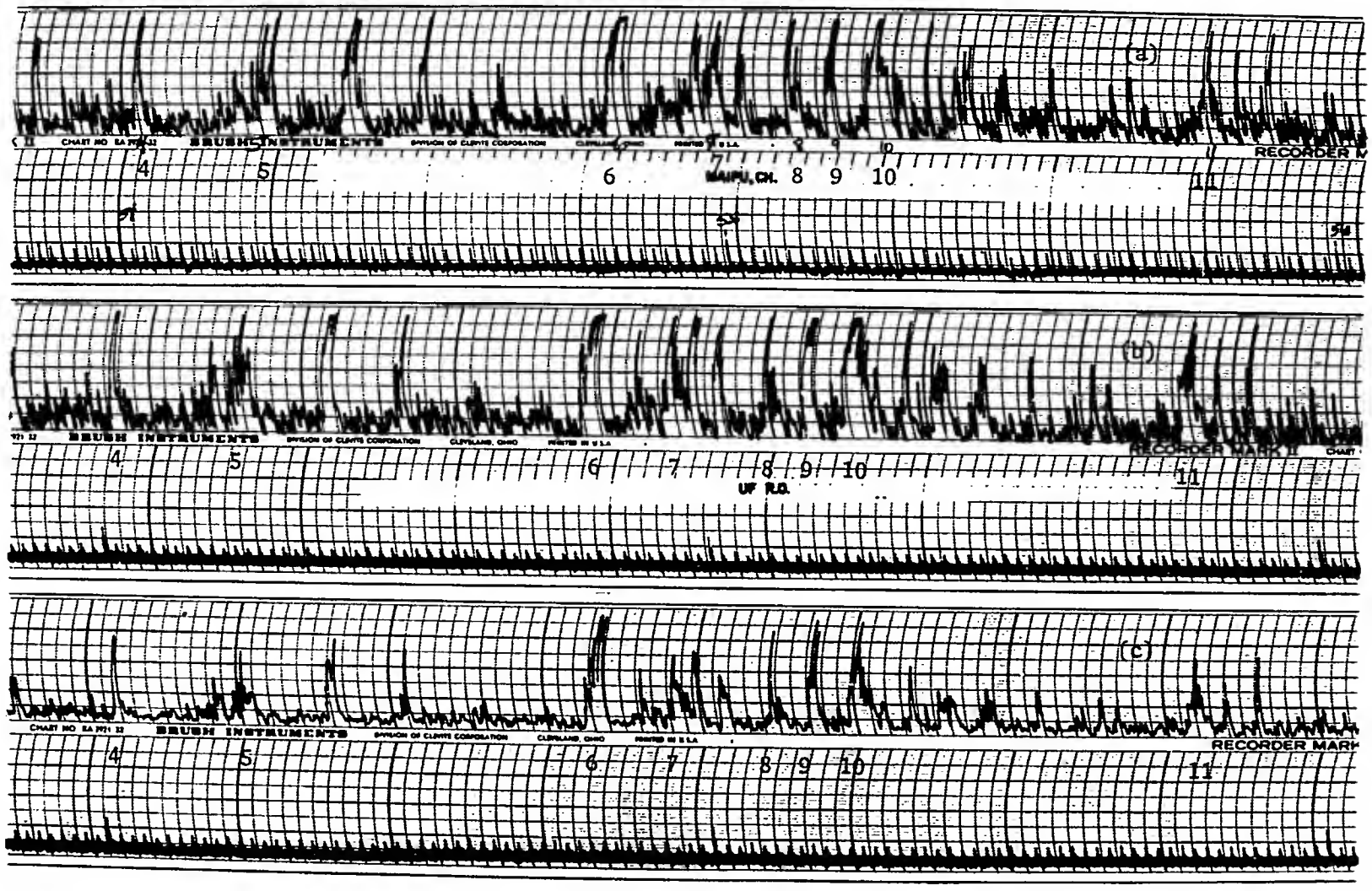

Figure V.3 -- Chart Records Showing Detected Data from MAIPU (a), UFRO Channel A (b) and UFRO Channel B (c) Beginning at $9^h35^m54^s.82$ U.T. on 30 April 1970. Bursts 4, 5, 6, 7, 8, 9, 10 and 11 Are Labelled. The Tallest Marks Visible in the Time Channels Are Second Ticks.

seconds after $9^h35^m51^s$. The digitized period extended for 1920 data points (51.3 milliseconds) from the times given. All bursts that are analyzed are contained within these intervals.

Table V.1

Burst No.	MAIPU (local time)	UFRO (local time)	U.T.
1	0.618	0.610	0.6193
2	1.168	1.160	1.1693
3	1.288	1.280	1.2893
4	2.998	2.990	2.9993
5	3.208	3.200	3.2093
6	3.778	3.770	3.7793
7	3.928	3.920	3.9293
8	4.078	4.070	4.0793
9	4.138	4.130	4.1393
10	4.213	4.205	4.2143
11	4.7607	4.750	4.7619

Two types of bursts were selected for analysis. The first type, consisting of numbers 1, 3, 4 and 9, were of short duration (about 20 milliseconds) and had sharp rise-times and great intensity. The second type, numbers 2, 5, 6, 7, 8, 10 and 11, were of longer duration (about 50 milliseconds) but are still classified as S-Bursts according to the system of Gallet mentioned in Chapter I. The ratio of Jupiter signal + galactic noise to galactic noise alone was exceptionally high for all of these bursts as compared with that for the L-Burst discussed in Chapter IV.

Figure V.4 reproduces chart recordings and incremental plotter graphs of burst number 5. The chart recordings are shown for MAIPU data and time channels on line (b) and for UFRO data and time channels on line (d). The taller marks visible in the time channels are 20-millisecond marks, and the shorter are 1-millisecond marks. The computer incremental plotter graphs are shown for MAIPU on line (a) and for UFRO on line (c). The time scale for the computer plots is expanded by about eight-to-one over that for the chart recordings. The digitization rate used for this data was 37,500 data points/real-time second. The feature marked by A on all four lines corresponds to the same feature in each burst.

V-3. Analysis of the Digitized Data

IBM cards containing 1920 data points for each burst from each station served to transport the data from the IBM 1800 at the University of Florida Medical Center, where it was digitized, to the IBM 360/65 at the University of Florida Computing Center, where it was processed. The two phase-quadrature channels, which will be referred to as UFRO-A and UFRO-B, were digitized separately. The Appendix contains a listing of the changes made to CROCO in order to process this data. The principal changes were necessary because of the different number of data points in a burst as compared with the L-Burst in Chapter IV. A program was written in IBM 360 Assembler Language to convert the column binary formatted data cards to files on magnetic tape for simpler access by CROCO. The data for a given burst from a station was arranged on the tape in the form of 24 records of 80 data points each. The first station written for each burst

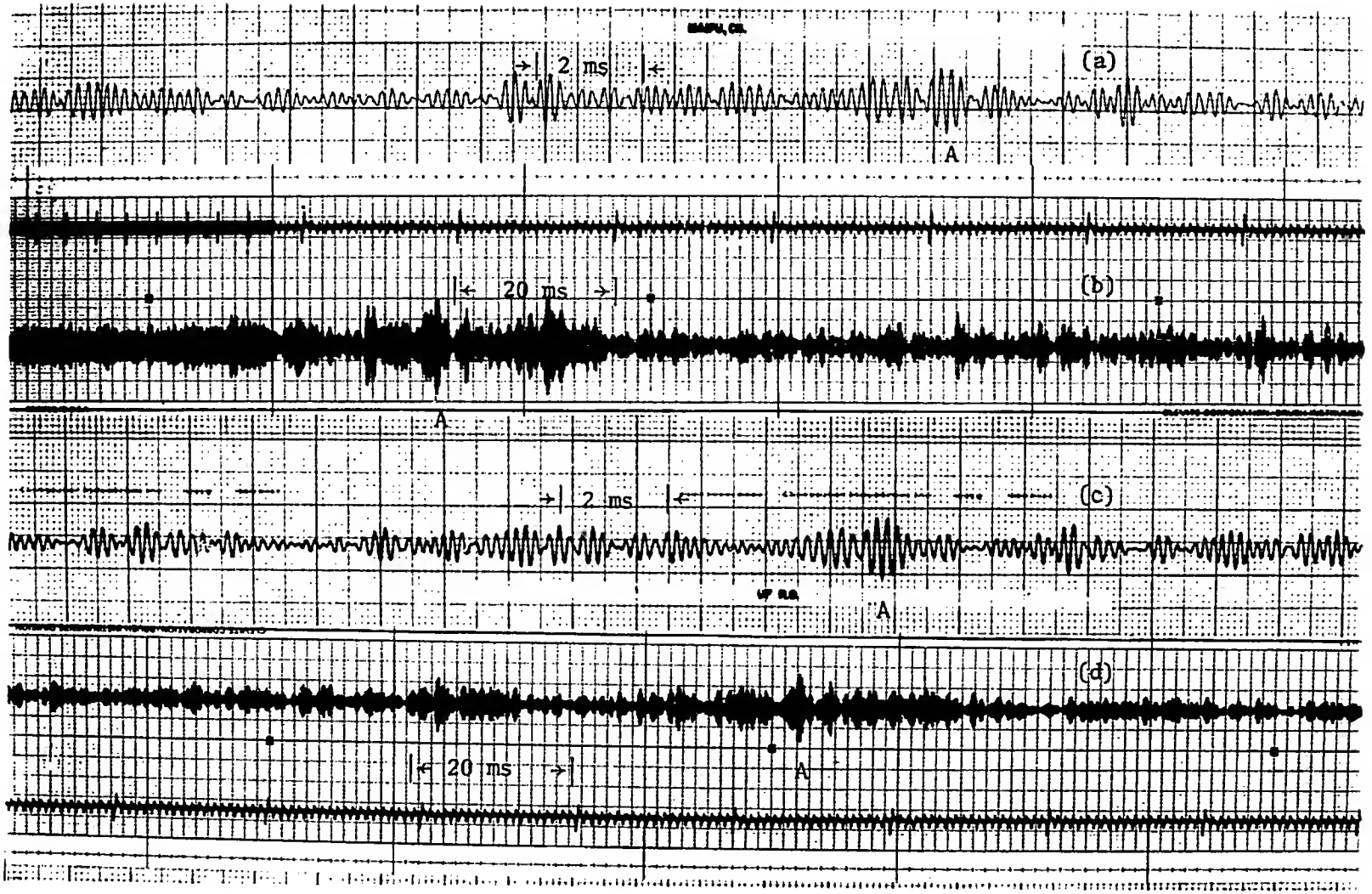

Figure V.4 -- Computer Plots of S-Burst Number 5 from MAIPU (a) and UFRO (c). Chart Records for the Same Burst from MAIPU (b) and UFRO (d). The Features Marked by A Are Aligned for the Best Relative Time Shift.

was MAIPU, the second was UFRO-A and the third was UFRO-B. The first several statements in the adapted version of CROCO select the appropriate burst using IFIL1 (which ranges from 1 through 11) and read the data for that burst into arrays XI (which receives MAIPU data) and IGV (which receives both channels of UFRO data). IFIL2 selects which channel of UFRO data will be cross correlated with MAIPU data by CROCO. The baseline adjustment portion of BADE was added to CROCO in the vicinity of statements 104 and 501 since the phase-locking of the A-to-D conversion procedure had eliminated the need for the remainder of the program BADE.

In certain cases it was necessary to provide detected data to CROCO. Since only heterodyned data was digitized, several statements were placed in the input portion of CROCO to square-law detect the heterodyned data, filter it using a 1-millisecond time constant, and adjust its baseline to the average of the burst. The added sections, which are shown in the Appendix, could easily be removed if it were desired to return CROCO to the form used to process heterodyned data.

Two types of analyses were performed on the S-Burst data. The bursts that were of short duration and extreme intensity were used to test the sweeping beam hypothesis. The longer bursts were used in an effort to determine the fringe rate of the interferometer. In order to perform the sweeping beam test it was necessary to cross correlate both the heterodyned and square-law detected data. The fringe rate and fringe stability calculations could be completed using only the cross correlated heterodyned data.

V-4. Burst Arrival Time Analysis

A method to improve the timing precision using the properties of the Jovian radio burst was demonstrated in Chapter IV. The analysis, using 1970 data with its better timing and faster rise-times, was expected to raise the maximum detectable sweep rate over that found using the burst in Chapter IV due to the much greater timing resolution used in digitizing the later data (37,500 data points/second as compared with 14,200 data points/second for the 1969 data).

Figures V.5, V.6, V.7, and V.8 show the various cross correlation functions plotted against relative shift, τ, for the short bursts (1, 3, 4 and 9). Since these bursts have such fast rise-times, it was felt that the best shifts determined for the envelopes would be more reliable than those found in Chapter IV for the 1969 L-Burst. The (a) line of each of the four figures represents a plot of C^2, the output of CROCO using detected data, versus the relative shift, τ, for an integration interval of 18.7 milliseconds (700 data points), which spans each burst completely. The relative shift means that data point E_{0j} in Equation 4) (Chapter III) will be multiplied by $E'_{0\ j+k}$, where k = (digitization rate)X(τ). Here, station 1 (as indicated by the subscript on E_0) was MAIPU and station 2 was either UFRO-A or UFRO-B. In the figures it is seen that the range of shifts indicates that the MAIPU data table is being read 10 to 40 data points ahead of the UFRO table. The (b) lines of Figures V.5, V.6, V.7 and V.8 show $\sqrt{C_A^2 + C_B^2}$ plotted versus relative shift, where C_A is the value of C for a time near the center of the burst using heterodyned data from MAIPU and UFRO-A and C_B is similar except that data from UFRO-B is

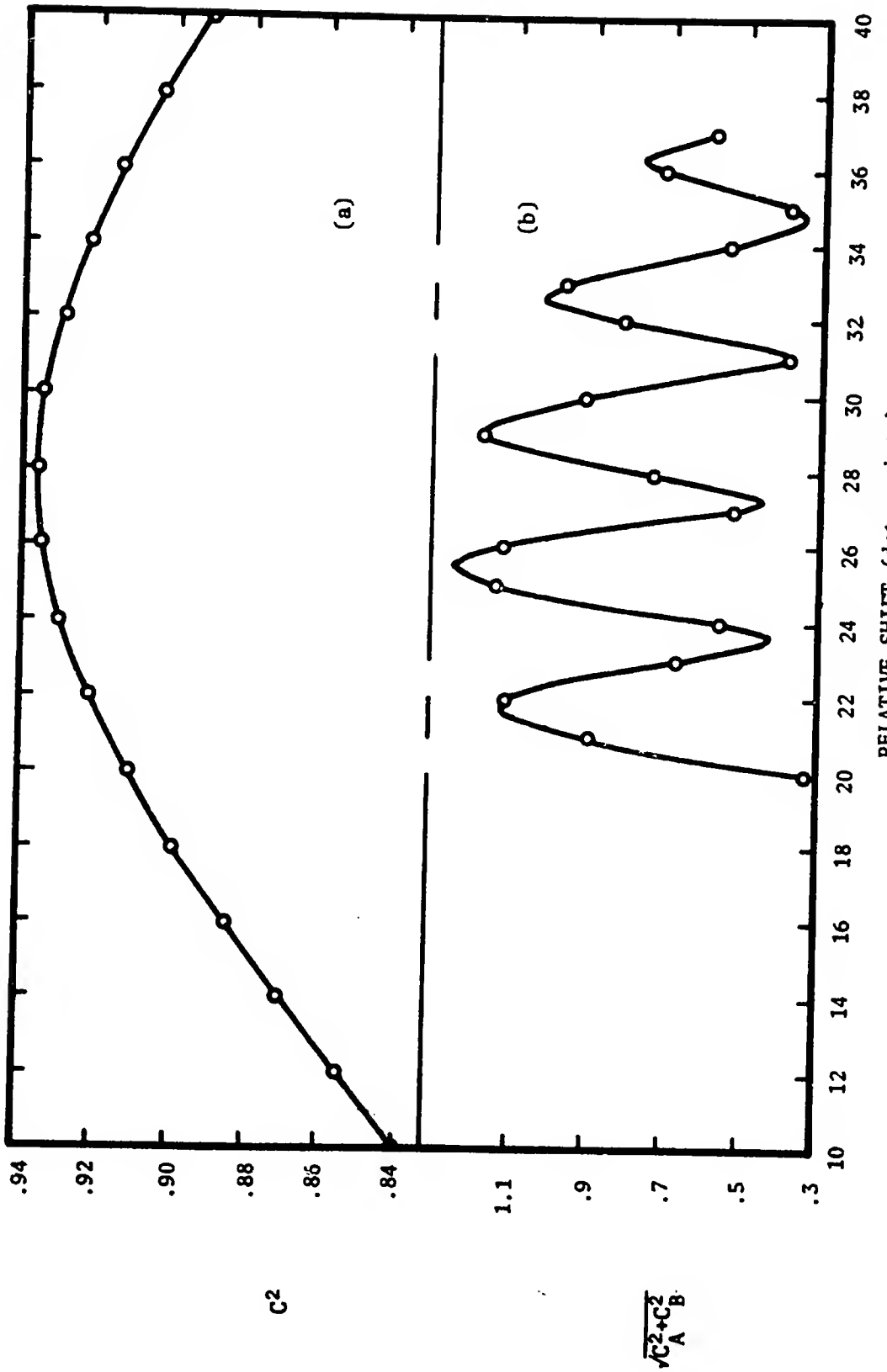

Figure V.5 -- (a) C^2 Versus Relative Shift for Burst Number 1. (b) $\sqrt{C_A^2+C_B^2}$ Versus Relative Shift for Burst Number 1.

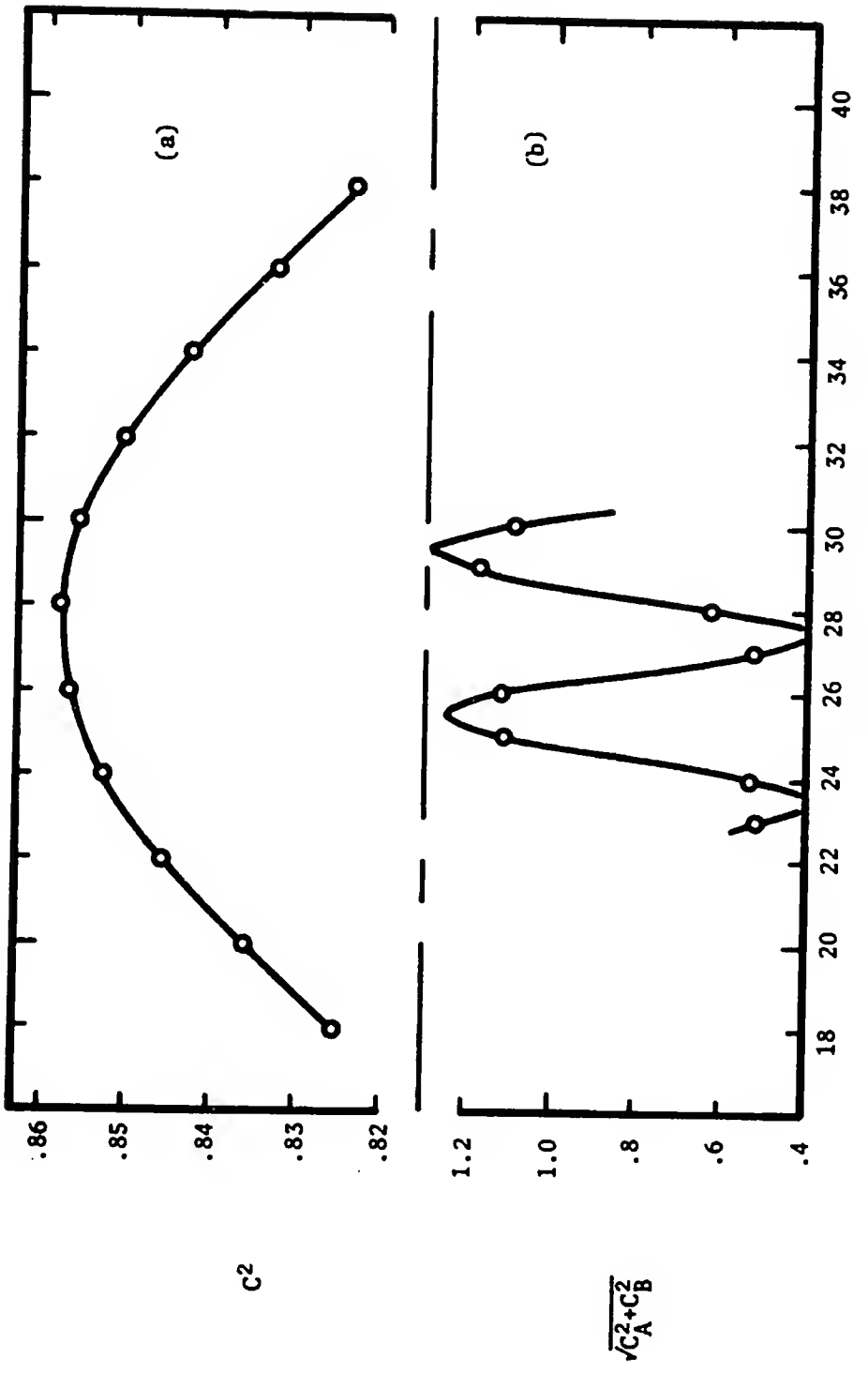

Figure V.6 -- (a) C^2 Versus Relative Shift for Burst Number 3. (b) $\sqrt{C_A^2+C_B^2}$ Versus Relative Shift for Burst Number 3.

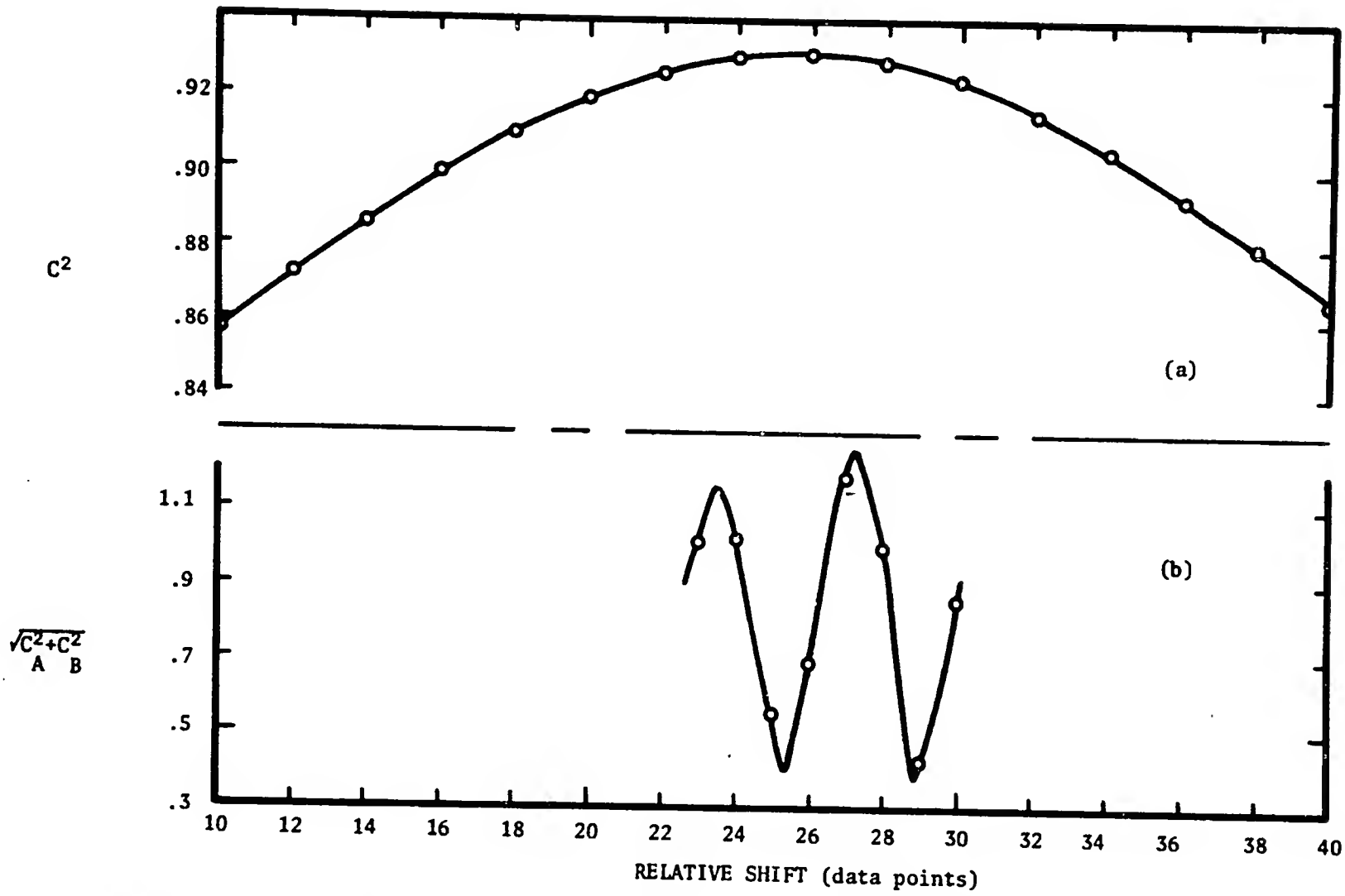

Figure V.7 -- (a) C^2 Versus Relative Shift for Burst Number 4. (b) $\sqrt{C_A^2+C_B^2}$ Versus Relative Shift for Burst Number 4.

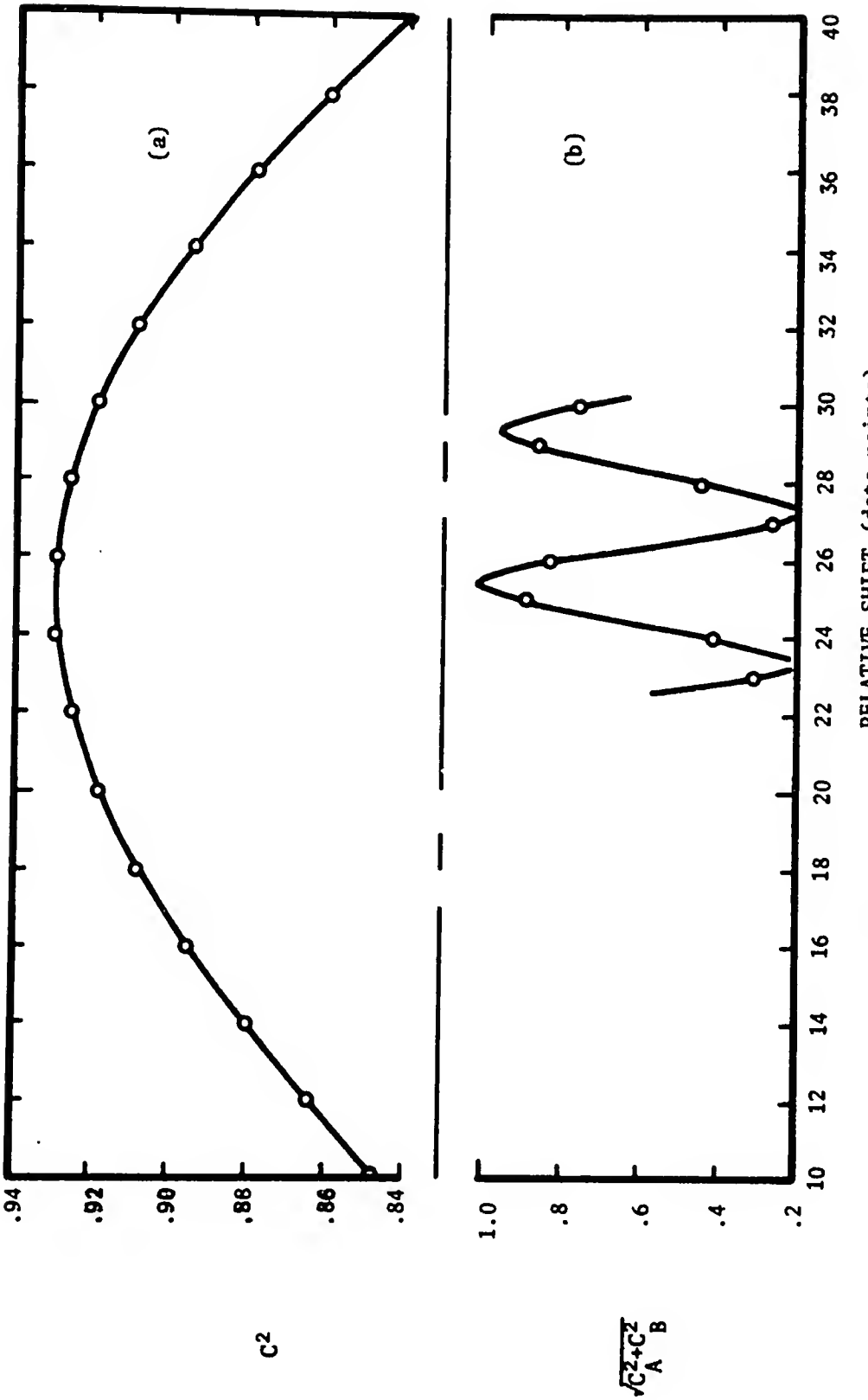

Figure V.8 -- (a) C^2 Versus Relative Shift for Burst Number 9. (b) $\sqrt{C_A^2+C_B^2}$ Versus Relative Shift for Burst Number 9.

used instead of UFRO-A. The integration interval, N, is 6.6 milliseconds (250 data points) and is located near the most intense portion of the burst.

It was shown in Chapter II that the best shift, i.e., that value of τ that maximized this square-root, could be found regardless of the phase of the fringes. In a burst as short as the ones under consideration, it is very unlikely that the fringe would be passing through a maximum during the burst, making this technique necessary. The oscillatory pattern of maxima and minima is due to the small ratio of bandwidth to center frequency that was used. The receivers were operating with Collins mechanical filters having 2.1 kHz bandwidths with passbands centered at 5 kHz. The Jupiter signal, as shown in the computer plots in Figure V.4a and c, is seen to be quasi-sinusoidal with the frequency varying in a random manner but over a relatively small range as restricted by the mechanical filters in the receiver I.F. amplifiers. It may be recalled that the autocorrelation function for a sine wave consists of a similar oscillation, except that all of the maxima are the same height and all of the minima are zero. A given maximum and the adjacent minimum are one-half of the period of the sine wave apart. In Figure V.5b it is seen that the maxima vary in height in an orderly way such that a central maximum can be detected at a relative shift of 25.5 data points. The spacing between maxima averages about 3.7 data points (1 millisecond) which is one-half of the period of the center frequency of the passband (5 kHz). This apparent halving of the "period" of C versus τ as compared to the autocorrelation example above is caused by the plotting of

$\sqrt{C_A^2 + C_B^2}$ which serves to "rectify" the cross correlation function.

Table V.2 summarizes the values of the best shift, τ_{best}, for both heterodyned and detected data for the bursts shown in Figures V.5, V.6, V.7 and V.8.

Table V.2

Burst No.	τ_{best} (het. data) Data Points	τ_{best} (det. data) Data Points	$\Delta\tau$ Data Points	Max. Timing Error
1	25.5	28.0	-2.5	(±1.8 d.p.)
3	29.4	27.6	+1.8	(±1.8 d.p.)
4	27.2	25.6	+1.6	(±1.8 d.p.)
9	25.4	25.0	+0.4	(±1.8 d.p.)

The quantity, $\Delta\tau$, is calculated from $\Delta\tau = \tau_{best}$(het. data) - τ_{best}(det. data).

There are two mechanisms that must be considered in order to determine the cause of the observed delays, $\Delta\tau$. The first concerns the accuracy in timing the arrival of a pulse considering that the pulse transversed a filter in a receiver which had a bandwidth of 2 kHz. The time for a significant change in signal level allowed by such a filter is on the order of 500 microseconds. However, the envelope cross correlation technique should be able to detect the arrival times at least an order of magnitude more accurately than this since the technique consists of matching the slopes of the rise- and fall-times of bursts received at different places. Any delay, $\Delta\tau$, less than 50 microseconds (1.8 data points) should be interpreted as being on the edge of, or beyond, the limit of detectability for data received using the 2.1 kHz bandwidth. The delay, $\Delta\tau$, measured for burst number 9 is clearly below

the minimum detectable delay since it has a value of 0.4 data points (11 microseconds). On this account, the evidence from burst 9 will not be considered further.

The second mechanism for consideration involves a beam of radiation from Jupiter being swept across the earth so that it is received at one station a short time before it is received at another station some distance away. Using the example given in Figure IV.12, the delay, $\Delta\tau$, would have a value of -3 time units (not data points) if station 1 were interpreted as UFRO and station 2 as MAIPU. Notice that the best relative shift for the heterodyned data in the example is zero time units and is +3 time units for the detected data (the envelopes), i.e., the MAIPU data table is read about 3 time units later than the UFRO data table in calculating the best shifted cross correlation function for the detected data. Therefore, using the example as a model, if the delays were caused by a sweeping beam, those $\Delta\tau$'s with a negative sign would indicate that the beam had a component sweeping from UFRO to MAIPU and a positive sign would indicate a sweep in the reverse direction. Table V.3 shows the values of $\Delta\tau$ expressed in milliseconds for bursts 1, 3 and 4 and the angular sweep rate parallel to the baseline components, D, D_{NS} and D_{EW}. These components subtended angles of 2.18 seconds of arc, 1.05 seconds of arc and 0.064 seconds of arc, respectively, as seen from Jupiter at the time the bursts were received. The $\Delta\tau$'s for bursts 3 and 4 are at the time resolution limit of the system, while that for burst 1 is just above the limit (within the range of detection). They are shown to indicate that, if sweeping beams are present, their sweep rates must have been at this rate or greater.

Table V.3

Burst No.	Δτ(msec)	Minimum Possible Sweep Rate (degrees/second) Parallel to D	Parallel to D_{NS}	Parallel to D_{EW}
1	-0.065	9.3	8.7	0.27
3	+0.048	12.5	11.8	0.37
4	+0.043	14.0	13.1	0.41
Max. Det.	±0.050	11.9	11.1	0.35

In Chapter IV it was indicated that the maximum east-west sweep rate parallel to the ecliptic, as caused by Jupiter's rotation, was on the order of 0°.01/second. It is obvious from Table V.3 that no beams were detected with such a slow sweep rate. A possible north-south sweeping might have been contributed by the motion of bunches of electrons along the curved magnetic field lines as they radiated. The model assumed in Chapter IV predicted sweep rates on the order of 5°/second or higher. It can be concluded from the data presented in Table V.3 that the bursts analyzed in this section were not connected with beams that swept at a rate less than 9°/second, if the beams were swept at all. Since the Δτ for burst 1 was within the time resolution limit, it should be interpreted as a reason to make more observations with broader bandwidth equipment. This one data point does not establish the existence of sweeping beams, but it should encourage an extended search.

V-5. Measurement of the Size of the Source

Figures V.9 and V.10 complete the graphical presentation of the cross correlation function plotted against relative shift for the rest of the bursts. Table V.4 is a summary of the best relative shifts for these bursts.

Table V.4

Burst No.	Best Relative Shift (data points)
2	29.6
5	27.0
6	23.5
7	28.2
10	23.5
11	24.3

Burst number 8 was not included since an error in locating the digitization interval for UFRO-B prevented using that data to calculate C_B.

There are two features in the figures that must be considered at this point. The first is the failure of each burst to have the same best relative shift. This accounted for by considering the physical relationship of the A-to-D converter sync tone and the data channel on the analog magnetic tape. A simple calculation shows that a dynamic skew of $0.^{\circ}6$ (a line drawn perpendicular to the edge of the tape changes by this angle with respect to the head gap as the tape moves) can account for the 6 data point range in best relative shift. This calculation assumes that the track separation is 0.125 inches and the

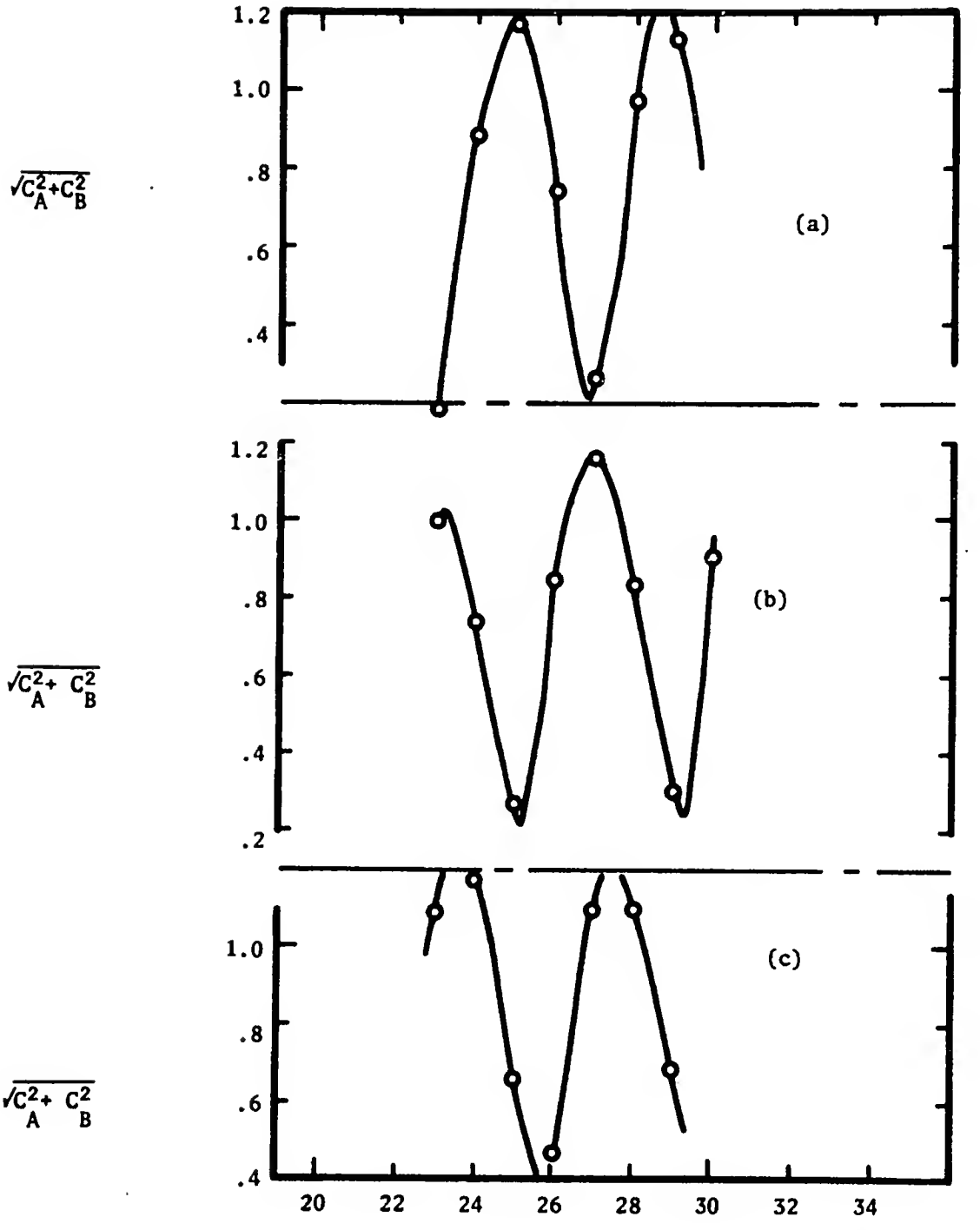

Figure V.9 -- $\sqrt{C_A^2 + C_B^2}$ Versus Relative Shift for (a) Burst Number 2, (b) Burst Number 5 and (c) Burst Number 6.

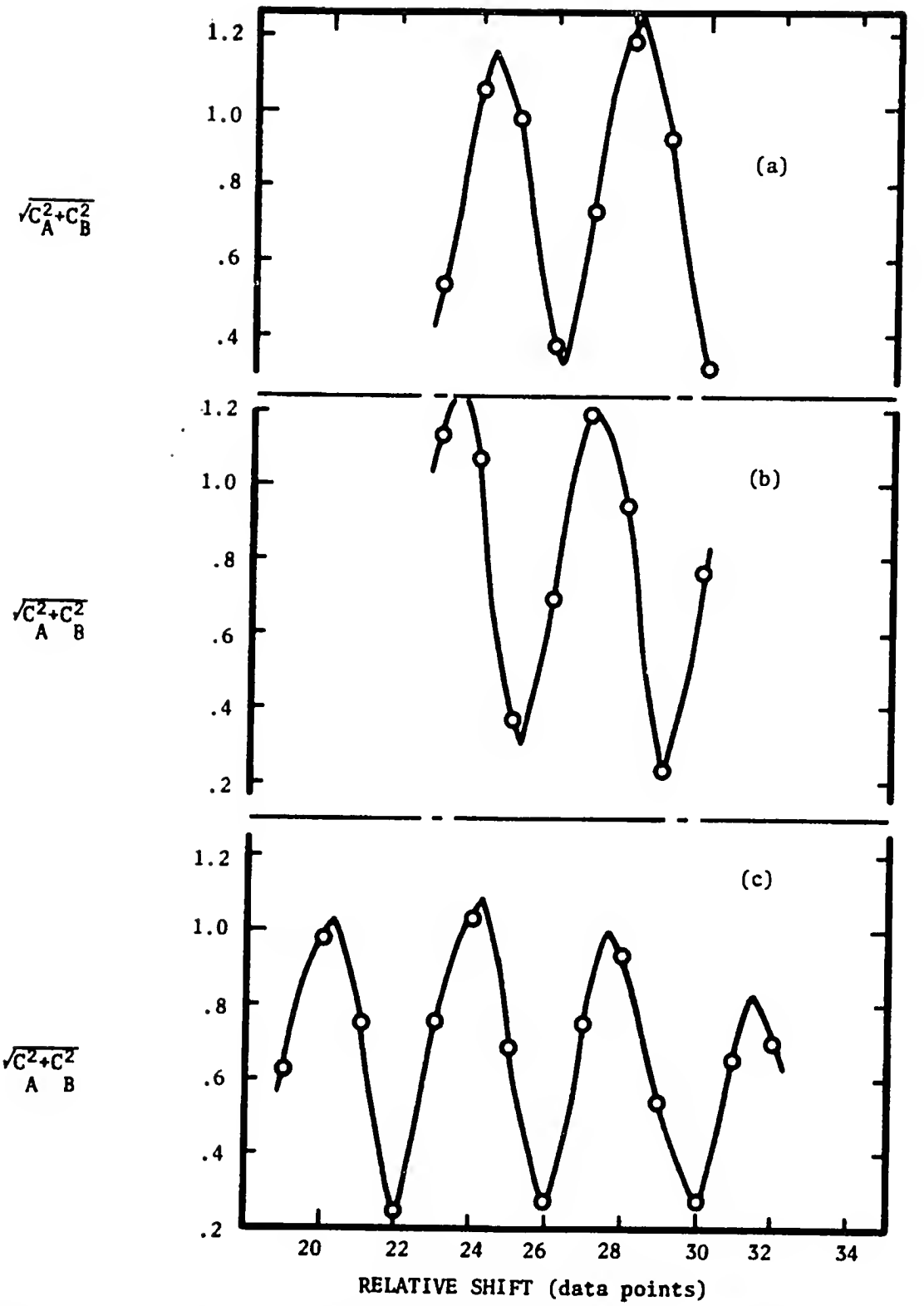

Figure V.10 -- $\sqrt{C_A^2+C_B^2}$ Versus Relative Shift for (a) Burst Number 7, (b) Burst Number 10 and (c) Burst Number 11.

recording rate is 7.5 inches/second. This value of dynamic skew has been detected in the 0.25 inch magnetic tape recorders used for recording the data. In the future the sync tone will be placed in the data channel to eliminate this problem.

The other feature that is obvious in Figure V.5, for example, is that the minima in $\sqrt{C_A^2 + C_B^2}$ versus relative shift do not go to zero. If the local oscillators at UFRO that provided the L.O. injection for the A and B channels had been exactly 90° out of phase, these minima would have been zero and the peak maximum would have been unity. The phase angle can be calculated for a burst that has a negligible amount of galactic contamination and can be compared with other similarly strong bursts to corroborate the possibility of this error. Using the equations on page 31 in Chapter II and choosing suitable values for the variables, the error can be evaluated as shown in the next paragraph.

Let $V_{\text{1st pair}} = C_A = V_0(s_\lambda)$ and $V_{\text{2nd pair}} = C_B = V_0(s_\lambda) \cos(90° - \sigma)$,

where σ is the deviation in the relative phase at UFRO from 90°. Solving the equations simultaneously for σ gives the following:

$$\sin \sigma = \left[\frac{C_A^2 + C_B^2}{V_0^2(s_\lambda)} - 1 \right]^{\frac{1}{2}}$$

. Using burst 1, which is relatively strong and is therefore more likely to have a fringe visibility close to unity, σ is found to be 34°. A comparison of the value of $\sqrt{C_A^2 + C_B^2}$ for the best relative shift from other strong bursts shows that σ does not vary appreciably over the 4 seconds covered by the data analysis. This is as would be expected for an equipment problem

such as this. It is not possible with the present data to determine the value of the fringe visibility without assuming that it is unity for at least one burst. Since C_A does reach a value of 0.8 for burst 1, this is not a bad assumption considering that C_A plotted as a function of time may not be at a fringe maximum during burst 1. Using this assumption, the σ-corrected value of $\sqrt{C_A^2 + C_B^2}$ averaged over all bursts (taking into account the varying degree of galactic noise contamination) is 1.01 ± 0.07. The maximum angular diameter of an incoherent, Gaussian distributed source is 0.1 seconds of arc (320 km at Jupiter). The mean angular size is 0.0 seconds of arc, with an error of +0.1 seconds and -0.0 seconds.

It was hoped at the time that the data was digitized that the fringe rate (C_A plotted versus time) would be such that data spaced over the approximately 4-second interval chosen would allow the reconstruction of the fringes. A graph of C_A versus time is given in Figure V.11, where the bursts and their values of C_A are labelled. Some segments of data were long enough to allow a portion of the fringe to be seen. In this case lines were drawn to show the part of the fringe that is visible. It was, in general, impossible to determine one curve that fit all of the values of C_A plotted versus time. While this might be interpreted as due to the "jumping about" of the source causing the fringes to fail to maintain phase, it is felt that due to the lack of values of C_A between those plotted, the interpretation should be withheld until the intermediate data points can be calculated.

Using the fraction of the fringe period that is present in burst 7, a value for the fringe rate at that time can be calculated. It is on the

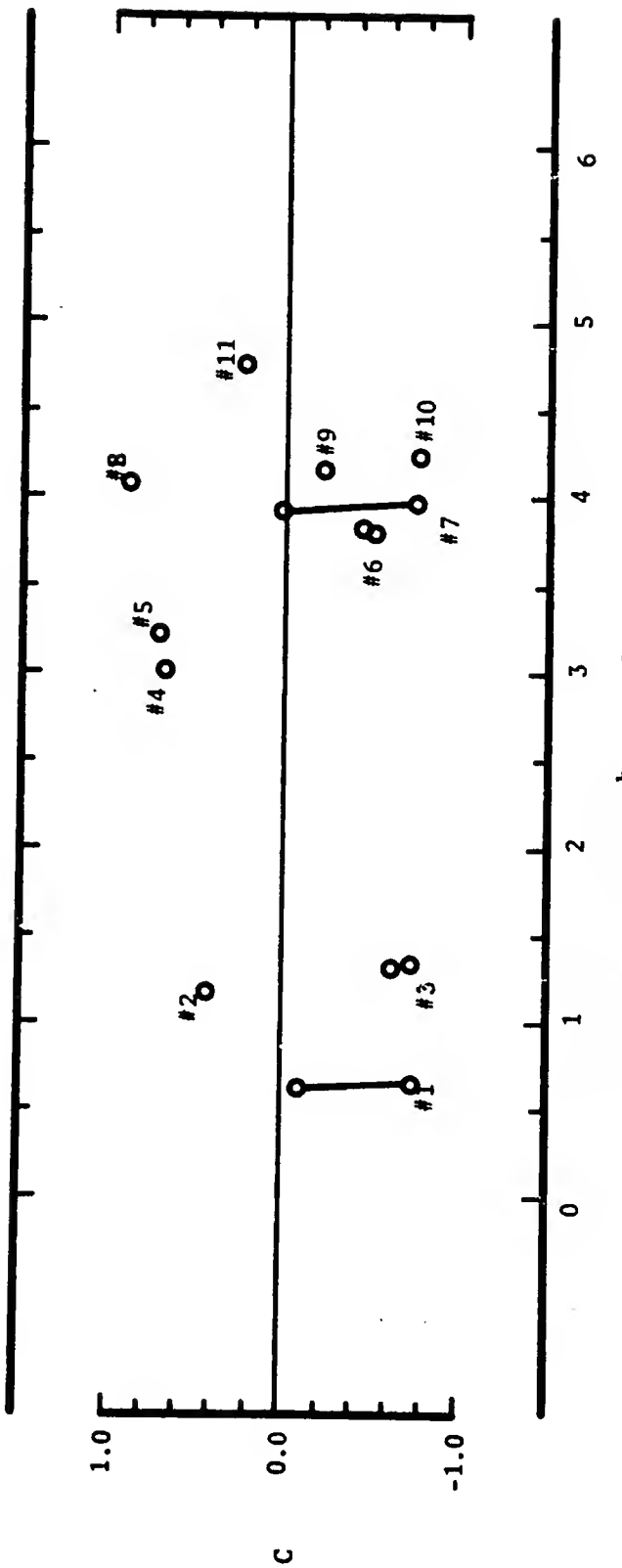

Figure V.11 -- Cross Correlation Function (C) Versus Time for all S-Bursts in Series. Connected Data Points Are Taken from the Same Burst Number.

order of 9 fringes/second, which compares favorably with the predicted value of 9.3 fringes/second due to the earth's rotation.

V-6. Brief Summary of the 1970 Data Analysis

While an upper limit of 11.9 degrees/second has been placed on the beam sweep detection capability of the system used in 1970 by the narrow bandwidth of the receivers, it was shown that at least one burst seemed to indicate a sweep rate a little less than this value, about 9 degrees/second. It is concluded that while all of the apparent sweep rates are so close to the limit of detectability that none may be significant, there is sufficient evidence for beam sweeping to justify a continuation of the search with wider bandwidth receivers. If the observed apparent sweep rates are real, they would indicate beaming from electron bunches moving along curved field lines. Sweep rates due to rotation effects would be much lower and are therefore ruled out.

The maximum fringe amplitude actually measured was 0.8, but it was felt that this value corresponds to a point not at a fringe maximum. For the baseline used, the σ-corrected $\sqrt{C_A^2 + C_B^2}$ averaged over all bursts having a value of 1.01 ± 0.07 indicates that the maximum size of the source (as given by the extreme lower limit of 0.94) is less than 0.1 seconds of arc, if the source is assumed to be an incoherent, Gaussian distributed radiator.

Since so few segments of the fringe were calculated, no evidence could be cited concerning the stability of the fringes and hence of the source. It is indicated that in the future, when A-to-D conversion

facilities become available that remove the limit on the number of data points that can be handled, this data should be reprocessed for the purpose of examining the source position stability problem.

CHAPTER VI

ANALYSIS OF DATA RECEIVED IN 1971

VI-1. Instrumentation, Timing and Baseline Orientation

The receiving systems described in the previous chapter for the 1970 Jupiter season were used again in 1971 with a few modifications. Two more stations were added to the University of Florida interferometer network. A receiver identical to the one used in Chile was put on the air at Western Kentucky University Radio Observatory near Bowling Green, Kentucky. A commercial receiver employing the same local oscillator frequency synthesis technique as used in the other interferometer receivers was operated by members of Southwest Research Institute at a radio observatory near San Antonio, Texas. The observing sessions during the 1971 apparition produced several reels of magnetic tape containing mostly L-Burst activity. A single L-Burst, found on tapes from UFRO and MAIPU, is discussed in this chapter. There were several promising bursts on the tape from SWRI Radio Observatory that were seen on chart recordings of the detected data from that station. No chart recordings have been made from the tapes from WKU.

The removal of the rubidium vapor clock that was used at MAIPU in 1970 required that alternate means of calibrating the local clock be used. The one-second ticks generated by a stable crystal oscillator

at the National Observatory in Chile were used to key a tone which amplitude modulated a radio transmitter. The transmitted signal was received simultaneously at MAIPU and at the NASA satellite tracking station near Santiago, Chile. Since the distances to the receiving stations are short and are about equal, the time correction supplied by the NASA station could be applied directly to the local one-second ticks generated at MAIPU. The NASA time correction was not available when the data was cross correlated so the correction will be compared with the value of the best relative shift presented later in this chapter.

At the UFRO the LORAN-C receiver, having been repaired, was used to supply the LORAN-C bursts to the tape recorder. The one-second tick transmitted by the East Coast chain master station at Cape Fear, South Carolina, was used to calibrate the locally generated time marks at the UFRO. Since the LORAN-C bursts were time multiplexed onto the data channels, the time correction was applied after the slowed-down tapes were displayed on chart recordings. Transmission time from the master station was taken into account. The method used is outlined by L. D. Shapiro in two papers (1968a and 1968b).

The L-Burst discussed in this chapter was received at UFRO and MAIPU on 12 April 1971 at $8^h51^m23^s.387$ U.T. Figure VI.1a shows the directions to the sun and to Jupiter as seen from a point above the earth at the North Pole of the ecliptic. The figure is a projection of these directions in the plane of the ecliptic. The right ascension of Jupiter was $16^h16^m38^s$, and its declination was -20°17'30". The right ascension of the sun at the time the burst was received was $1^h20^m20^s$.

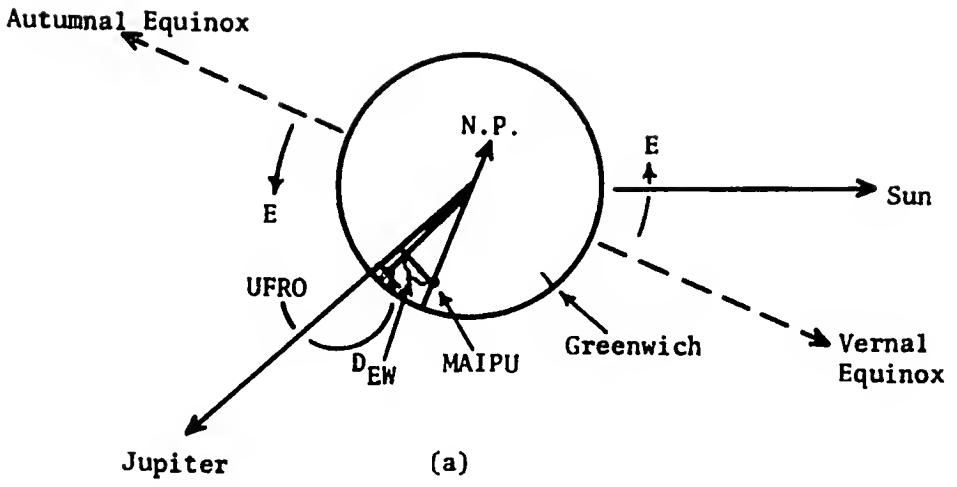

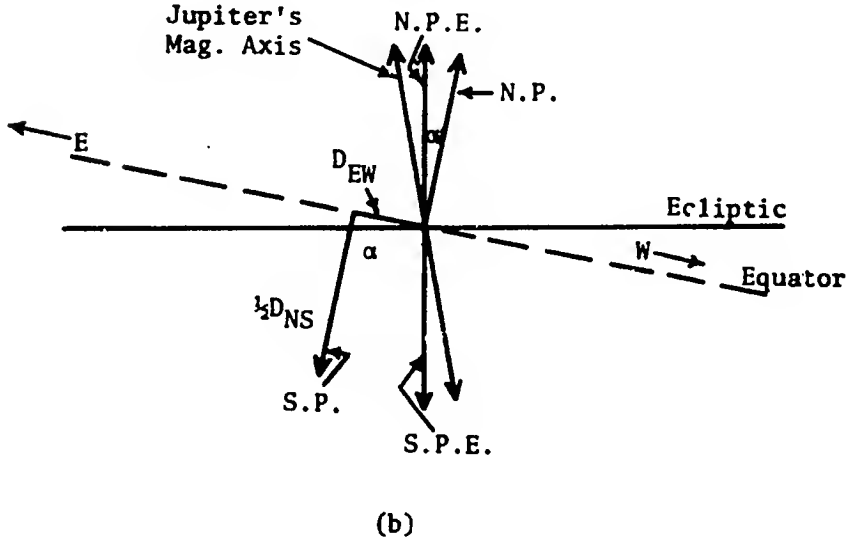

Figure VI.1 -- (a) View of Earth, Jupiter and the Sun from Above the North Pole on 12 April 1971, (b) D_{NS} and D_{EW} Projected on the Plane Perpendicular to the Line-of-Sight to Jupiter.

The straight-line distance (i.e., chord of the great circle arc) from UFRO to MAIPU is 6980 km (419,000 λ) and is designated as D. Figure VI.1b shows the components of this distance projected on a plane that is perpendicular to the line-of-sight from the stations to Jupiter. The figure shows how the baseline components would appear to an observer located at the center of the earth facing Jupiter if he used the directions on the side of the earth facing that planet. D_{NS} is the component of D parallel to the earth's rotational axis projected on the plane perpendicular to the line-of-sight. It had a length of 6240 km at the time the burst was received. D_{EW}, the component of the baseline, D, parallel to the earth's equator projected onto the plane perpendicular to the line-of-sight, had a length of 1570 km. B_{EW} is the length of D parallel to the ecliptic projected onto the same plane. Its length can be calculated from $B_{EW} = D_{NS} \sin \alpha \pm D_{EW} \cos \alpha$, as given in Chapter IV. Using $\alpha = 11°$, B_{EW} is found to have a length of 2730 km. The component of D parallel to the plane of the earth's equator, coupled with the earth's rotational angular velocity, determines the natural fringe rate of the interferometer. The length of this component is 2125 km, and the natural fringe rate has a period of 0.108 seconds or a frequency of 9.3 Hz.

VI-2. The Nature of the Received Data

The L-Burst that was received at UFRO and MAIPU on 12 April 1971 was recorded on analog magnetic tape as outlined in Chapter III. The antennas at both stations were right-hand circularly polarized. The burst was located for study by scanning the tapes while listening and recording on a chart recorder any sections containing interesting activity.

Of the many bursts received during the morning of 12 April, this was the only one that was received simultaneously at both stations. Figure VI.2 shows the actual chart recordings of the detected data, which start at $8^h51^m23^s$ U.T. and last approximately 3.75 seconds. The only marks visible in the time channels are one-second ticks. The local one-second mark on the MAIPU record (Figure VI.2a) lags the National Observatory time mark by 873.0 milliseconds. The UFRO one-second marks lag the LORAN-C time reference by 586.6 milliseconds. The envelopes are well correlated in appearance, and they arrived at each station simultaneously within the time resolution of the chart recordings. The ratio of the Jupiter signal + galactic noise power to the galactic noise power alone was on the order of 9 db for the MAIPU burst and 8 db for the UFRO burst.

The corresponding sections of the two original analog data tapes were slowed down by a ratio of eight-to-one and recorded on a single length of magnetic tape. The slow-down was required in order for the A-to-D converter on the IBM 1800 to reach the desired digitization rate of 37,500 data points/second in each channel. The bursts were arranged on the tape in such a way that one minute of MAIPU data was followed by one minute of UFRO-A data which, in turn, was followed by one minute of UFRO-B data. The burst of interest was contained within the data from each station on the tape. The place to begin digitization was marked on each section of the tape for visual identification by the computer operator.

The program, DACSX, signalled the operator of the IBM 1800 to start the analog magnetic tape drive and immediately start the computer. Digitization proceeded at a rate of 37,500 data points from each channel

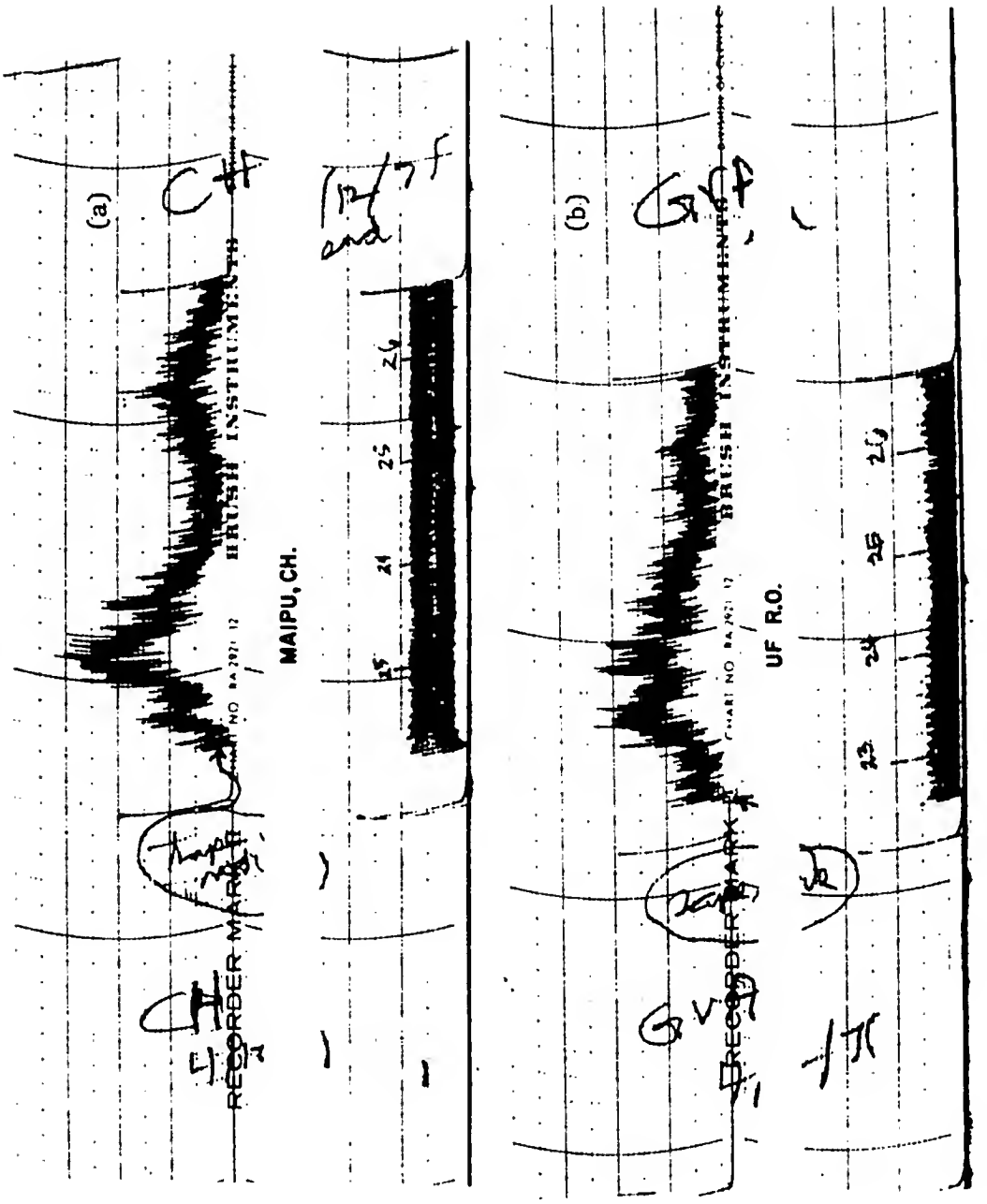

Figure VI.2 -- Actual Chart Records of Detected Data from MAIPU (a) and UFRO (b). Data Starts at $8^h51^m23^s$U.T.

(one data channel and one time channel) under control of the sync tone in the time channel on the analog magnetic tape. At the end of six seconds, digitization stopped. The programs, LOOK and TRNFR, found and saved 84,480 data points from each channel (a total of 168,960 points from one station). The process was repeated for the same time increment from the other stations. The 1,060 cards for each station were punched from the data channel using the column binary format (one data point per column on the card). The time channel data points were printed on the line printer along with the data channel points in order to verify that the synchronizer was working. A segment of the heterodyned data channel was plotted on the incremental plotter by the computer. The plots, starting about 716 milliseconds into the burst, are shown in Figure VI,3. The points marked A are aligned when the two data channels have the correct relative shift.

The 3,180 cards were read by the IBM 360 with the help of the Assembler Language converter program mentioned in the previous chapter. The data was written on digital magnetic tape in a form that CROCO, with a little modification, could read. The data format on the tape was arranged such that there were 24 records of 80 data points each (1920 data points) from MAIPU followed by 24 records of data from UFRO-A and then followed by 24 records of data from UFRO-B. The cycle was repeated 44 times in order to write all 253,440 data points on the digital tape.

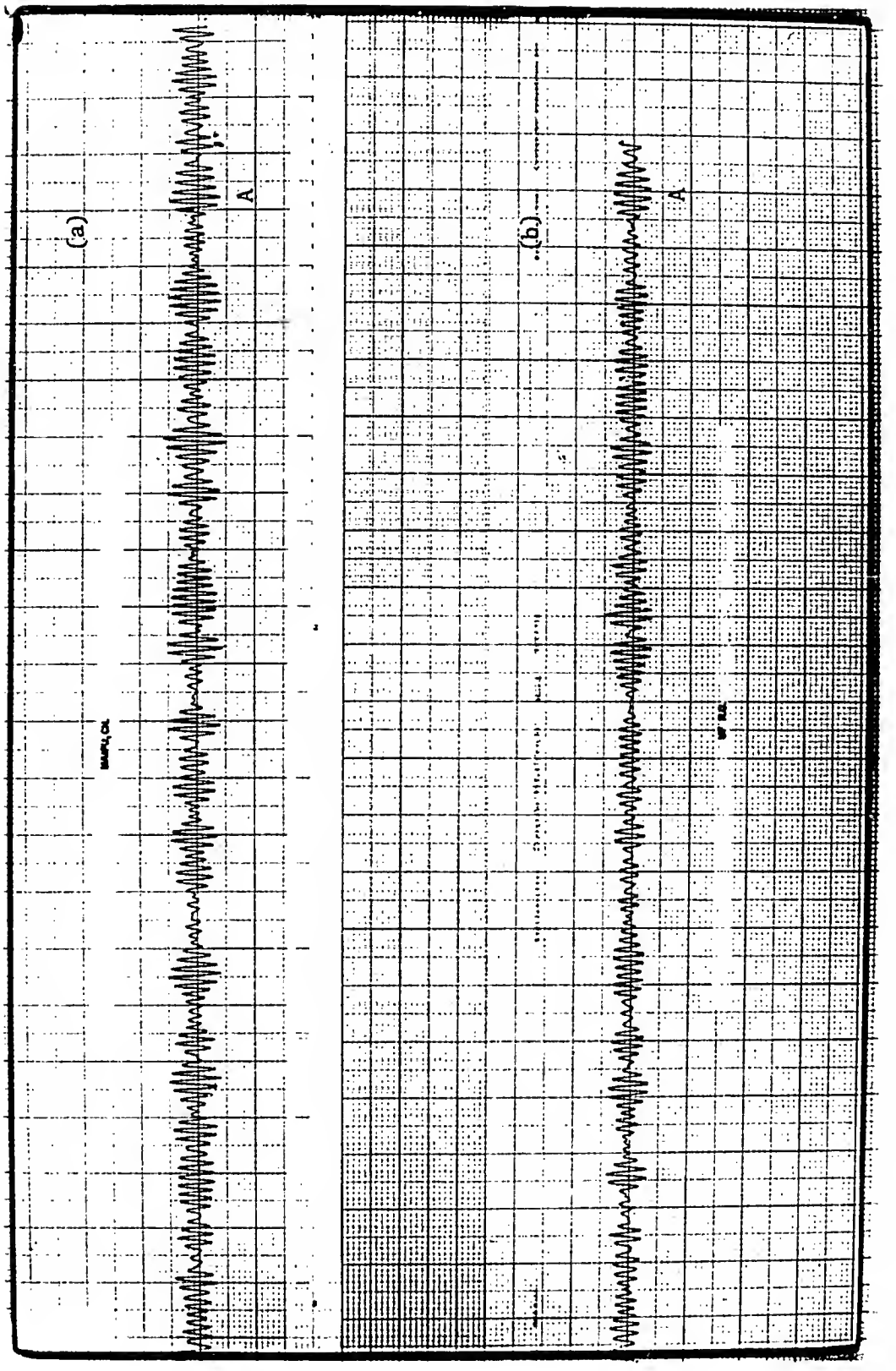

Figure VI.3 -- Computer Plot of Data from MAIPU (a) and UFRO (b) Showing a Region Located 716 Milliseconds After the Beginning of the Burst. Features Marked A Are Aligned for the Best Relative Time Shift.

VI-3. Analysis of the Data

The modifications to the input section of CROCO are shown in the Appendix. They cause CROCO to read 24 records from MAIPU, then read the corresponding 24 records from UFRO-A followed by the same part of UFRO-B. The particular section of the burst to be considered is selected by the variable IFIL1 which ranges in value from 1 to 44 and selects 1920 data point segments of the burst, accordingly. IFIL2 has values of 1 or 2, thereby selecting data from UFRO-A or UFRO-B, respectively, for comparison with the MAIPU data. The square-law detector adaptor section given in Chapter V can be inserted, as before, to calculate C^2, the cross correlation function of the envelopes.

Using the square-law detector adaptor section, CROCO calculated C^2 as a function of relative shift for the section of data that was plotted in Figure VI.3 (the 1920 data point segment beginning at 716 milliseconds after the starting time of digitization). The integration period was 0.018 seconds (N = 700 data points). A plot of C^2 versus relative shift is shown in Figure VI.4a. The maximum value of C^2 is 0.65 and occurs at a relative shift of -99 data points. The relative shift corresponds to the data table for UFRO being read 99 data points ahead of the MAIPU data table. The shift accounts for 2.225 milliseconds of the 3.7 millisecond correction supplied by the NASA satellite tracking station to the time standard of the National Observatory of Chile. The remaining 1.5 milliseconds can be accounted for by the time required for the burst to traverse the difference in distance between the two stations and Jupiter. The time shift corresponds to about 450 km, with UFRO nearer than MAIPU to Jupiter, which is consistent with Figure VI.1a.

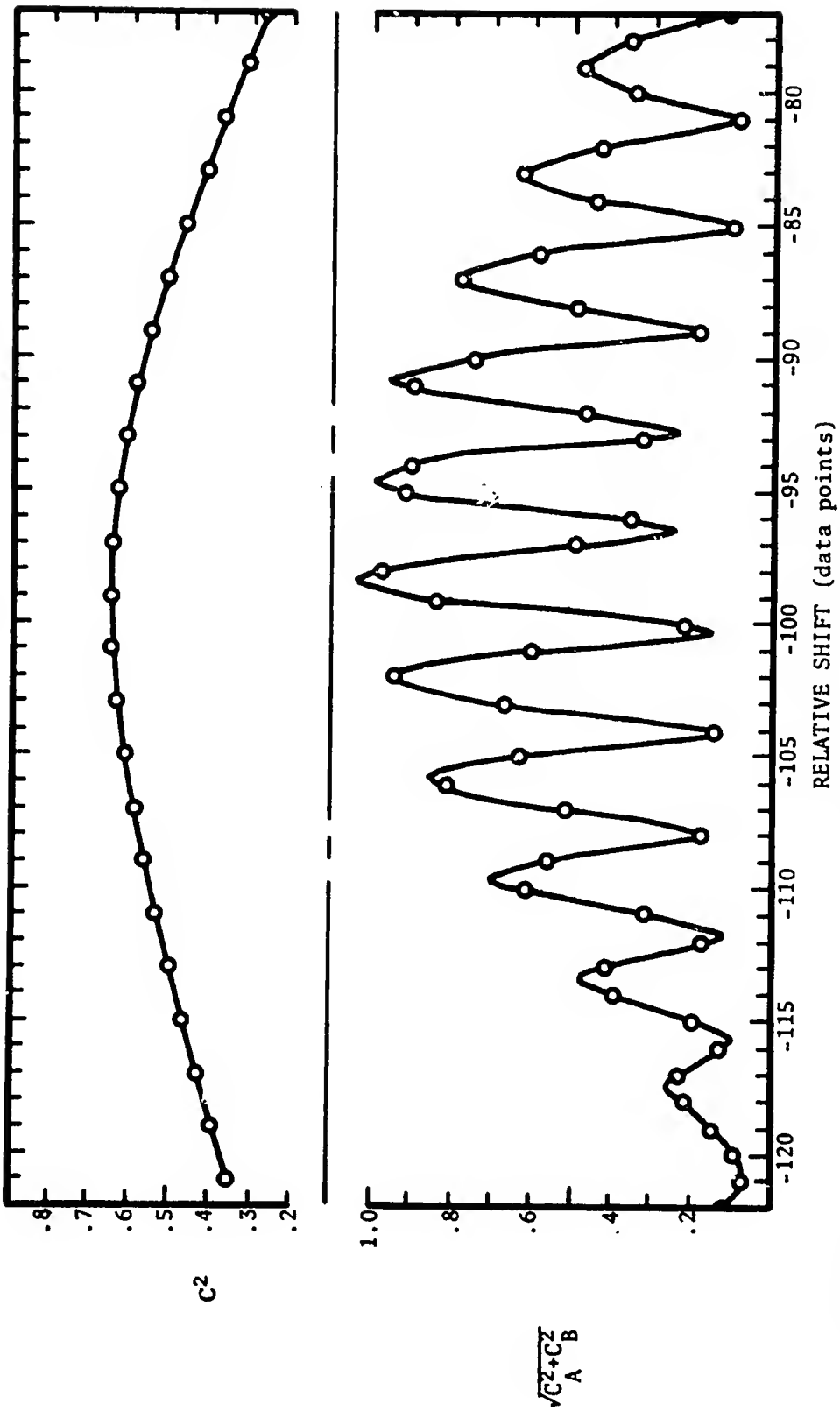

Figure VI.4 -- (a) C^2 Versus Relative Shift and (b) $\sqrt{C_A^2+C_B^2}$ Versus Relative Shift for Segment Number 14 of L-Burst.

Removal of the square-law detector adaptor section allowed the heterodyned data to be cross correlated using CROCO. The phase quadrature channels from UFRO were each correlated with the MAIPU data to form cross correlation functions $C_A(t,\tau)$ and $C_B(t,\tau)$. The graph of $\sqrt{C_A^2 + C_B^2}$ versus relative shift, τ, for time (t) set at 716 milliseconds into the burst, is given in Figure VI.4b. The integration period was 12 milliseconds (N = 450 data points). Examination of the central maximum in this graph shows that the best relative shift for the heterodyned data is 98.4 data points. From similar graphs for successively later times in the burst, the best relative shifts were seen to vary by about 0.4 data points in the next 12 milliseconds. This is attributed to the dynamic skew in the analog magnetic tape recorders. The effect is of no concern in the data considered in this chapter. Another mechanical defect is noted in Figure VI.4b as it was in Chapter V. The maximum value of $\sqrt{C_A^2 + C_B^2}$ is greater than unity, indicating that the local oscillator injections at UFRO were not exactly 90° out of phase. Since the best relative shift can still be determined and since the burst had a duration greater than one fringe period, no harm was done by this maladjustment.

Figure VI.5a shows the chart recordings of detected data from the two stations for a time interval containing the L-Burst. Figures VI.5b and c show $C_A(t,\tau)$ plotted versus time for a relative shift of -99 data points and the denominator of the cross correlation function (NORM) plotted versus time for the same shift. The maximum value for the cross correlation function, $|C(t,\tau)_{max}|$, occurs for a fringe maximum near t = 0.64 seconds and equals 0.86. An equation given by

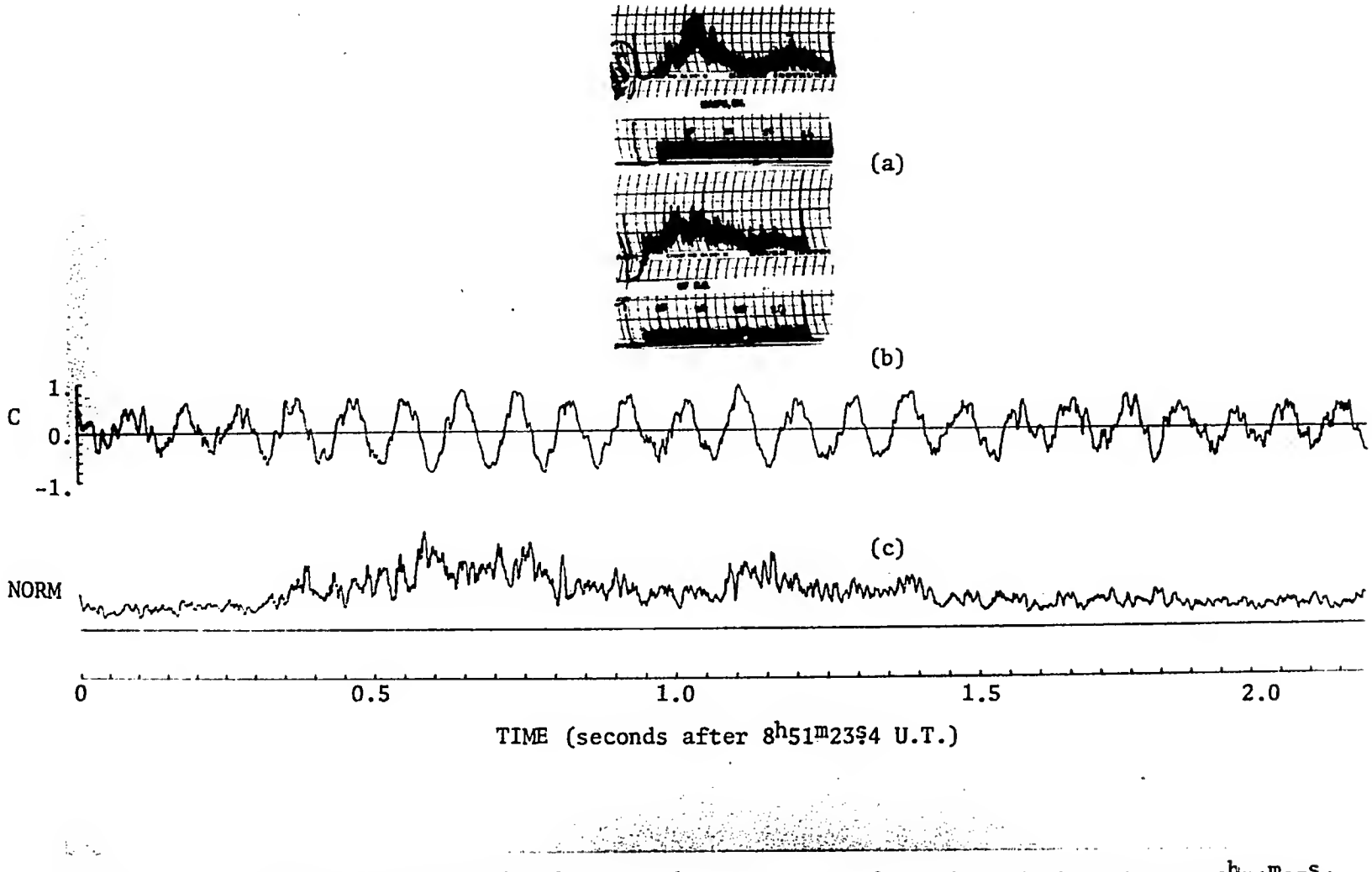

Figure VI.5 -- Actual Chart Records of Detected Data Running for 4 Seconds Starting at $8^h51^m23^s.4$ Are Shown at (a). Cross Correlation Function (b) and Normalization (c) Plotted Versus Time.

Brown (1970) can be used to correct this value for the galactic noise contamination. The equation is $C_n = C' \left[1 + \frac{1}{\left(\frac{P_{JG}}{P_G} - 1\right)} \right]$, where C_n is the corrected correlation coefficient, C' the uncorrected value, P_{JG} the power due to the Jupiter signal + the galactic background and P_G the galactic noise power alone. As indicated in Section VI-2, the power ratio was 6.3, which makes the correction factor for this particular data point 1.19. The corrected value of the amplitude of the cross correlation function at t = 0.64 seconds is, then, 1.02. If all fringe maxima are corrected for the galactic noise contamination at the times that they occur, their average value will be 1.02 with an RMS deviation of 0.10. Within the accuracy of the correction method, it is seen that the heterodyned Jupiter signals are well correlated.

VI-4. Physical Conclusions from the 1971 L-Burst

The corrected average value of the amplitude of the cross correlation function, 1.02 ± 0.10, indicates that the source of this burst was not resolved by this interferometer. Since the baseline was 419,000 λ, it is concluded that an incoherent, Gaussian distributed source must have had an angular diameter of less than 0.1 second of arc using the extreme value of the corrected fringe amplitude consistent with the RMS deviation (0.92). The maximum linear diameter of the source must have been less than 330 km ± 10% on Jupiter.

The temporal fringes shown in the graph of the cross correlation function plotted versus time in Figure VI.5b are caused by at least two factors. The greater part of the fringe rate is due to the rotation

of the earth carrying the interferometer antenna pattern in an eastward sense with respect to the Earth-Jupiter line. The fringe rate due to this effect alone is 9.3 Hz, corresponding to a period of 0.108 seconds. The average fringe rate was 11.2 Hz (0.089 second period) which indicates that other factors are also present. The most probable factor is that the local oscillators at UFRO and MAIPU were offset by a small frequency, γ in Equation 1) in Chapter II. If this were the only factor, the value of γ would have been 1.9 Hz, which corresponds to the local crystal oscillators being offset 0.16 Hz. Another possible contributing factor involves the motion of the source with respect to the Earth-Jupiter line. Alternatively, the difference between the natural fringe rate (due to the earth's rotation) and the observed fringe rate can be accounted for by assuming that the source has a westward component of velocity equal to 440 km/second at Jupiter. The actual case, no doubt, involves a certain amount of both effects; however, the frequency calibration of the local crystal oscillators was not accurate enough to rule out the frequency offset factor. The relative orbital motion of the earth and Jupiter at the time of the burst was less than 16 km/second which would contribute very little to the fringe rate.

The stability of the fringe period can be used to give information on any changes in the constant relative motion of the source and the antenna pattern. Figure VI.6 is a graph of the times of the + to - transitions of the fringe plotted versus the fringe number. It will be noticed that there are no major trends away from the line, which has a slope equal to the average fringe period line (drawn for a period of 0.089 seconds). This implies that the source did not undergo uniform acceleration during the burst period (about 2.2 seconds).

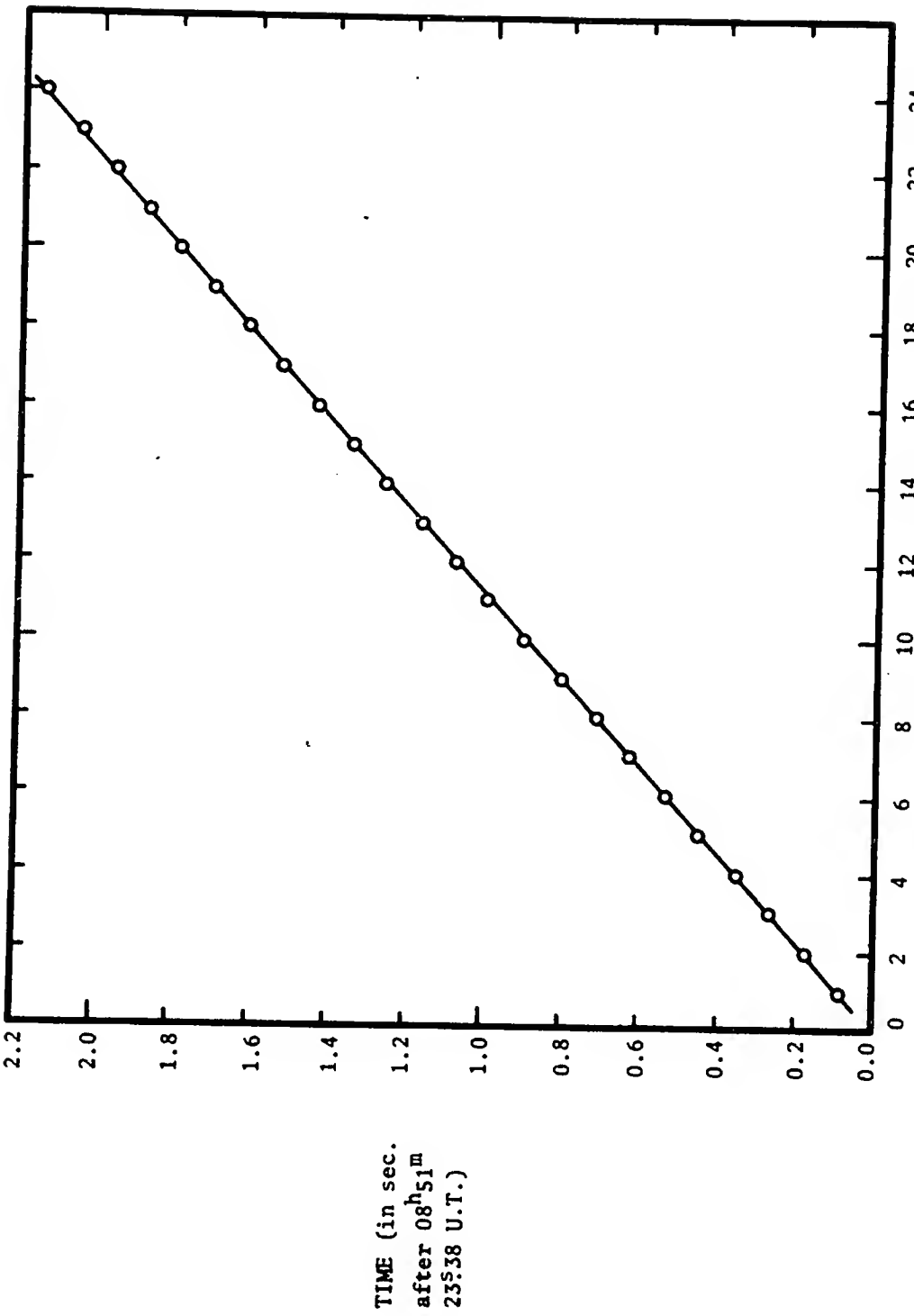

Figure VI.6 -- Time of the + to - Transition of the Fringe Versus the Number of the Fringe for the L-Burst Recorded on 12 April 1971.

Further, the source did not "jump about" randomly since this effect would have caused abrupt changes in the phase of the fringe pattern. This would be manifest in Figure VI.6 as abrupt major deviations of the data from the straight line having the average fringe period.

Figure VI.7 is a graph of the fringe period of each cycle versus the fringe number. There is a certain amount of variation of this data about the average fringe period line (drawn for a period of 0.089 seconds). The RMS standard deviation of the periods from the average period is 4.7 milliseconds or 5.3%. The deviation could be accounted for by a combination of two effects. The first is that the source may be "jumping about" in a random manner. An average "jump" of about 5% of the distance between first nulls of the interferometer pattern would correspond to a distance of 85 km on Jupiter. The greater amount of the deviation is probably caused by the variation in best shift due to dynamic skew in the analog tape drives. The output of CROCO for various relative shifts shows this effect to amount to about 5%.

The theory of Douglas and Smith (1967) concerning the formation of L-Bursts proposes that the structure for many bursts is caused by an isophotal pattern induced by inhomogeneities in the solar wind, having dimensions on the order of 100 km, drifting across the receiving station. Their data indicates that for stations separated on the order of 100 km in an east-west direction parallel to the ecliptic, those bursts that can be correlated between stations tend to arrive at one station before the other. The time of arrival is determined by Jupiter's position with respect to opposition. The burst received by the University of Florida interferometer showed good envelope correlation on a baseline that was an order of magnitude longer than the ones used by Douglas and Smith.

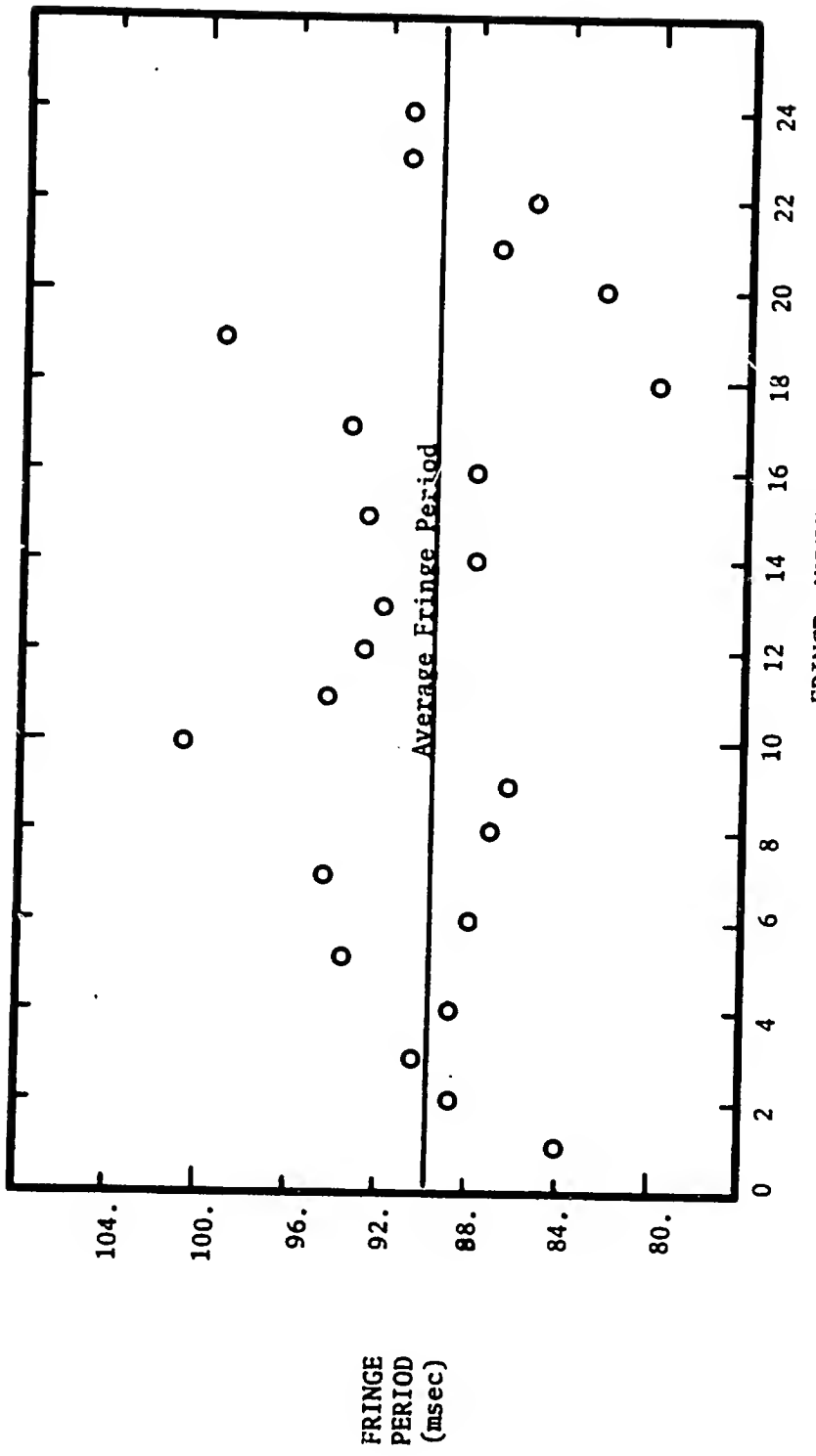

Figure VI.7 -- Fringe Period Versus Fringe Number for the L-Burst of 12 April 1971.

Since the baseline length parallel to the ecliptic, B_{EW}, is so much longer than the coherence length of the supposed inhomogeneities in the solar wind, it must be concluded that the shape of the envelope of the 1971 L-Burst was established at, or near, Jupiter by a process different than that proposed by Douglas and Smith. The most likely conclusion is that the source on Jupiter can impose time variations on the order of the ones seen in Figure VI.2. There was no delay in the arrival time of the burst at the two receiving stations, despite the large component of the baseline parallel to the ecliptic.

In summary, the source of the L-Burst of 12 April 1971 has been shown to be smaller than 0.1 second of arc, if it is assumed to be an incoherent, Gaussian distributed radiator. Its motion with respect to the antenna pattern was constant, and any "jumps" had a component parallel to the baseline of less than 5% of a fringe (85 km on Jupiter). The source apparently imposed all observed time variations on the envelope, since they could be correlated for such a long baseline.

CHAPTER VII

CONCLUSIONS

For the past three years, Jupiter has been monitored at 18 MHz using a very-long-baseline interferometer for the purpose of measuring some properties of its decametric radio source. Several successful sets of data were recorded using two different receiving systems that have been discussed in previous chapters. Both S- and L-Bursts were observed and analyzed. These bursts all originated from approximately the same source, B, under the same Io phase condition (Io was approximately 90° from superior geocentric conjunction). Table VII.1 shows the LCM-Io coordinates for the three sets of data.

Table VII.1

Date and Time of Data	Central Meridian Longitude System λ_{III} (1957.0)	Angle from Superior Geocentric Conjunction of Io
2 January 1969 8^h22^m UT	152°	96°
30 April 1970 9^h36^m UT	170°	90°
12 April 1971 8^h51^m UT	145°	97°

The measurements of the size of the source can best be summarized by presenting Figure VII.1, which shows the fringe visibility function for an incoherent, one-dimensional Gaussian distributed radiator plotted versus baseline length. The three curves correspond to the fringe visibility functions for sources having angular diameters (at the half power points) of 0.5, 0.25 and 0.1 seconds of arc. The measured values of the cross correlation coefficient, C, have been determined by averaging all values for each type of burst for a given baseline length. The average value of C for an L-Burst was found by summing the galactic noise-corrected fringe amplitude at all fringe maxima (both positive and negative) in the burst. This sum was divided by the number of maxima used. The RMS deviation was then calculated and used to determine the extent of the error bars in the figure. The equation for correcting the fringe amplitude for galactic noise contamination was given in Chapter VI and is only reasonably accurate for fringe amplitudes near unity. Some of the error is due to the correction process. The single data point on Figure VII.1 that was determined from S-Bursts is less accurately known than the data points for the L-Bursts.

The $\sqrt{C_A^2 + C_B^2}$ for all S-Bursts, using the value found for the best shift, was corrected for the non-quadrature local oscillator condition at UFRO by assuming that the fringe visibility of burst 1 was unity. This determined the actual phase offset of the local oscillator injections, which was applied to the other bursts along with the galactic noise correction. The average of these values and the RMS deviation are plotted in the figure.

It is concluded that the most probable angular diameter of the source, if it is incoherent with a Gaussian angular distribution,

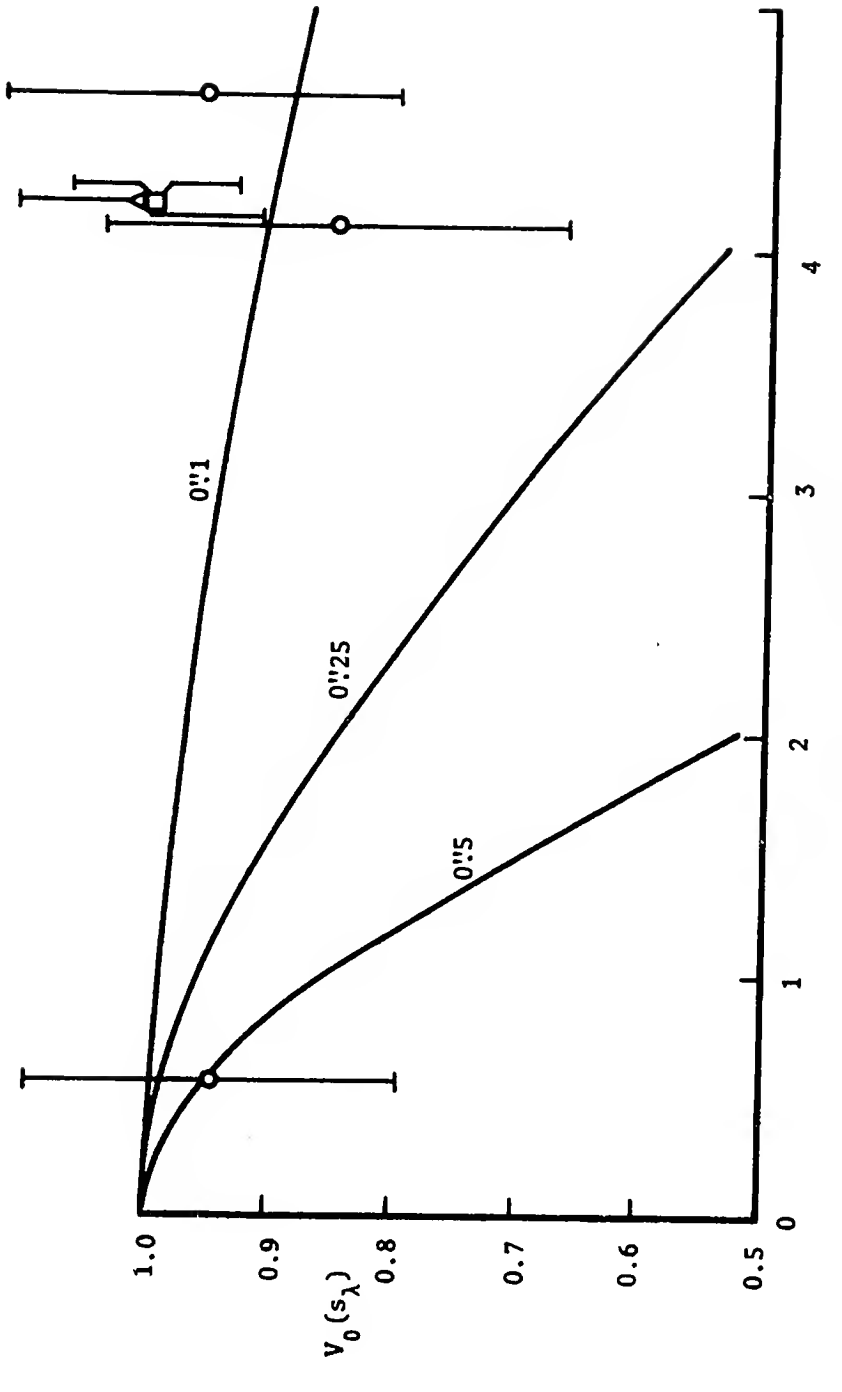

Figure VII.1 -- Graph of $V_0(s_\lambda)$ Versus Baseline Length for a Gaussian Source of Various Angular Widths. Circled Data Points Are the Averaged Fringe Amplitudes for the 1969 Data. A Triangle Indicates the Averaged Fringe Amplitude for the 1970 Data, and a Square Indicates the Same for the 1971 Data.

is less than 0.1 second of arc. Since Jupiter was at different distances from the earth for the three sets of data, this angular diameter corresponds to linear dimensions ranging from 254 km to 330 km. The assumption of incoherence is required in order to be able to use the fringe visibility to reconstruct the source brightness distribution as was shown in derivation at the bottom of page 23 in Chapter II. The interferometer can give no information on the size of a coherent source using the visibility function alone. Wide bandwidth experiments carried out by Flagg and Carr (1967) and others seem to indicate that, at least for short bursts, the source is relatively small. This conclusion is inferred from the very short rise- and fall-times of separate bursts. While most current models employ a source spatial distribution that is coherent, the information presented by the source size measurements given here will serve as a constraint on any theories that propose an incoherent radiator.

The analysis performed to detect the possible presence of sweeping beams of radiation from the decametric source succeeded in establishing minimum detectable sweep rates on the order of, or greater than, any predicted by current theories on the origin of the radiation. There was only one possible sweep rate that was detected for an S-Burst that was less than the maximum detectable rate of 10°/second, out of the several bursts measured. All sweep rates that are due to motions of the source caused by the rotation of the planet, orbital motion of Io, etc., are ruled out since they have values less than 0°.01/second. The only motion that is still possible (other than no sweeping at all), that has been predicted by current theories, is that due to the motion of a cloud of electrons along the magnetic field lines of the planet as

they radiate. The minimum rate that such a beam must have swept, based on this data, is greater than 10°/second. The time resolution of this analysis is at least twice that used by other investigators, e.g., Dulk (1970), and in the north-south direction where the greatest sweep rates are expected, it approaches an order of magnitude improvement.

The theory of Douglas and Smith (1967) successfully accounts for the origin of many L-Bursts using a mechanism involving inhomogeneities of approximately 100 km size in the solar wind, which cause an isophotal pattern of radiation to drift across the receiving stations. If an interferometer with a baseline longer than the coherence length of the isophotal pattern is used to investigate the Jovian radiation, it is expected that any interference due to the inhomogeneities (assuming they are located about 1 to 2 AU from the earth on a line between the earth and Jupiter) would not be seen. Many L-Bursts were observed that could be correlated at the ends of the University of Florida interferometer. During the one-minute interval that contained the 1969 L-Burst, some 50% of the approximately 23 bursts observed were envelope-correlated on the longest baseline (WKU-MAIPU). In a five-minute period containing the 1971 L-Burst, there were 18 bursts received at UFRO and 12 at MAIPU. Three were envelope-correlated on this baseline. The 1969 bursts had an average duration of 0.4 seconds, while the 1971 bursts averaged on the order of 2 seconds in duration.

It is concluded that the L-Bursts analyzed in the previous chapters, along with several others occurring about the same time, received their envelope shape at, or near, Jupiter. It is probable that the source itself imposed the time variations observed.

It has been shown that the sources of the two L-Bursts analyzed remained in approximately the same position with respect to the antenna power pattern for the durations of the bursts. The 1969 burst, due to the greater statistical noise on the fringes (caused by the higher fringe rate requiring a short integration time to be used in the cross correlation), placed a high tolerance on the "jumping about" of the source of 125 km in 150 milliseconds. Under better conditions, the 1971 data imposed a limit of 85 km for 2.2 seconds. The latter data indicated that the source possibly had a westward velocity of as much as 440 km/second, which is more than an order of magnitude greater than the surface velocity of the planet due to diurnal rotation. It was desired to perform a similar analysis on the series of S-Bursts since it would be very instructive to know if the bursts came from the same source location. This analysis was impossible to perform due to the limited amount of data that could be handled in the A-to-D conversion system presently available.

The research reported in this dissertation indicates that, with the acquisition of a new A-to-D conversion system, the question of the stability of the position of the source should be studied using longer continuous runs of data. This analysis should give answers to the question of the relative location of the sources of each S-Burst in a series like that presented in Chapter V. The time history of the source position for L-Bursts could be studied similarly for periods of several seconds or minutes.

The experiments proposed in the first chapter have been performed over the past three years. A little more information has been added to man's experience with Nature. While this series of measurements

does not give a complete picture of the source of Jovian decametric radiation, it does place new limits on any theory of the source mechanisms that are in existence or will be proposed in the future. It has been shown that, if the source is assumed to be incoherent, its angular diameter must be less than 0".1 of arc. If the source of an S-Burst is assumed to beam its radiation and if the beam rotates with respect to the Earth-Jupiter line, then the sweep-rate must be greater than 10°/second in the north-south direction. It was also shown that the position of the source of an L-Burst does not change more than 85 km with respect to the antenna pattern during the period of a typical burst (2 seconds). It will, no doubt, be necessary for many more measurements to be made and much more thinking to be done before a suitable model for the source mechanism is created. Then, man will have taken one more step along the path to understanding of the world in which he lives. Two serious detours could occur during this quest. Nature could change the rules of operation of the universe. Beneath all of man's quest for understanding is the faith that the universe is in some sense orderly and that the same rules of operation will always be followed. This is an act of faith, however. The other serious detour would occur if man lost interest in a rational understanding of his world. Man has not always thought that a rational understanding was necessary. This would be, by far, the most serious occurrence of the two. Will man ever be at home in a universe that he understands?

APPENDIX


BADE
AND
BASQ

```
C      THIS PROGRAM DETERMINES THE BASELINE AND CALCULATES THE DEVIATION
C      FROM THE BASELINE FOR DATA FROM EACH STATION
       INTEGER XBAR,SUM
       INTEGER Z(2240)
       INTEGER Y(2240)
       DIMENSION IAR(3520)
       DATA IAR,Z     ,Y/3520*0,2240*0,2240*0/
   81  READ (5,2)IFILE,JFILE,NBEG,NEX,ISQ,INT,JNDLT
    2  FORMAT(7I5)
       IF (IFILE)   11,11,1
    1  DO 3 MI=1,3520
    3  IAR(MI)=0
       DO 102 K360=1,293
  102  READ(5,101)(IAR((K360-1)*12+J),J=1,12)
  101  FORMAT(12I6)
       READ(5,101)(IAR(3516+J),J=1,4)
       SUM=0
       DO 5 M=1,3520
    5  SUM=SUM+IAR(M)
       XBAR=SUM/3520
       DO 7 MJ=1,3520
    7  IAR(MJ)=IAR(MJ)-XBAR
       WRITE(6,10) IFILE,XBAR
   10  FORMAT('0','XBAR FOR FILE ',I1,' IS ',I8)
C      THIS PROGRAM DELETES NEX EXCESS DATA POINTS AND PLACES 2240 DATA
C      POINTS STARTING WITH NBEG IN A NEW FILE.
C      IFILE TELLS WHICH FILE WILL BE READ, JFILE TELLS WHICH FILE
C      WILL BE WRITTEN INTO.
C      THE VARIABLE ISQ IS SET TO ZERO IF THE DATA IS NOT TO BE INTEGRATE
C      D, IT IS SET TO ONE IF IT IS TO BE INTEGRATED.
       IF(NEX)77,77,88
   77  NEX=1
   88   N=3520/NEX
       J=0
```

```
      I=0
      NI=N
      YP=IAR(NBEG)
   33 I=I+1
      JIG=I-J
      JIL=I+NBEG
      IF(I-NI)34,35,35
   34 IF ( JIL     -3520)21,21,6
   21 YP=IAR(JIL)
      Y(JIG)=YP
      IF(JIG-2240)33,6,6
   35 IF(JIL-3519         )22,22,6
   22 YP=IAR(JIL+1)
      Y(JIG)=YP
      J=J+1
      NI=NI+N
      I=I+1
      IF(JIG-2240)33,6,6
    6 IF(ISQ)113,113,121
  121 JL=0
  227 JN=0
  122 SUSQ=0.
      DO 123 IN=1,INT
      JIN=IN+JN
      YS=Y(JIN)
  123 SUSQ=SUSQ +YS*YS
      JL=JL+1
      JN=JN+JNDLT
      ZP=SQRT(SUSQ)
      Z(JL)=ZP
  225 IF((JN+INT)-2240)122,122,124
  124 CONTINUE
      WRITE (6,125)JL,JFILE,NBEG,INT
  125 FORMAT('0THE FIRST',I5,' POINTS IN FILE', I3,' ARE DETECTED AND IN
```

```
   4TEGRATED DATA SUCH THAT THE FILE STARTS WITH THE',I5,' DATA POINT'
   7/' THE INTEGRATION PERIOD IS ',I5,'.')
223 GO TO 81
113 DO 321 NL=1,186
    WRITE(6,324)(Y(NN+12*(NL-1)),NN=1,12),IFILE,NL
321 WRITE(7,322)(Y(NN+12*(NL-1)),NN=1,12),IFILE,NL
322 FORMAT(12I6,T76,I1,T78,I3)
324 FORMAT(' ',12I6,T76,I1,T78,I3)
    NL=187
    WRITE(6,324)(Y(NN+12*(NL-1)),NN=1,8),IFILE,NL
    WRITE(7,322)(Y(NN+186),NN=1,8),IFILE,NL
    NBEGI=NBEG+1
    WRITE(6,90) IFILE,JFILE,JFILE,NBEGI
 90 FORMAT('0DATA FROM FILE',I5,' HAS BEEN TRANSFERRED TO FILE',I5,'
   6SUCH THAT FILE',I5,' STARTS WITH THE',I5,' DATA POINT.')
    GO TO 81
 11 STOP
    END
```

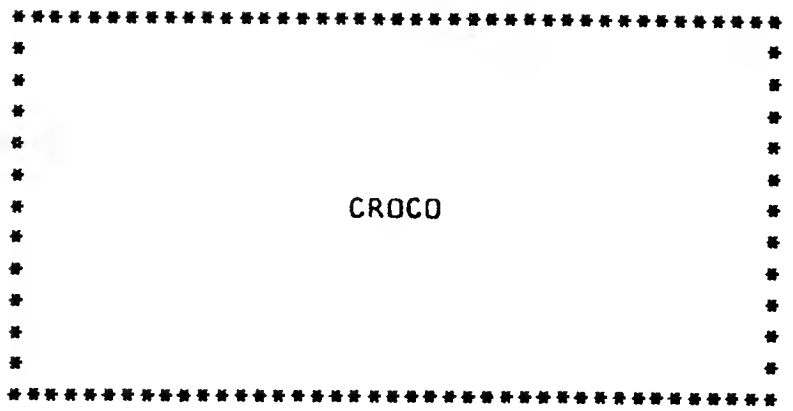
CROCO

```
C     THIS PROGRAM CALCULATES CORRELATION COEFFICIENTS BETWEEN DATA FROM
C     TWO STATIONS. STATION 1 WILL REMAIN FIXED AND THE DATA FROM
C     STATION 2 WILL BE SHIFTED BY KDELT DATA POINT INTERVALS BETWEEN
C     ITAU AND JTAU.  INTEGRATION TIME IS N DATAPOINTS.
C     IFIL1 DESIGNATES STATION 1. IFIL2 DESIGNATES THE STATION TO BE
C     COMPARED WITH IFIL1.
C     THE DATE OF THE BURST IS ENTERED INTO IDATE SUCH THAT IDATE(1) IS
C     THE MONTH NUMBER, IDATE(2) IS THE DAY NUMBER AND IDATE(3) IS THE
C     YEAR (FOR EXAMPLE, 1/2/69 IS 2 JAN. 1969).
C     LBEG IS THE DATA POINT ON WHICH CROSS CORRELATING STARTS.
C     KDELT TELLS HOW MANY DATA POINTS TO STEP ITAU EACH CYCLE THROUGH
C     DATA FOR EACH PAIR OF STATIONS.
C     LDELT TELLS THE NUMBER OF DATA POINTS TO BE STEPPED IN SHIFTING
C     THE INTEGRATION REGION.
C     NDPS IS THE DATA POINT ON WHICH LDELT STEPPING STOPS.
C     JTAU IS THE DATA POINT NUMBER WHERE SHIFTING STOPS.
C     DPS IS SET TO THE DIGITIZATION RATE.
      INTEGER A(101),AST
      INTEGER XI(2232),YI(2232),X,Y
      DIMENSION IG(4,2232)
      DIMENSION PXC(3),IDATE(3),NOW(5)
      DATA A(51),AST,BLNK/'*','*',' '/
      DATA X,Y,XI,YI,IFIL1,IFIL2              /2*0 ,2232*0,2232*0,0,0/
      DATA NDPS/2200/
C     THIS PART READS IN DATA FROM THE STATIONS TO BE COMPARED.
C     DATA IS READ FROM CARDS. THERE ARE 186 CARDS CONTAINING 12 DATA
C     POINTS EACH FOR EACH STATION. COLUMN 76 CONTAINS A STATION CODE
C     NUMBER (1 FOR WKU, 2 FOR UFRO, 3 FOR MAIPU, 4 FOR FPC).
    9 READ(5,10)(IRL,IR,(IG(IRL,IRN+12*(IR-1)),IRN=1,12))
   10 FORMAT (T76,I1,T78,I3,T1,12I6)
      IF (IR)901,901,9
  901 READ(5,71)IDATE(1),IDATE(2),JHOUR,XSEC,IFIL1,IFIL2,ITAU,N,KDELT,LD
     5ELT,IDATE(3),DPS,JTAU,NDPS,LBEG
   71 FORMAT(2I2,T6,I5,F10.6,7I5,F5.0,3I5)
```

```
      IF (IFIL1)94,94,1113
 1113 PINT=N/DPS
  902 DO 1013 IF3=1,2232
      XI(IF3)=IG(IFIL1,IF3)
 1013 YI(IF3)=IG(IFIL2,IF3)
      WRITE(6,82) IDATE,JHOUR,XSEC
   82 FORMAT('1','THE DATE OF THIS DATA IS ',I2,'/',I2,'/',I2,' AT',I5,'
     6 U.T. AND ',F10.4,' SECONDS.')
      CALL TODAY(NOW)
      WRITE(6,30)NOW
   30 FORMAT('0','THE DATE OF THIS PROCESSING RUN IS ',5A4,'.')
      WRITE(6,1112)PINT
 1112 FORMAT('0THE INTEGRATION TIME FOR THIS DATA IS ',F10.8,' SEC.')
      ITAUS=IABS(ITAU)
      JTAUS=IABS(JTAU)
      IF(ITAUS-JTAUS)130,130,131
  130 ITAUA=JTAUS
      GO TO 133
  131 ITAUA=ITAUS
  133 K=-ITAU
   84 WRITE(6,11111) IFIL1,IFIL2,K,NOW
11111 FORMAT('1STATION ',I1,' LEADS STATION ',I1,' BY ',I5,' DATA PTS ON
     6 ',5A4)
      WRITE(6,81)
   81 FORMAT('0','THE DATA CARD FOR THIS RUN IS ')
      WRITE(6,181)
  181 FORMAT('0IDATE(1) IDATE(2) JHOUR  XSEC   IFIL1 IFIL2 ITAU N  KDELT
     6 LDELT IDATE(3)  DPS  JTAU NDPS     LBEG')
      WRITE(6,281)IDATE(1),IDATE(2),JHOUR,XSEC,IFIL1,IFIL2,ITAU,N,KDELT,
     2LDELT,IDATE(3),DPS,JTAU,NDPS,LBEG
  281 FORMAT(' ',3X,I2,7X,I2,4X,I5,1X,F7.4,2(2X,I2,1X),I5,I5,2I5,I8,F10.
     80,I4,I6,I6)
      WRITE(6,83)
   83 FORMAT('0','  NORM   XCOR1 XCOR2 XCOR3   LP ',T68,'CROSS CORRELATI
```

```
     7ON COEFFICIENT')
      WRITE(6,87)
   87 FORMAT('0',T31,'-1.',T41,'-.8',T51,'-.6',T61,'-.4',T71,'-.2',T83,'
     HO',T92,'.2',T102,'.4',T112,'.6',T122,'.8',T132,'1.')
      WRITE(6,88)
   88 FORMAT(' ',T24,11(9X,'I'))
      L=LBEG
      LP=1
   36 DO 35 NJ=1,3
   35 PXC(NJ)=0.
      PNM=0.
      DO 336 NJ=1,101
  336 A(NJ)=BLNK
      A(51)=AST
C     THE FOLLOWING LOOP ON NI CALCULATES ONE LINE OF OUTPUT.
    3 DO 8 NI=1,3
    4 SUXYK =0.
      SUSQX =0.
       SUSQY =0.
      MU1=L+ITAUA
      IF(MU1+N-NDPS)18,18,92
   18 IF(MU1+N-NDPS-K)19,19,92
C     THIS LOOP ON M CALCULATES ONE VALUE OF THE CORRELATION COEFFICIENT
   19 DO 5 M=1,N
      MU=MU1+M
      MV=MU-K
      X=XI(MU)
      Y=YI(MV)
      SUXYK=SUXYK+X*Y
      SUSQX=SUSQX+X*X
    5 SUSQY=SUSQY+Y*Y
      SQ=SQRT(SUSQX*SUSQY)
      IF(SQ)22,22,23
   22 PXC(NI)=0.
```

```
      GO TO 8
   23 PXC(NI)=SUXYK/SQ
      IF(NI-1)37,37,8
   37 PNM=SQ
      JPXC=50.*PXC(NI)+51.5
C     THIS LOOP DECIDES THE POSITION OF THE ASTERISK ON THE GRAPH.
      DO 138 NL=1,101
      IF (JPXC-NL)138,136,138
  136 A(NL)=AST
      GO TO 8
  138 CONTINUE
    8 L=L+LDELT
      WRITE(6,31)PNM,PXC,LP,A
   31 FORMAT(' ',E8.2,3F6.3,1X,I4,101A1)
      LP=LP+3
      GO TO 36
   92 WRITE(6,31)PNM,PXC,LP,A
   91 WRITE(6,88)
      WRITE(6,87)
      K=K+KDELT
      IF(K-JTAU)84,84,901
   94 STOP
      END
```

MODIFICATIONS TO

CROCO

REQUIRED FOR S-BURSTS

RECEIVED ON

4/30/70

```
C     THIS PROGRAM CALCULATES CORRELATION COEFFICIENTS BETWEEN DATA FROM
C     TWO STATIONS. STATION 1 WILL REMAIN FIXED AND THE DATA FROM
C     STATION 2 WILL BE SHIFTED BY KDELT DATA POINT INTERVALS BETWEEN
C     ITAU AND JTAU.  INTEGRATION TIME IS N DATAPOINTS.
C     IFIL1 IS THE NUMBER OF THE BURST TO BE CORRELATED.  IT HAS A VALUE
C     BETWEEN 1 AND 11.  IFIL2 GIVES THE CHANNEL OF GAINESVILLE DATA TO
C     BE USED FOR CORRELATION.  IFIL2 IS 1 FOR GVA, 2 FOR GVB.
C     DATA IS ARRANGE IN 80 DATA POINT RECORDS.  THERE ARE 24 RECORDS
C     FOR CH, 24 FOR GVA AND 24 FOR GVB FOR BURST NO. 1. THE CYCLE
C     REPEATS FOR 11 BURSTS.
C     LBEG IS THE DATA POINT ON WHICH CROSS CORRELATING STARTS.
C     DATA FROM CHILE WILL BE LOADED INTO ARRAY XI.
C     KDELT TELLS HOW MANY DATA POINTS TO STEP ITAU EACH CYCLE THROUGH
C     DATA FOR EACH PAIR OF STATIONS.
C     LDELT TELLS THE NUMBER OF DATA POINTS TO BE STEPPED IN SHIFTING
C     THE INTEGRATION REGION.
C     NDPS IS THE DATA POINT ON WHICH LDELT STEPPING STOPS.
C     JTAU IS THE DATA POINT NUMBER WHERE SHIFTING STOPS.
C     DPS IS SET TO THE DIGITIZATION RATE.
      INTEGER A(101),AST
      DIMENSION PXC(3),IDATE(3),NOW(5)
      DATA A(51),AST,BLNK/'*','*',' '/
      INTEGER XI(1920),YI(1920)
      DIMENSION IGV(2,1920)
      DATA X,Y,XI,YI,IFIL1,IFIL2,JFIL1      /2*0.,1920*0,1920*0,0,0,0/
      DATA JFIL3/0/
      DATA NDPS/1920/
  901 READ(5,71)IDATE(1),IDATE(2),JHOUR,XSEC,IFIL1,IFIL2,ITAU,N,KDELT,LD
     5ELT,IDATE(3),DPS,JTAU,NDPS,LBEG
   71 FORMAT(2I2,T6,I5,F10.6,7I5,F5.0,3I5)
      IF (IFIL1)94,94,1113
 1113 PINT=N/DPS
      IF (JFIL1-IFIL1)107,108,107
  107 IREC1=72*(IFIL1-1)
```

```
      IF(IREC1)208,209,208
  208 DO 103 NREC=1,IREC1
  103 READ(11)
  209 DO 101 IREC=1,24
  101 READ(11)(XI((       IREC-1)*80+JREC),JREC=1,80)
      ASUM=0
      DO 104 IEK=1,1920
  104 ASUM=ASUM+XI(IEK)
      AAVG=ASUM/1920.
      DO 106 IEL=1,1920
  106 XI(IEL)=XI(IEL)-AAVG
      JFIL3=0
      DO 102 ICOL=1,2
      DO 102 IRECD=1,24
  102 READ(11)((IGV(ICOL,(IRECD- 1)*80+KREC)),KREC=1,80)
      REWIND 11
  108 IF(JFIL3-IFIL2)504,503,504
  504 DO 1 IE=1,1920
    1 YI(IE)=IGV(IFIL2,IE)
      JFIL1=IFIL1
      BSUM=0
      DO 501 IED=1,1920
  501 BSUM=BSUM+YI(IED)
      BAVG=BSUM/1920.
      DO 502 IEC=1,1920
  502 YI(IEC)=YI(IEC)-BAVG
  503 JFIL3=IFIL2
                                    *
                                    *
                                    *
      JFIL2=IFIL2+1
   84 WRITE(6,11111)      JFIL2,K,NOW
11111 FORMAT('1STATION   CH   LEADS STATION ',I1,' BY ',I5,' DATA PTS ON
     5 ',5A4,' GVA IS STATION 2, GVB IS STATION 3.')
```

```
C
C
C
      WRITE(6,508)IFIL1
  508 FORMAT('0THIS IS BURST NUMBER',I4,'.')
C
C
```

```
C*****************************************
C*                                       *
C* CARDS ADDED AFTER STATEMENT 101 TO    *
C*                                       *
C* SQUARE-LAW DETECT DATA IN ARRAY XI    *
C*                                       *
C*****************************************

      DO 513 ISQ=1,1880
      DSUM=0.
      DO 514 ISP=1,37
      ISL=ISQ+ISP-1
  514 DSUM=DSUM+XI(ISL)*XI(ISL)
  513 XI(ISQ)=SQRT(DSUM)
```

```
C*****************************************
C*                                       *
C* CARDS ADDED AFTER STATEMENT 1 TO      *
C*                                       *
C* SQUARE-LAW DETECT DATA IN ARRAY YI    *
C*                                       *
C*****************************************

      DO 525 JSQ=1,1880
      FSUM=0.
      DO 516 JSP=1,37
      JSL=JSQ+JSP-1
  516 FSUM=FSUM+YI(JSL)*YI(JSL)
  525 YI(JSQ)=SQRT(FSUM)
```

FURTHER

MODIFICATIONS TO

CROCO

REQUIRED FOR L-BURST

RECEIVED ON

4/12/71

```
C     THIS PROGRAM CALCULATES CORRELATION COEFFICIENTS BETWEEN DATA FROM
C     TWO STATIONS. STATION 1 WILL REMAIN FIXED AND THE DATA FROM
C     STATION 2 WILL BE SHIFTED BY KDELT DATA POINT INTERVALS BETWEEN
C     ITAU AND JTAU.  INTEGRATION TIME IS N DATAPOINTS.
C     IFIL1 IS THE NUMBER OF THE BURST TO BE CORRELATED.  IT HAS A VALUE
C     BETWEEN 1 AND 44.  IFIL2 GIVES THE CHANNEL OF GAINESVILLE DATA TO
C     BE USED FOR CORRELATION.  IFIL2 IS 1 FOR GVA, 2 FOR GVB.
C     DATA FOR CH IS IN THE FIRST 1056 RECORDS OF FILE 4. THAT FOR GVA
C     IS IN THE NEXT 1056 RECORDS AND THAT FOR GVB IS IN THE NEXT 1056.
C     THERE ARE 80 DATA POINTS PER RECORD.
C     DATA FROM CHILE WILL BE LOADED INTO ARRAY XI.
C     KDELT TELLS HOW MANY DATA POINTS TO STEP ITAU EACH CYCLE THROUGH
C     DATA FOR EACH PAIR OF STATIONS.
C     LDELT TELLS THE NUMBER OF DATA POINTS TO BE STEPPED IN SHIFTING
C     THE INTEGRATION REGION.
C     NDPS IS THE DATA POINT ON WHICH LDELT STEPPING STOPS.
C     JTAU IS THE DATA POINT NUMBER WHERE SHIFTING STOPS.
C     DPS IS SET TO THE DIGITIZATION RATE.
                                      *
                                      *
                                      *
  107 IREC1=24*(IFIL1-1)
                                      *
                                      *
                                      *
      DO 1020 NRC=25,1056
 1020 READ(11)
                                      *
                                      *
```

LIST OF REFERENCES

Bigg, E. K., "Influence of the Satellite Io on Jupiter's Decametric Radiation," Nature, 203, 1008-1010 (1964).

Block, W. F., M. P. Paul, T. D. Carr, G. R. Lebo, V. M. Robinson, and N. F. Six, "Interferometry of Jupiter at 18 MHz with a 52800 λ Baseline," Astrophys. Letters, 5, 133-136 (1970).

Bracewell, R. N., The Fourier Transform and Its Applications (McGraw-Hill Book Company, New York, 1965).

Brown, G. W., Long Baseline Interferometry of Jupiter's Decametric Radiation (Ph.D. Dissertation, University of Florida, 1970).

Brown, R. Hanbury, and R. Q. Twiss, "A New Type of Interferometer for Use in Radio Astronomy," Phil. Mag., 45, 663-682 (1954).

Brown, G. W., T. D. Carr, and W. F. Block, "Long-Baseline Interferometry of S-Bursts from Jupiter," Astrophys. Letters, 1, 89 (1968).

Burke, B. F., and K. L. Franklin, "Observations of a Variable Radio Source Associated with the Planet Jupiter," J. Geophys. Res., 60, 213-217 (1955).

Carr, T. D., M. A. Lynch, M. P. Paul, G. W. Brown, J. May, N. F. Six, V. M. Robinson, and W. F. Block, "Very Long Baseline Interferometry of Jupiter at 18 MHz," Radio Science, 5, 1223-1226 (1970).

Carr, T. D., G. W. Brown, A. G. Smith, C. S. Higgins, H. Bollhagen, J. May, and J. Levy, "Spectral Distribution of the Decametric Radiation from Jupiter in 1961," Astrophys. J., 140, 778-795 (1964).

Carr, T. D., J. May, C. N. Olsson, G. F. Walls, NEREM Record 7, 22 (1965) (IEEE Cat. No. F-60).

Carr, T. D., A. G. Smith, H. Bollhagen, N. F. Six, and N. E. Chatterton, "Recent Decameter Wavelength Observations of Jupiter, Saturn, and Venus," Astrophys. J., 134, 105-125 (1961).

Cooper, B. F. C., "Correlators with Two-Bit Quantization," Aus. J. Phys., 23, 521-527 (1970).

Douglas, J. N.,and H. J. Smith, "Decametric Radiation from Jupiter," Astron. J., 68, 163-180 (1963).

Douglas, J. N.,and H. J. Smith, "Presence and Correlation of Fine Structure in Jovian Decametric Radiation," Nature, 192, 741 (1961).

Douglas, J. N.,and H. J. Smith, "Interplanetary Scintillation in Jovian Decametric Radiation," Astrophys. J., 148, 885-903 (1967).

Dulk, G. A., "Io-Related Radio Emission from Jupiter," Science, 148, 1585 (1965).

Dulk, G. A., "Characteristics of Jupiter's Decametric Radio Source Measured with Arc-Second Resolution," Astrophys. J., 159, 671-684 (1970).

Dulk, G. A., B. Rayhrer, and R. Lawrence, "The Size of Jupiter's Decametric Radio Source," Astrophys. J., 150, 117-120 (1967).

Flagg, R. S., and T. D. Carr, "Wide Bandwidth Observations of the Decametric Bursts from Jupiter," Astrophys. Letters, 1, 47 (1967).

Gallet, R. M., "Radio Observations of Jupiter II," Planets and Satellites, ed. by Kuiper, G. P., and Middlehurst, B. M. (University of Chicago Press, Chicago, Illinois, 1961), 509.

Gardner, F. F., and C. A. Shain, "Further Observations of Radio Emission from the Planet Jupiter," Aus. J. Phys., 11, 55 (1958).

Goldreich, P., and D. Lynden-Bell, "Io, a Jovian Unipolar Inductor," Astrophys. J., 156, 59-78 (1969).

Hewlett-Packard Company, Frequency and Time Standards, Application Note 52 (Palo Alto, California, 1965), 4-4 -- 4-6.

Kraus, J. D., Radio Astronomy (McGraw-Hill Book Company, New York, 1965).

May, J., Studies of Radio Noise Bursts from Jupiter (Master's Thesis, University of Florida, 1965).

Mayer, C. H., T. P. McCullough, and R. M. Sloanaker, "Observations of Mars and Jupiter at a Wavelength of 3.15 cm," Astrophys. J., 127, 11-16 (1958).

Paul, M. P., Waveform and Source Size Studies of Jupiter's Decametric Radiation (Ph.D. Dissertation, University of Florida, 1969).

Radhakrishnan, V., and J. A. Roberts, "Polarization and Angular Extent of the 960 Mc/sec Radiation from Jupiter," Phys. Rev. Letters, 4, 493-494 (1961).

Riihimaa, J. J., "High Resolution Spectral Observations of Jupiter's Decametric Radio Emission," Nature, 202, 467 (1964).

Riihimaa, J. J., "Modulation Lanes in the Dynamic Spectra of Jovian L Bursts," Astron. & Astrophys., 4, 180-188 (1970).

Schatten, K. H., and N. F. Ness, "The Magnetic-Field Geometry of Jupiter and Its Relation to Io-Modulated Jovian Decametric Radio Emission," Astrophys. J., 165, 621-631 (1971).

Schmahl, E. J., Io, an Alfven-Wave Generator (Ph.D. Dissertation, University of Colorado, 1970).

Shain, C. A., "Location on Jupiter of a Source of Radio Noise," Nature, 176, 836-837 (1955).

Shain, C. A., "18.3 Mc/s Radiation from Jupiter," Aus. J. Phys., 9, 61-73 (1956).

Shapiro, L. D., "Loran-C Timing and Frequency Comparison," Frequency, 22-24 (March, 1968a).

Shapiro, L. D., "Time Synchronization from Loran-C," IEEE Spectrum, 46-55 (August, 1968b).

Slee, O. B., and C. S. Higgins, "Long Baseline Interferometry of Jovian Decametric Radio Bursts," Nature, 197, 781-783 (1963).

Slee, O. B., and C. S. Higgins, "The Solar Wind and Jovian Decametric Radio Emission," Aus. J. Phys., 21, 341-368 (1968).

Sloanaker, R. M., "Apparent Temperature of Jupiter at a Wavelength of 10 cm," Astron. J., 64, 346 (1959).

Stannard, K. M., G. A. Dulk, and B. Rayhrer, "Very Long Baseline Interferometry of Decametric Radiation from Jupiter," Radio Science, 5, 1271-1280 (1970).

Weinreb, S., M.I.T. Research Laboratory of Electronics Report No. 412, 119 (1963).

BIOGRAPHICAL SKETCH

Michel Allan Lynch was born in Oklahoma City, Oklahoma, on 6 December 1939. After representing Oklahoma City in two National Science Fairs, he graduated from high school in 1957. He made a trip to Turkey as a representative of the Oklahoma Wing of the Civil Air Patrol during the summer of 1957. That fall he matriculated at the University of Oklahoma. His work completed for a bachelor's degree in Physics in January of 1961, he was employed by Texas Instruments, Inc. in their Central Research Division in Richardson, Texas.

Mr. Lynch's graduate career began in 1961 at Rice University. He completed a master's degree at the University of Oklahoma with work in acoustics directed by Dr. C. A. Plint in 1966. From 1966 through 1968, he was a member of the faculty of the Department of Physics at Oklahoma City University. In the summer of 1967, he married the former Mary Elizabeth Coates.

An appointment in the summer of 1968 as a participant in the RPCT program in the Department of Physics and Astronomy at the University of Florida brought him to the Southeast. He joined the faculty of the University College in the Department of Physical Sciences in the fall of that year. After working on equipment for the very-long-baseline interferometer during 1968, he entered the Graduate School of the University of Florida to complete the requirements for the Ph.D.

His hobbies are the design and construction of various electronic projects. He also enjoys cabinet and musical instrument construction. With a pilot license that he obtained as an undergraduate, he is known to fly when time permits. He currently resides with his wife, Mary, and collie, Sebastian, in Gainesville.

I certify that I have read this study and that in my opinion it conforms to acceptable standards of scholarly presentation and is fully adequate, in scope and quality, as a dissertation for the degree of Doctor of Philosophy.

Thomas D. Carr

Thomas D. Carr, Chairman
Professor of Physics and
Astronomy

I certify that I have read this study and that in my opinion it conforms to acceptable standards of scholarly presentation and is fully adequate, in scope and quality, as a dissertation for the degree of Doctor of Philosophy.

Alex. G. Smith
Professor of Physics and
Astronomy

I certify that I have read this study and that in my opinion it conforms to acceptable standards of scholarly presentation and is fully adequate, in scope and quality, as a dissertation for the degree of Doctor of Philosophy.

Kwan-Yu Chen
Associate Professor of Astronomy
and Physical Sciences

I certify that I have read this study and that in my opinion it conforms to acceptable standards of scholarly presentation and is fully adequate, in scope and quality, as a dissertation for the degree of Doctor of Philosophy.

George R. Lebo
Assistant Professor of Astronomy

I certify that I have read this study and that in my opinion it conforms to acceptable standards of scholarly presentation and is fully adequate, in scope and quality, as a dissertation for the degree of Doctor of Philosophy.

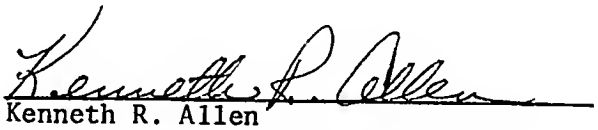

Kenneth R. Allen
Assistant Professor of Physics

This dissertation was submitted to the Department of Physics and Astronomy in the College of Arts and Sciences and to the Graduate Council, and was accepted as partial fulfillment of the requirements for the degree of Doctor of Philosophy.

June, 1972

Dean, Graduate School

UNIVERSITY OF FLORIDA
3 1262 08554 5340